

**Design, Fabrication and Testing of a Configurable Full-Field Stimulus
Source for Electroretinography**

BY

GIULIA CROCIONI
B.S., Politecnico di Milano, July 2017

THESIS

Submitted as partial fulfillment of the requirements
for the degree of Master of Science in Bioengineering
in the Graduate College of the
University of Illinois at Chicago, 2019

Chicago, Illinois

Defense Committee:

John Hetling, Chair and Advisor
Hananeh Esmailbeigi
Giambattista Gruosso, Politecnico di Milano

ACKNOWLEDGEMENTS

I would first like to thank my thesis advisor Dr. John Hetling of the Department of Bioengineering at University of Illinois at Chicago. He was a great mentor and he steered me in the right direction every time I needed it. Without his inputs and suggestions this project could not have been successfully conducted.

I would also like to thank my Italian advisor Dr. Giambattista Grusso of the Department of Electronics, Information, and Bioengineering, at Politecnico di Milano. He always followed me actively and helped me during this project, despite the distance. I am gratefully indebted for his very valuable help on this thesis.

Finally, a huge and special thanks goes to my parents, to my boyfriend and to my friends for having always supported me during the development of this thesis. I couldn't have done it without them. Thank you.

GC

TABLE OF CONTENTS

<u>CHAPTER</u>	<u>PAGE</u>
1 INTRODUCTION	1
1.1 The human retina	1
1.2 The electroretinogram	4
1.2.1 The multifocal electroretinogram	8
1.2.2 The pattern electroretinogram	8
1.3 Electroretinogram stimulus sources	10
1.3.1 Ganzfield stimulator	10
1.3.2 Cathode-Ray Tubes	12
1.3.3 Liquid Crystal Displays	14
1.3.4 Plasma Displays Panels	16
1.3.5 Light Emitting Diodes	16
1.3.6 Stimulus sources available on the market	18
1.4 The peripheral pattern electroretinogram (pERG) and the three dimensional stimulus source	18
1.4.1 Glaucoma	20
1.4.2 Glaucoma detection	20
1.4.3 Traditional tests	21
1.4.4 The first prototype: the peripheral pattern electroretino- gram (ppERG) system	23
1.4.5 The improved peripheral pattern electroretinogram (ppERG) prototype	27
2 SPECIFIC AIM	35
3 SPECIFIC AIM 1	37
3.1 Methods	37
3.2 Design requirements	39
3.2.1 Visual field	39
3.2.2 Check shape, size and number	41
3.2.3 Optical properties	41
3.2.4 Electronic layout	43
3.3 Design results	44
3.3.1 Visual field	44
3.3.2 Check shape, size and number	46
3.3.3 Optical properties	50
3.3.4 Electronic layout	72

TABLE OF CONTENTS (Continued)

<u>CHAPTER</u>		<u>PAGE</u>
4	SPECIFIC AIM 2	84
	4.1 Materials	84
	4.1.1 First layer	84
	4.1.2 Second layer	85
	4.1.3 Third layer	85
	4.1.4 Fourth layer	86
	4.1.5 Printed circuit board (PCB)	87
	4.1.6 Base and side walls	91
	4.1.7 Black coating	91
	4.1.8 White coating	91
	4.2 Assembling	92
	4.3 Results	94
5	SPECIFIC AIM 3	95
	5.1 Methods	95
	5.1.1 Luminance measurements	95
	5.1.2 Uniformity measurements	96
	5.1.3 Contrast measurements	99
	5.2 Results	102
	5.2.1 Luminance measurements	102
	5.2.2 Uniformity measurements	103
	5.2.3 Contrast measurements	110
6	DISCUSSION	114
	6.1 Conclusions	114
	6.2 Limitations and future works	117
	APPENDICES	120
	Appendix A	121
	Appendix B	128
	Appendix C	129
	Appendix D	154
	CITED LITERATURE	169
	VITA	173

LIST OF TABLES

<u>TABLE</u>		<u>PAGE</u>
I	COMPARISON BETWEEN VISUAL ELECTROPHYSIOLOGY STIMULUS SOURCES ON THE MARKET.	19
II	CHECK SIZES FOR EACH ROW.	47
III	STIMULUS STRENGTH AND DURATION REQUIREMENTS OF MAIN FULL-FIELD electroretinogram (ERG) PROTOCOLS	62
IV	MEAN STIMULUS STRENGTH FOR EACH light emitting diode (LED) CHANNEL AND FOR EACH STIMULUS DURATION	63
V	MEAN STIMULUS STRENGTH FOR EACH LED CHANNEL USING HIGHER CURRENT (500 mA)	65
VI	MEAN LUMINANCE (TOTAL TIME PERIOD 15 MIN) OF EACH CHECK COLOUR USING LOW CURRENTS (1.2 AND 2 mA) TO POWER EACH LED CHANNEL	66
VII	MEAN ON-LUMINANCE (350 mA, TOTAL TIME PERIOD 15 MIN) OF EACH LED COLOUR CHANNEL	66
VIII	COEFFICIENT OF VARIATION % GIVEN BY THE TWO LUMINANCE MEASUREMENTS MADE IN ORDER TO ANALYSE STABILITY IN TIME OF MC-E LED CHANNELS	69
IX	COEFFICIENT OF VARIATION % OF GRAYSCALE INTENSITY LEVEL OF THE PIXELS ALONG THE TWO LINES, FOR EACH COLOUR CHANNEL.	72
X	SPECIFICATIONS AND REQUIREMENTS OF THE ORDERED PCBs .	88
XI	COEFFICIENT OF VARIATION % GIVEN BY THE LUMINANCE MEASUREMENTS MADE IN ORDER TO ANALYSE MAXIMUM LUMINANCE UNIFORMITY OF PIXELS BELONGING TO THE SAME ROW, FOR EACH COLOUR, POWERING EACH LED WITH 200 mA.	103
XII	COEFFICIENT OF STANDARD DEVIATION % OF GREYSCAL INTENSITY LEVEL OF EACH PIXEL OF EACH ROW USING THE LED RED CHANNEL.	106

LIST OF TABLES (Continued)

<u>TABLE</u>		<u>PAGE</u>
XIII	COEFFICIENT OF STANDARD DEVIATION % OF GREYSCAL INTENSITY LEVEL OF EACH PIXEL OF EACH ROW USING THE LED GREEN CHANNEL.	107
XIV	COEFFICIENT OF STANDARD DEVIATION % OF GREYSCAL INTENSITY LEVEL OF EACH PIXEL OF EACH ROW USING THE LED BLUE CHANNEL.	108
XV	COEFFICIENT OF STANDARD DEVIATION % OF GREYSCAL INTENSITY LEVEL OF EACH PIXEL OF EACH ROW USING THE LED WHITE CHANNEL.	109
XVI	CONTRAST RATIO AND RELATIVE CONTRAST % FOR EACH pERG PHASE 16-BIT GRAYSCALE IMAGE.	113
XVII	Global Contrast Factor (GCF) AND RELATIVE CONTRAST % FOR EACH pERG PHASE 16-BIT GRAYSCALE IMAGE.	113

LIST OF FIGURES

<u>FIGURE</u>		<u>PAGE</u>
1	Photopic and scotopic efficacy curves, adopted from ^[1]	2
2	Cross section of the human retina, adopted from ^[2]	3
3	Retinal cells which originate components of ERG, adopted from ^[3]	4
4	Multifocal electroretinogram (mfERG) waveform, adopted from ^[4]	9
5	PERG waveform, adopted from ^[5]	10
6	The Nicolet Ganzfeld stimulator (Nicolet - Instruments of Discovery).	12
7	An example of Cathod-Ray Tubes (CRT), adopted from ^[6]	14
8	Normal anatomy vs glaucoma.	21
9	Targeting regions of pERG.	24
10	Targeting regions of ppERG.	24
11	Peripheral pERG system.	25
12	Cross-sectional view of the LED unit.	26
13	LED units disposition.	27
14	Example of response recorded with the first ppERG system.	28
15	First prototype of the ppERG stimulus source.	29
16	Distal view of the improved pattern stimulus source.	30
17	Flow of circuit connections in the second prototype, adopted from ^[7]	31
18	Improved ppERG system response matched with conventional pERG.	33
19	Improved ppERG system response.	34
20	Test-retest repeatability of ppERG system.	34
21	Renders of possible ERG patterns.	36
22	Organization of rows and columns of the dome.	38

LIST OF FIGURES (Continued)

<u>FIGURE</u>		<u>PAGE</u>
23	Representative lateral section of one redesigned pixel.	39
24	Red curve: human visual field limits for a healthy right eye.	40
25	Visual field subtended by ppERG prototype.	45
26	Lateral angle subtended by the new three dimensional stimulus source.	45
27	Partial Solidworks design procedure.	48
28	Frontal view of the first shell.	49
29	Top view of the circumference with radius 40 cm of the first shell.	50
30	The first shell (400 mm radius) obtained with the explained procedure.	51
31	Complete design of the dome.	51
32	The Cree®XLamp MC-E LED, adopted from ^[8]	53
33	Mechanical dimensions of XLamp MC-E LED, adopted from ^[8]	53
34	Eeschema Schematic of the PCB.	54
35	FR-4 cross-sectional geometry with thermal vias, adopted from ^[9]	55
36	Fingerprints used in the designed PCB.	56
37	Final PCB in the Kicad tool Pcbnew.	57
38	Final PCB shown with 3D Viewer.	58
39	First phase of the photoengraving technique.	59
40	Development of the positive photoresist (PR)	60
41	Last phases of the photoengraving technique.	60
42	Temperature variation over time for each LED color channel.	67
43	The photographs used, one for each LED color.	70
44	Lines along which grayscale intensity levels were evaluated.	70
45	Greyscale intensity level of the pixels along the lines.	71
46	Timing diagram of SN74HC595, taken from ^[10]	74

LIST OF FIGURES (Continued)

<u>FIGURE</u>		<u>PAGE</u>
47	Front panel of the LabVIEW Virtual Instrument (VI) developed. . . .	81
48	The block diagram of the LabVIEW VI developed.	83
49	From the left, the first layer piece for one pixel of rows A, B and C. .	85
50	From the left, the second layer piece for one pixel of rows A, B and C.	86
51	From the left, the third layer piece for one pixel of rows A, B and C. .	87
52	From the left, the fourth layer piece for one pixel of rows A, B and C.	88
53	One of the PCBs with the LED mounted on it.	89
54	Final PCBs.	90
55	From the left, the aluminum walls for one pixel of rows A, B and C. .	93
56	The assembled prototype during the hot gluing of the PCBs.	93
57	Different views of the prototype assembled.	94
58	Binary images obtained.	98
59	Binaryzed version of the images of pERG protocol phases.	101
60	Original photographs of the assembled device with all LEDs on. . . .	105
61	Photographs used to analyse contrast between the assembled checks.	112
62	Partial schematics of 32 LEDs control	128
63	Surface 1 section of row A	130
64	Surface 1 section of row B	131
65	Surface 1 section of row C	132
66	Surface 1 front view of each row (A-M).	133
67	Surface 2 section of row A	134
68	Surface 2 section of row B	135
69	Surface 2 section of row C	136
70	Surface 2 front view of each row (A-M).	137

LIST OF FIGURES (Continued)

<u>FIGURE</u>		<u>PAGE</u>
71	Surface 3 section of row A	138
72	Surface 3 section of row B	139
73	Surface 3 section of row C	140
74	Surface 3 front view of each row (A-M)	141
75	Surface 4 section of row A	142
76	Surface 4 section of row B	143
77	Surface 4 section of row C	144
78	Surface 4 front view of each row (A-M)	145
79	Base wall section of row A	146
80	Base wall section of row B	147
81	Base wall section of row C	148
82	Base wall front view of each row (A-M)	149
83	Side wall section of row A	150
84	Side wall section of row B	151
85	Side wall section of row C	152
86	Side wall front view of each row (A-M)	153

Listings

A.1	Algorithm for Solidworks dome construction	121
A.2	Algorithm for the electronic control of 36 LEDs	122
A.3	Algorithm to analyse the luminance uniformity of checks	126

LIST OF ABBREVIATIONS

AR	Anti-Reflection
AWG	American Wire Gauge
CAD	Computer-Aided Design
CAE	Computer-Aided Engineering
CRT	Cathod-Ray Tubes
CSLO	Confocal Scanning Laser Ophthalmoscopy
DC	Direct Current
DLP	Digital Light Projection
ERG	Electroretinogram
GCF	Global Contrast Factor
GND	Ground
HVF	Humphrey Visual Field
IDE	Integrated Development Environment
IOP	Intraocular Pressure
IRB	Institutional Review Board
ISCEV	International Society for Clinical Electrophysiology of Vision

LIST OF ABBREVIATIONS (Continued)

ISO	International Organization of Standard
LCD	Liquid Crystal Display
LED	Light Emitting Diode
LIFA	LabVIEW Interface for Arduino
mfERG	Multifocal Electroretinogram
NI-VISA	National Instruments VISA
NPTH	Non Plated Through-hole
ONH	Optic Nerve Head
OCT	Optical Coherence Tomography
OE	Output-enable Pin
O-LED	Organic LED
OP	Oscillatory Potential
PCB	Printed Circuit Board
pERG	Pattern Electroretinogram
PhNR	Photopic Negative Response
ppERG	Peripheral Pattern Electroretinogram
PR	Photoresist
PTH	Plated Through-hole

LIST OF ABBREVIATIONS (Continued)

RCLK	Storage Register
RGB	Red, Green and Blue
RGBW	Red, Green, Blue and White
RGC	Retinal Ganglion Cell
RNFL	Retinal Nerve Fiber Layer
RPE	Retinal Pigment Epithelium
RPS	Reversals Per Second
SAP	Standard Automated Perimetry
SER	Serial
SLP	Scanning Laser Polarimetry
SMD	Surface-mount Device
SRCLK	Shift Register Clock
SRCLR	Direct Overriding Clear
VI	Virtual Instrument
VISA	Virtual Instrument Software Architecture

SUMMARY

The retina is the fundamental component of vision as it contains the photoreceptors, specialized cells which convert light stimuli into electrical signals, and which represent the first stage of the visual process. The electroretinogram (ERG) is a functional test widely used in clinical practice to help diagnose diseases of the retina and optic nerve. In fact, it measures the electrical response to a light stimulus of retinal cells and different ERG tests can be used to probe different retinal areas and cells. The tests most used are the full-field ERG, which consists of flashes of variable intensity and frequency, the multifocal electroretinogram (mfERG), which consists of illuminating in a pseudo-random way hexagonal elements on a monitor, and finally the pattern electroretinogram (pERG), which consists in high-contrast reversals of a grating pattern. While the first is performed by probing the entire retina, mfERG and pERG testing is usually limited to its central portion.

The stimulators most commonly used in visual electrophysiology are Ganzfeld stimulators, spherical devices used to perform full-field ERG, and flat monitors, which are able to display patterns to perform standard mfERG and pERG. Devices capable of performing all the tests of interest are obtained by integrating a Ganzfeld stimulator with an internal or external monitor. The stimulators can use different technologies, but light emitting diodes (LEDs) are becoming very popular since they are almost ideal light sources.

SUMMARY (Continued)

The conventional pERG testing is limited to the central part of the human visual field and this limits the sensitivity of the test. Since pERG probes retinal ganglion cells (RGCs), and since the first cells to be damaged by glaucoma are peripheral RGCs, it may be extremely helpful in early detection of this optic neuropathy. Thus, the Neural Engineering Vision Laboratory at UIC developed a three dimensional stimulus source able to perform peripheral pattern electroretinogram (ppERG). The flat monitors used in standard tests are not really suited for the detection of peripheral early disfunctions, since they do not probe the entire human visual field. Thus, the developed stimulator consisted in a hemispherical dome tilted with white LEDs in its peripheral part and its validation gave satisfactory results, obtaining waveforms similar to those obtained with conventional pERG.

The purpose of this thesis is to build a stimulus source for electroretinography that is capable of presenting an arbitrary pattern of pixels to the entire visual field, thus bringing together the functionalities of Ganzfeld stimulators, standard monitors and ppERG stimulus source. The pattern of pixels shall be configurable to present stimuli for flash ERG, pERG, and mfERG protocols to any arbitrary sector of the visual field, giving also the possibility to use different colours.

CHAPTER 1

INTRODUCTION

1.1 The human retina

The retina is a layer of tissue which covers the interior surface of the eye and which is light-sensitive. Photoreceptors, the primary retinal sensory cells, lie in the outer part of the retina against the retinal pigment epithelium (RPE), which is attached to the choroid, the vascular layer. The RPE is the layer that nourishes retinal cells and resynthesizes photosensitive molecules. Each photoreceptor cell is composed by the outer segment, which contains light-absorbing molecules, the inner segment, which contains nucleus and organelles, and a synaptic terminal.^[3] There are two types of photoreceptors: cones and rods. The former are used for daylight (photopic) vision and they are mainly concentrated in a small region near the center of human eye retina, known as macula. In its central area there is a small rod-free depression composed of densely packed cones, the fovea centralis. It provides the sharpest vision, which is characterized by maximum acuity and color sensitivity. Humans have three types of cones: cones sensitive to middle wavelengths (M-cones, green), cones sensitive to long wavelengths (L-cones, red), mainly found in the fovea centralis, and cones sensitive to short wavelengths (S-cones, blue), mainly found outside the fovea. The S-cones are only 2% of the total, but their sensitivity is greater than M- and L-cones ones. Rods are used for low-light (scotopic) vision and are more sensitive and

numerous (~ 120 million) than cones (~ 6 -7 million). The photopic and the scotopic efficacy curves are shown in Figure 1. The luminous efficacy represents the ability of a light source in producing visible light, and it is measured in lumens per watt. The wavelength at which the human eye is most sensitive is 555 nm, which is both the intersection of the two curves and the peak of the daylight vision sensitivity. The scotopic efficacy curve is shifted to shorter wavelengths, resulting in a rod light response that has a high peak in the blue-green, but is almost absent in the red.^[1]

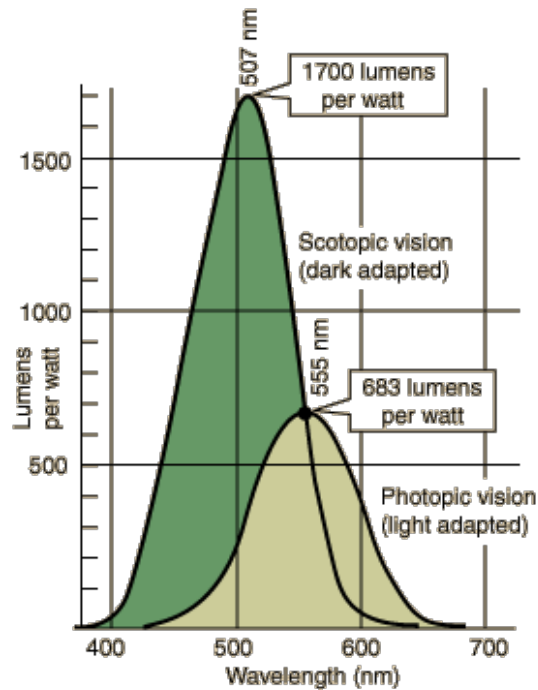


Figure 1: Photopic and scotopic efficacy curves, adopted from^[1].
The permission to reprint this copyright material is in the Appendix D.

When light is absorbed by photoreceptors visual pigments, the information is conveyed to bipolar cells, horizontal cells, amacrine cells and finally to retinal ganglion cells (RGCs). The integration of inputs from the outer retina generates in each RGC a receptive field with a centre-surround organization (contrast enhance mechanism).^[3] RGCs are retinal neurons that have to convert the electrical signal of the outer retina to the action potentials, which represent the language used in the central nervous system. They represent the last stage of visual processing in the retina, projecting directly to the thalamus through the optic nerve.^[11]

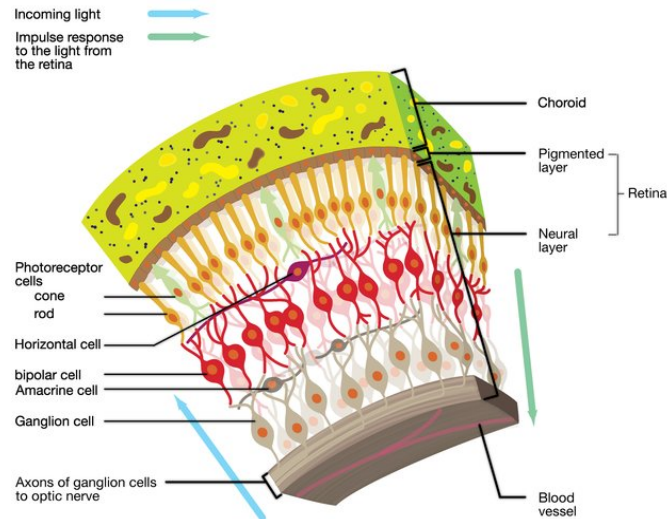


Figure 2: Cross section of the human retina, adopted from^[2].
The permission to reprint this copyright material is in the Appendix D.

1.2 The electroretinogram

The electroretinogram (ERG) is a functional test that measures the electrical activity in response to a light stimulus of both neural and non-neuronal cells in the retina, under different states of retinal adaptation to light and dark. The signal is often measured as a sum of retinal electrical activity using electrodes embedded in a corneal contact lens or fiber electrodes. ERG waveform is composed by discrete components and each of them is linked to specific retinal cells, as can be seen in Figure 3.

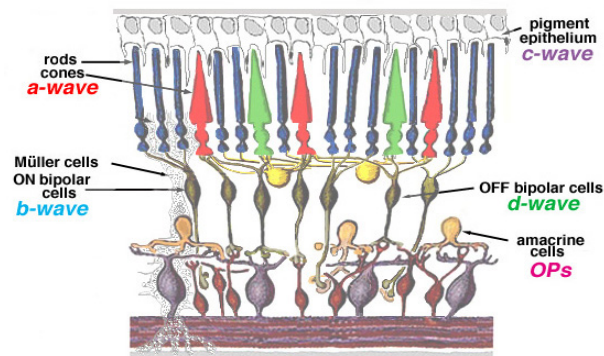


Figure 3: Retinal cells which originate components of ERG, adopted from^[3].

Typically, while the a-wave is produced by the photoreceptors, the b-wave is mainly correlated with ON bipolar cells and Müller cells (retinal glial cells), and finally the c-wave is due to the polarization of the pigment epithelium^[12]. Oscillatory potentials (OPs) are low

amplitude wavelets (frequency range 100-150 Hz) on the rising phase of the b-wave that can appear when the ERG stimulus is a bright light. Although their cell origin is not yet clear, they may be associated with ganglion cells, amacrine cells and bipolar cells negative feedback pathways. The d-wave is produced by the OFF bipolar cells and can be seen only using long duration light stimuli (>100 ms), which are able to separate in time the ON and OFF phases of the ERG. Response amplitudes (in the range of microvolts) and implicit times can be analysed in order to detect retinal disorders, and they depend on the light or dark adaptation of the eye and on the color, luminance and rate of the light stimulus. Additionally, these parameters allow the separation of rod (night vision) and cone (day vision) systems.^[3]

Under background illumination, rod system saturates and since it is not able to respond to increment or decrement of light stimuli, the light adapted ERG represents the cone system response. In this case ERG is characterized by small amplitudes and is very fast (time to peak about 30-32 ms). On the other hand, applying the same light stimulus after about 30 min of adaptation in darkness, the rod system is very sensitive and despite the dark adapted ERG represents a mixed rod-cone response, the rod system contribution is significantly greater. In this case ERG is characterized by larger amplitudes and is slower (time to peak of the b-wave about 60 ms).^[3]

Due to the different peak wavelength sensitivity for rods (about 507 nm, blue-green region) and cones (about 555 nm, green-yellow region), also different color stimuli can isolate these two systems. Rods are more sensitive than cones by a factor 10^3 , but the latter

recover faster than the former. Considering a subject in the dark adapted state, a dim blue stimulus produces a slow positive wave associated to rods. On the other hand, a bright red stimulus elicits a fast ERG component which peaks around 30 ms (cone-mediated response) and a slow ERG component which peaks around 100 ms (rod-mediated response).^[3]

Another parameter which influences the ERG response is the intensity of the light stimulus. In dark adapted conditions, a dim light stimulus can elicit a small slow b-wave. Its amplitude increases as the intensity of the light stimulus increases. In this case the kinetics becomes faster and a negative wave (a-wave) appears before the positive wave (b-wave).^[3]

Finally, also different stimulus rates can be used to separate rod and cone contributions to the ERG. In fact, a light adapted 30 Hz flicker allows the isolation of cones from rods, since rod system can only follow stimulus with a flickering rate up to 15 Hz.^[3]

The International Society for Clinical Electrophysiology of Vision (ISCEV) presented the standard series for the full-field clinical electroretinography, which include 6 protocols:

- Dark-adapted 0.01 ERG. ON bipolar cells response driven by rod system;
- Dark-adapted 3 ERG. Rod and cone systems drive this response (rod dominated), which represents both bipolar cells and photoreceptors activity;
- Dark-adapted 10 ERG. Photoreceptor response is reflected in enhanced a-waves;
- Dark-adapted oscillatory potentials. Mainly amacrine cells responses;
- Light-adapted 3 ERG. Cone system responses in which photoreceptors and cone OFF bipolar cells reflect their activity in the a-wave, while both ON and OFF cone bipolar cells give rise to the b-wave.

- Light-adapted 30 Hz flicker ERG. Response driven by the cone pathway.

The numbers in the protocols name represent the flash strength in luminance per second.^[13] The unit of measurement of luminance is candela per square meter (cd m^{-2}), and it represents the physical measure of the visible light which leaves a point on a surface in a given direction^[14]. Photopic (ph) luminance refers to photopic environments (day vision), during which cone photoreceptors are active. On the other hand, scotopic (sc) luminance refers to scotopic environments (night vision), during which rod photoreceptors are active.^[3]

The dark-adapted red flash ERG is an ISCEV extended protocol which elicits a healthy subject response with the first positive component cone-mediated (peak at 30-50 ms) and a second positive component red-mediated (peak at about 100 ms). It can be used to probe both rod and cone system function, thus contributing to make some diagnosis.^[15]

The photopic negative response (PhNR) of the light-adapted flash ERG is an additional extension to the ERG Standard. It uses a brief red flash on a blue background and after the b-wave it elicits a negative component. The short-wavelength background saturates the rod system, and the slow response reflects RGCs function. PhNR reduced amplitude can be due to optic neuropathies such as glaucoma.^[16]

Another ISCEV extended protocol is the photopic On-Off ERG. On- (a-wave negative and b-wave positive) and Off- (d-wave positive) responses are elicited using a 150-200 ms light stimulus and suppressing the rods through the background. This additional testing may be useful to identify post- phototransduction or receptor disorders. The background

and flash colour is typically white, but also blue and green have been successfully used. Even a green background together with orange stimuli have been used to suppress rods and S-cones, selectively stimulating L- and M-cones.^[17]

Other types of electroretinographies include multifocal electroretinogram (mfERG) and pattern electroretinogram (pERG).

1.2.1 The multifocal electroretinogram

MfERG was developed by Erich Sutter in the 1990s and probes retinal responses within the first 30 degrees of the human visual field. Light stimuli for the cone-driven retina (light-adapted conditions) come from hexagonal elements which constitute several arrays presented on a display monitor. The hexagonal elements are smaller in the center and larger in the periphery, and are stimulated using the m-sequence, which is a pseudo-random light and dark sequence. The latter is followed by all hexagons, but each of them starts at a different sequence position. The frame frequency range goes from 60 Hz to 75 Hz. The resulting response is characterized by a negative component (N1), a positive component (P1), and finally another negative component (N2). The typical waveform of a mfERG response is shown in Figure 4. MfERGs can be used to detect retinal defects, such as anomalies due to glaucoma that can be found earlier using this technique rather than automated perimetry.^[4,18]

1.2.2 The pattern electroretinogram

The pERG is a non-invasive functional test in which there is the recording of the eye response to high-contrast reversals of a grating pattern or a checkerboard. As the mfERG,

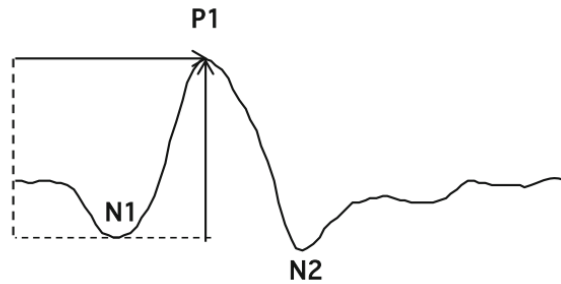


Figure 4: MfERG waveform, adopted from^[4].

The vertical arrow shows the trough-to-peak amplitude, while the horizontal arrow shows the implicit time. The permission to reprint this copyright material is in the Appendix D.

the standard test probes retinal responses within the first 30 degrees of the human visual field^[5]. The first description of pERG was done by Riggs et al. in 1964. In the recorded response the linear components of ERG (e.g. a-waves and b-waves) disappear because of the constant average luminance of the stimulus.^[19] Thus, pERG signal is composed only by the nonlinear components, which are related to the functional efficiency of RGCs. In fact, according to studies in mammals the degeneration of RGCs bodies and axons causes the elimination of pERG components.^[20,21] The typical waveform of a pERG response is shown in Figure 5. The earliest component is the negative peak N35, the second larger and positive peak is P50 and the last one is the negative N95. The transient signal is typically recorded at reversal rates lower than 6 reversals per second (reversals per second (RPS)) and is ~ 200 milliseconds long. P50 component occurs between 45-60 ms with 2-8 μV of amplitude and the N95 occurs between 90-100 ms.^[5] The component that most represents RGCs is the N95^[22] and consequently its amplitude reduction corresponds to

RGCs degeneration, allowing electrophysiological evaluations. This tool has an important role both in reasearch and clinic, in particular in the evaluation of RGCs integrity, and consequently in the detection of eye diseases such as glaucoma.^[20,21] According to clinical studies pERG is extremely sensitive to glaucomatous functional degeneration^[22], and the response of eyes affected by this disease results abnormal^[23].

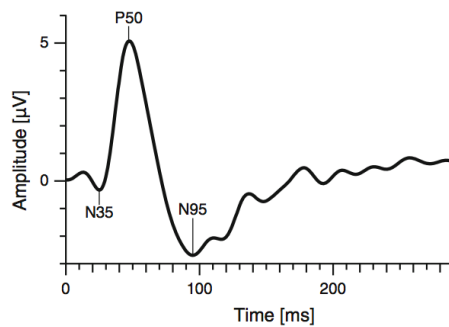


Figure 5: PERG waveform, adopted from^[5].
The permission to reprint this copyright material is in the Appendix D.

1.3 Electretinogram stimulus sources

The most common types of stimulators in visual electrophysiology were explored and then some of those commercially available for clinical use were compared.

1.3.1 Ganzfield stimulator

The Ganzfield stimulator is widely used in clinical routine for electroretinography. It consists of a bowl of around 250 mm radius and it provides an unstructured stimulus,

meaning that it does not display any pattern. The light enters the sphere through one bowl aperture while the head of the patient is positioned inside a larger port in such a way that his visual field is entirely occupied by the inner bowl surface, which is coated with a highly reflective white paint. Filters are used to modify stimuli colour and intensity. The light sources are commonly xenon flash lamps, but they can also be incandescent lamps and shutter systems or LEDs.^[24]

Xenon flash lamps consist of a glass tube that is filled with xenon gas, an anode and a cathode placed through its ends, and another electrode (the trigger one) placed outside it. Light flashes are produced by the discharge of the energy stored in a capacitor through the gas, which has become electrically conductive because of its ionization, caused by an high voltage pulse applied to the trigger electrode. The flash duration depends on the capacitors size and on the discharge circuit impedance and varies from microseconds to milliseconds, while the flash wavelength depends on the gas and on its pressure. One drawback of xenon flash systems is that due to the voltages applied across the tube (300-800 V) and the voltage needed to trigger the system (10000-20000 V), the safety risks are high and all cables must be properly insulated. Moreover, in addition to the fact that the light output is difficult to stabilize completely, xenon flash systems can easily originate electrical artifacts. A Ganzfeld stimulator in which the light source is a xenon flash tube is shown in Figure 6.^[24]

Incandescent lamps and shutter systems do not provide a light output as high as that of xenon flash tubes, but their output energy generated by low voltage power supplies can



Figure 6: The Nicolet Ganzfeld stimulator (Nicolet - Instruments of Discovery).

be relatively high. Additionally, the light output stabilization can be achieved through a feedback system both optical and electrical, which can be easily implemented. However, the drawback in clinical practice is the electromechanical shutter. In fact, contrast ratios and transmission efficiency can be decreased because of the shutter switching of the large amounts of light, which are necessary for a Ganzfeld stimulator.^[24]

1.3.2 Cathode-Ray Tubes

Cathode-Ray Tubes (CRTs) are formed by glass in the shape of a conical flask, which has a broad front surface coated internally with a phosphor. A cathode placed in the neck of the flask is heated and emits an electron beam, which is accelerated toward an anode using a

high voltage. Then the accelerated electron beam excites the phosphor, which emits light. The easiest way to drive a CRT is to use an unfocused electron beam, which excites the entire screen surface coated with the phosphor, causing its illumination. Another mode consists in using a vector display, in which the beam of electrons is focused to a small spot and an electrical field deflects the beam in both the horizontal and vertical directions.^[24]

In the TV tube this beam is deflected and moved about the phosphor surface through the modulation of the current in the electrodes, which are external coils, thus generating a magnetic field. A sequence of illuminated lines is written on the entire area of the display by moving fast the beam in the horizontal direction from left to right. After each line the beam is switched off, and a much more slowly increasing current in the vertical coils moves it downward, while it returns from right to left. Since light emission duration is equal to the excitation one, high luminance output in tubes with slow refresh rates can be obtained using phosphors highly persistent, which are not suitable for high raster rate tubes. The colour of the emitted light is determined by the phosphor used. The vertical refresh rate is considered the total scan time, and computer displays of modern stimulus systems typically have an image refresh rate of 10 ms (100 Hz). Despite the way the screen area is drawn may cause problems in displaying light stimuli, the several features available make these devices adaptable to visual electrophysiological stimulators.^[24] An example of CRT found in a oscilloscope is shown in Figure 7.



Figure 7: An example of CRT, adopted from^[6].

1.3.3 Liquid Crystal Displays

In Liquid Crystal Displays (LCDs) the light plane of polarization rotates depending on the voltage applied to a layer of liquid crystals, causing the transmission of light to increase. Two surfaces are coated with a linear polarizer and are arranged at 90 degrees to each other in order to attenuate the transmission through the device. The electrodes are arranged in a matrix in which each of them alters the voltage of a pixel, allowing the display of complex patterns. Each pixel is constituted by a red, a green and a blue transmitting region, and individual transistors incorporated into the glass substrate can drive each subpixel. A drawback of LCDs used as stimulus displays is that the color system must be adjusted depending on the type of display used. In fact, the cold cathode fluorescent lamp which normally illuminates the LCD panel has an uneven spectral output, which then

is passed through red, green and blue (RGB) filters, resulting in an irregular composition of wavelengths in the resultant output. Another concern is that the rate of change of the stimulus is limited by the refresh rate, which is significantly slower than the one of high-resolution CRTs (100 Hz). Moreover, there can be luminance transients on the reversal of a checkerboard display due to the lack of constancy in pixel switching times. Together with the fact that the signal is not passed directly to the screen as in CRT displays, but is stored in memory until the next screen refresh, the two latter drawbacks make the prediction of when the stimulus generator transition will appear on the screen very uncertain. Finally, contrast and chromatic distortions are experienced as the subject moves from the optical axis of the screen. However, recent technological improvements (e.g. refresh rates of 4 ms) may make LCDs more suitable to be used as stimulators.^[24]

Data projectors commonly use LCD shutter devices, can provide high luminance, large stimulus area and can avoid color distortions using halogen illumination. However, concerns remain about the refresh rates and response times. The projectors can be also based on three CRTs, one each for red, green and blue, and Digital Light Projection (DLP) systems (Texas Instruments). Temporal and chromatic performances are similar to the ones of CRT displays, but costs and sizes are greater. DLP projectors contain several memory cells on each of which a micro-mirror is mounted. The state switching of one of the cells triggers a change in the corresponding mirror angle, resulting in a deviation of the illumination beam through the projection lens. The duty time each pixel is on modulates the intensity, and the modulation of a rotating filter wheel provides RGB separation.^[24]

1.3.4 Plasma Displays Panels

Plasma displays panels are based on RGB phosphor triplets and can provide high resolution and large stimulus area. Pixels cells containing xenon or neon gas form the display, and vertical and horizontal electrodes are superimposed on them. The UV light emitted by the fluorescent gas when the electrodes are excited stimulates the phosphors, thus producing visible light. The electrodes arrays are controlled by a circuitry similar to the LCD panels one, and there may be time problems even though the refresh rate is better.^[24]

1.3.5 Light Emitting Diodes

Light Emitting Diodes (LEDs) are epitaxial semiconductor junction diodes. They are composed by two doped semiconductive layers, the first which contains free electrons in excess, the second which contains positive charges (holes) in excess. When the diode is forward biased, positive charges move from the positive material to the negative one, and electrons move in the opposite direction. Thus, the energy gap between the two surfaces is excited by the current, and when an electron-hole pair recombines a certain amount of energy is emitted in the form of a photon, which has a characteristic wavelength depending on the energy band gap. They can produce a light emitted over a narrow bandwidth, purer and more monochromatic than the one achievable through complex and expensive filters. White LEDs emit blue light through which a phosphor is excited. A short wavelength emitting junction is encapsulated in the phosphor itself, which in turn emits white light. Differently from white light spectrum obtained through red, green and blue light narrow spectral lines, the spectral output of a white LED is continuous and broad, consti-

tuting an advantage for ERG use. Wavelengths from ultraviolet to infrared are available, achieving even 10 nm steps along the visible spectrum. In order to control the intensity linearly, pulse width modulation can be used. The light output range of linearity is limited and can be improved by controlling the LEDs through a feedback loop of a current drive, but the depth of modulation cannot achieve the 100 %. Another drawback is that even at the maximum continuous forward current quoted by most manufactures, the light output for a fixed current progressively falls because of heating effects within the junction. While in orange and red LEDs this effect is more evident, it is less noticeable in shorter wavelengths. However, LEDs are almost ideal light sources due to small sizes, low costs, low voltages and currents requirements, and flexibility in providing continuous light output, very short flashes, or complex waveforms, using different intensities. In ERG high luminance is required and LEDs meet this requirement. In order to obtain an effective stimulus, usually several LEDs need to be connected in series, in parallel, or both, and this can be easily reached by carefully designing the circuit. LEDs have been used in several psychophysical and electrophysiological application, such as measuring spectral sensitivity, analyzing interactions between rods and cones, and in small checkerboard displays with high contrast. The luminance given by the current LEDs generation is high enough to illuminate full-size Ganzfeld spheres, with single coloured or broadband white light. Organic LEDs (O-LEDs) are based on polymers and can be printed on both plastic and glass substrates. The RGB color displays that can be produced are characterized by low cost, high luminance and high resolution, and they do not present the geometric limits typical of LCD panels.^[24]

1.3.6 Stimulus sources available on the market

Some of the devices used in clinical visual electrophysiology and available on the market were compared. Their main ERG specifications are shown in the Table I, and it can be noticed that almost all devices use LEDs as stimulus sources. Ganzfeld stimulators are usually used to perform Standard full-field ERG and its extensions (e.g. photopic On-Off ERG), while pERG and mfERG are usually performed on flat screens LCD or LED/O-LED based. UTAS SunBurstTM[25], EP-1000^[26] and MonPackONE^[27] can perform all the previously mentioned protocols because each of them is composed by both a Ganzfeld stimulator (for ERG full-field protocol and its extensions) and a flat monitor (for pERG and mfERG). In fact, there are no spherical Ganzfeld stimulators able to perform pERG and mfERG tests, which in fact are run on an external monitor (UTAS SunBurstTM, mfERG in EP-1000) or on a monitor placed inside the Ganzfeld stimulator itself (pERG in EP-1000, MonPackONE). In particular, in pERG testing LED based monitors are preferred to standard LCD monitors because the latter produce a flash of transient light every time the pattern changes phase^[24], resulting in an inconsistent luminance and risking to not stimulate only RGCs.

1.4 The peripheral pERG and the three dimensional stimulus source

PERG testing presents several advantages, such as objectivity and functional assessment, but conventional pERG is done targeting just the central part of the human visual field, limiting the sensitivity of the test.^[7] Some studies suggested that the RGCs of the peripheral retina are the first to be damaged by glaucoma, an optic neuropathy which can

TABLE I: COMPARISON BETWEEN VISUAL ELECTROPHYSIOLOGY STIMULUS SOURCES ON THE MARKET.

Device	UTAS SunBurst™ [25]	RETeval® [28]	Desktop Envoy™ [29]	ColorDome [30]	LCD Monitor [31]	EP-1000 [26]	MonPackONE [27]
Dimensions [mm]	/	70 x 100 x 230	98 x 70 x 45	260 x 360 x 310	630 x 370 x 24	<ul style="list-style-type: none"> Ganzfeld: 390 x 540 x 500 Multifocal monitor: 376.32 x 301.056 	/
Stimulus source	<ul style="list-style-type: none"> Ganzfeld stimulator LED 	LED	O-LED	<ul style="list-style-type: none"> Ganzfeld stimulator LED 	LCD	<ul style="list-style-type: none"> LED Pattern inside the Ganzfeld: monitor Multifocal monitor: LCD 	LED backlight monitor
Main ERG protocols	<ul style="list-style-type: none"> ISCEV Standard full-field ERG ISCEV Standard PhNR ERG ISCEV photopic On-Off ERG ISCEV Standard pERG ISCEV Standard mfERG 	<ul style="list-style-type: none"> ISCEV Standard full-field ERG ISCEV Standard PhNR ERG ISCEV photopic On-Off ERG 	ISCEV Standard pERG	<ul style="list-style-type: none"> ISCEV Standard full-field ERG ISCEV Standard PhNR ERG ISCEV Standard dark adapted red flash ERG ISCEV photopic On-Off ERG 	<ul style="list-style-type: none"> ISCEV Standard pERG ISCEV Standard mfERG 	<ul style="list-style-type: none"> ISCEV Standard full-field ERG ISCEV Standard pERG ISCEV Standard mfERG 	<ul style="list-style-type: none"> ISCEV Standard full-field ERG ISCEV Standard pERG ISCEV Standard mfERG
Stimulus field [degrees]	Full-field for flash ERG	Full-field	Compliant with standards (30)	Full-field	90	Full-field for flash ERG	Full-field for flash ERG
Stimulus Colour	White and other not specified colours	<ul style="list-style-type: none"> Red Green Blue White 	White	Any colour	Any colour	<ul style="list-style-type: none"> LED: red, green, blue, white 	<ul style="list-style-type: none"> Red, green, blue and their combinations
Luminance [cd m^{-2}]	/	/	> 500	/	1200	/	/
Flash strength [cd s m^{-2}]	<ul style="list-style-type: none"> Xenon flash: 2.5 - 2500 LED flash: 2.5×10^{-5} - 31 	<ul style="list-style-type: none"> Red LED flash: 0.0001-15 Green LED flash: 0.001-17 Blue LED flash: 0.0001-5 White LED flash: 0.002-30 	/	<ul style="list-style-type: none"> Max white xenon flash: >5000 Max white LED flash: >60 Overall flash: 10^{-9}-5000 	/	LED flash: 0.1-30	Up to 10

lead to blindness^[32,33]. Thus, the first prototype for peripheral pERG testing and RGCs monitoring was developed, and it is described in this section.

1.4.1 Glaucoma

Glaucoma is the leading disease of irreversible blindness. According to global estimations 60.5 million people were affected by this disease in 2010, and the number will increase to 111.8 million in 2040.^[34] Glaucoma is a group of optic neuropathies characterized by both structural damage to the optic nerve head and visual dysfunctions^[35]. The anterior chamber is a space between the innermost cornea surface and the iris, filled with aqueous humor. Where the cornea and the iris meet there is the open angle, at which the fluid leaves the chamber. In open-angle glaucoma, which is the most common type, the aqueous humor flows too slowly and therefore builds up, resulting in an increased intraocular pressure (IOP) which may damage RGCs axons within the optic nerve head (ONH), with consequent vision loss.^[11,36] RGCs dendrites are characterized by a high concentration of mitochondria, and their axons have to cross the retinal surface. Indeed, the process of dendritic summation and the generation of action potentials are extremely heavy in metabolic and energetic terms. Since glaucoma also causes the impairment of RGCs and their dendrites, the efficiency of the integration can be compromised, resulting in a reduced RGCs response to light.^[11]

1.4.2 Glaucoma detection

The vision lost from the disease cannot be recovered, and last stages of glaucoma bring to the blindness of the subject. Consequently, the early detection of this pathology is funda-

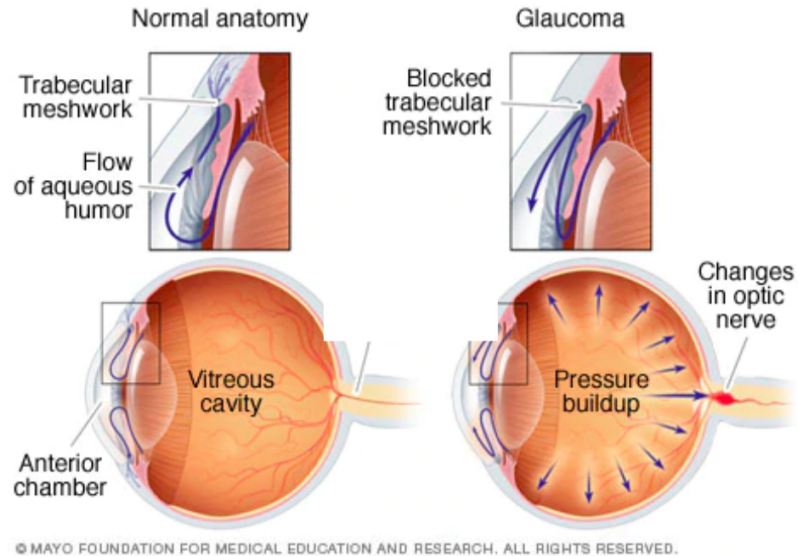


Figure 8: Normal anatomy vs glaucoma.

Used with permission of Mayo Foundation for Medical Education and Research, all rights reserved (see Appendix D).

mental in clinical practice and many clinical electrophysiological tests are available. These ophthalmic examinations mainly identify elevated IOP, ganglion cells death, morphological changes of the retinal nerve fiber layer (RNFL) and ONH. The window of time between the first functional damages and RGCs death can be exploited to detect and to contain the disease before permanent vision loss^[11].

1.4.3 Traditional tests

The diagnosis of glaucoma is done using both functional and structural tests. The first ones include standard automated perimetry (SAP) tests, the clinical gold standard^[37] for the assessment of visual function, such as Humphrey visual field (HVF) analyzer. In this

non-invasive tool, white light stimuli with different intensities are displayed at specific points within a defined field, and when the patient detects the light he has to press a hand-held button. HFV analyzer allows the evaluation of retinal sensitivity [dB], which represents the ability of the retina to detect light stimuli within the visual field.^[38] The changes in the retinal structure are identified through structural tests, such as scanning laser polarimetry (SLP), confocal scanning laser ophthalmoscopy (CSLO) and the optical coherence tomography (OCT). SLP determines tissue thickness, CSLO gives topographical information about the posterior eye, and OCT analyzes differences in tissue depth reflectivity. All three imaging technologies are used to quantify structures in the ONH region and to give information about other structural losses that characterize the development of glaucoma.^[37]

HVF and OCT have been used in glaucoma typical detection instead of pERG because of its limited sensitivity and specificity. However, tests such as HVF and OCT are not really suited for early detection of the disease because they give a response only after 20-50 % of the retinal ganglion cells are already dead.^[39] As already pointed out, detecting glaucoma before the cells have undergone apoptosis is fundamental to avoid permanent vision loss. Functional changes occur before structural ones, and this has been demonstrated by the time lag of approximately 8 years between functional changes and RNFL thinning in glaucoma suspects^[40].

1.4.4 The first prototype: the ppERG system

Conventional pERG testing is done targeting just the central part of the visual field (20-30°, full angle), and this may limit the sensitivity of the test. As shown in Figure 9, the angle at which glaucoma is known to start corresponds to the mid-far periphery of the visual field (30°, half angle). In fact, some studies suggest that the first glaucomatous damages of RGCs appear in the peripheral area of the retina^[32,33]. In standard tests flat monitors are used, but they are not really suited for the detection of peripheral early dysfunctions. The several advantages of pERG testing (e.g. objectivity and functional assessment) and the lack of a proper tool for peripheral pattern electroretinogram (ppERG) testing have given the motivation for the development of a three dimensional stimulus source for RGCs function detection and monitoring, in particular in glaucoma candidates. The target region of this new tool is shown in Figure 10, which corresponds to the mid-far periphery of the visual field.^[7]

The first prototype to perform ppERG test was developed by the senior design group from the Neural Engineering Vision Laboratory at the University of Illinois at Chicago. The targeted region of the ppERG system begun at 20 degrees up to the limits of the visual field, and focused on the recording of the pERG from the peripheral region of the retina. The three dimensional stimulus source was an hemispherical dome of 30 cm radius mounted inside a wooden housing, as shown in Figure 11. 120 LEDs were arranged in four circumferential rows and 30 radial columns. The LEDs of the individual columns were

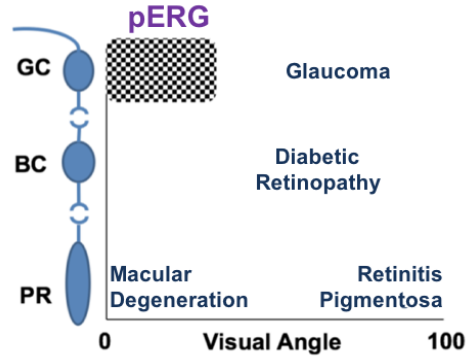


Figure 9: Targeting regions of pERG.

Most common eye blinding diseases related to retinal depth (y-axis) and eccentricity in terms of visual angle (x-axis), with pERG targeting region highlighted. Adopted from^[7], the permission to reprint this copyright material is in the Appendix D.

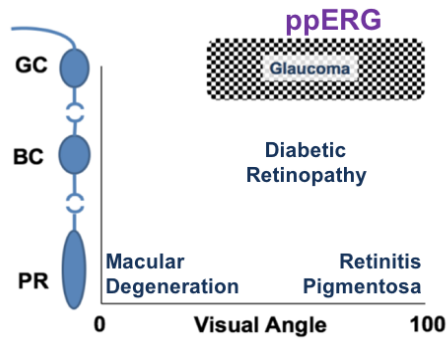


Figure 10: Targeting regions of ppERG.

Most common eye blinding diseases related to retinal depth (y-axis) and eccentricity in terms of visual angle (x-axis), with ppERG targeting region highlighted. Adopted from^[7], the permission to reprint this copyright material is in the Appendix D.

connected in series, while alternate LEDs in each row were connected in parallel, resulting in pERG phase A and phase B.^[7]

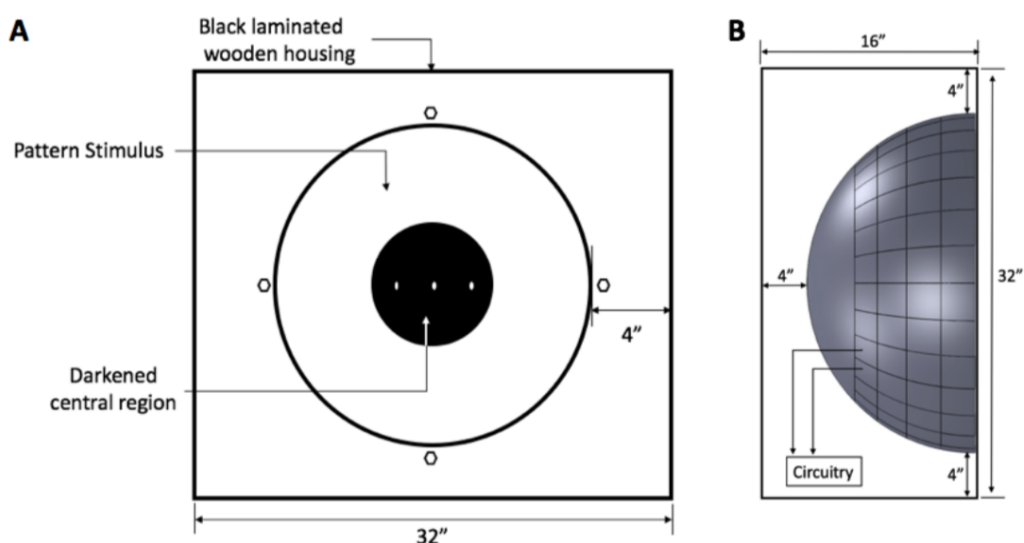


Figure 11: Peripheral pERG system.
 (A) Front view of the ppERG system mounted in the wooden box. (B) Side view of the ppERG system. All units are in inches. Adopted from^[7], the permission to reprint this copyright material is in the Appendix D.

Going from the innermost part to the outermost part of the dome, one LED unit was composed by an acrylic surface with metal fins glued to it, thin film diffusers and the BXRA-C0402 (Bridgelux, Fremont, CA) cool white LED, hold by a plastic mount custom designed. One example of LED unit is shown in Figure 12. Each fixed check size varied

with the viewing distance and the pattern went from 40 to 170 degrees of the visual field full angle, leaving the central 40 degrees blank. The central point that the patient had to fix during the test was a ping pong ball marked with a cross. The ON and OFF pattern typical of pERG was generated using custom designed software powered by a microcontroller (Arduino AtMega 2560). The used luminance of 80 ph cd m^{-2} respected ISCEV recommended standards^[5], with a reversal rate of 4.26 Hz. In Figure 14 the recorded response is shown in blue and it is compared to the response of a standard pERG test. Despite the two responses were similar, there were several malfunctions in hardware and software of the prototype, such as poor LED solder connections, not uniform phase luminance and inaccurate real time averaging.^[7]

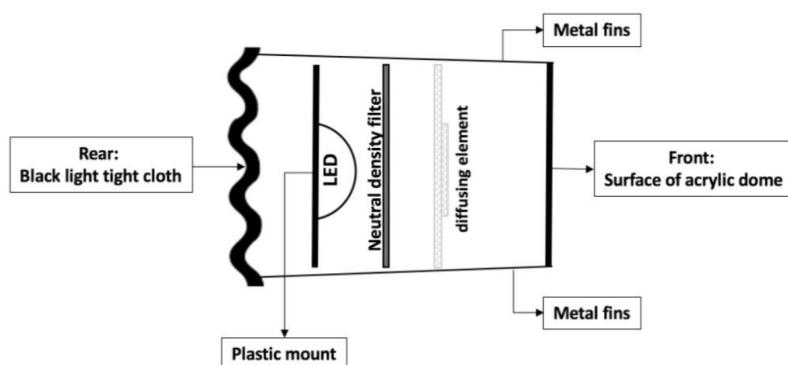


Figure 12: Cross-sectional view of the LED unit. Metals fins define the edge of the check. The black light tight cloth and the neutral density filters are additions done in the second prototype. Adopted from^[7], the permission to reprint this copyright material is in the Appendix D.

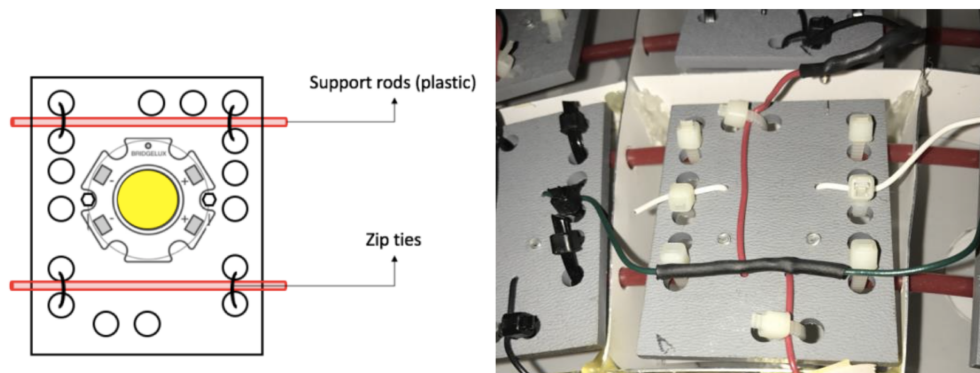


Figure 13: LED units disposition.

(Left) The LED was screwed onto the center of the custom designed plastic mount. (Right) LED unit mounted. Zip-ties hold in place the connecting wires. The green (and white) wires connect the positive terminal of LEDs in parallel (alternate row LEDs). The red wires connect the negative terminals of LEDs in series (in columns). Adopted from^[7], the permission to reprint this copyright material is in the Appendix D.

1.4.5 The improved peripheral pattern electroretinogram (ppERG) prototype

In 2018 the already existent prototype was improved in terms of robustness, luminance, pattern control and hardware/software functioning. After the replacement of bad LEDs, electrical connections were re-soldered and insulated, making LEDs robustly connected. Rows and column were labeled in order to easily identify the origin of possible malfunctions. The innermost row was considered to be number 1 (see figure 16), and the columns were labeled clockwise from the top. In each row a set of solid state switches (DG202BDJ-E3, Vishay Intertechnology, Malvern, PA), operational amplifiers (LM741, Texas Instruments, Dallas, TX) and transistors (MJH6284GOS-ND, ON Semiconductors, Phoenix, AZ) were inserted to control either the A or the B phase, while a

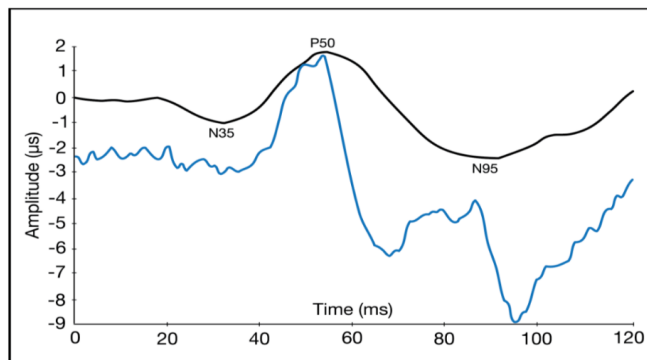


Figure 14: Example of response recorded with the first ppERG system. The response was recorded at a mean ON-luminance of 80 ph cd m⁻², viewing distance of 66 cm and a 4.26 Hz reversal rate. Blue trace: ppERG response. Black trace: conventional pERG response. Adopted from^[7], the permission to reprint this copyright material is in the Appendix D.

single switch was inserted in each column. This modularity made the identification and management of malfunctions very easy. In the Figure 17 the schematic flow of connections is shown. The reversing pattern phase can be depicted from the "A" and "B" markings on the square wave, which is provided by a function generator (Sony, Textronix, AFG310 Beaverton, OR). The frequency was set at 2.3 Hz, giving 4.6 RPS that is compliant with the ISCEV-recommended reversal rate^[5]. Inverting amplifiers were used to the square wave that controlled half the checks, allowing the creation of the ON-OFF pattern. Arduino through LabVIEW (National Instruments, Austin TX) controlled solid state switches and so the ON or OFF state of the LEDs. A direct current (DC) power supply (BK precision 9151, B&K Precision Corporation, Yorba Linda, CA) fixed at +5V voltage and high current transistors (two for row, one for phase) were used to provide the current to the LEDs. Solid

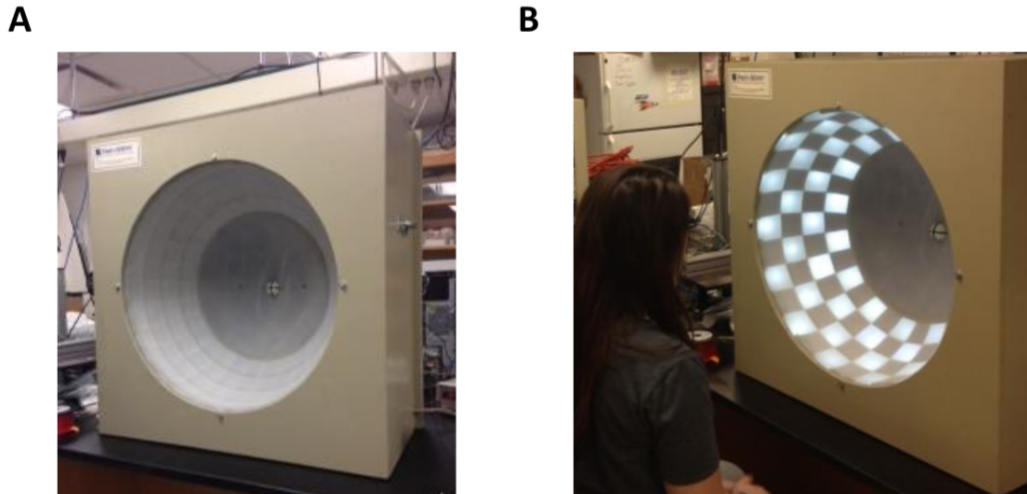


Figure 15: First prototype of the ppERG stimulus source. Adopted from^[7], the permission to reprint this copyright material is in the Appendix D.

state relays (VO14642AT-ND, Vishay Intertechnology, Malvern, PA) controlled by Arduino through LabVIEW gated the path to the negative-voltage point (set by a second DC power supply) for each column.^[7]

The achievement of high contrast between the ON and OFF checks was extremely important because of the linear relationship between pERG amplitude and contrast. Thus, the central 40 degrees (conventional pERG monitor, 14"x11") were painted matte black and a black light-tight cloth was wrapped around the acrylic hemisphere, resulting in a contrast between neighbouring units increased to 96%.^[7]

The standardization of the recording procedure is fundamental to decrease inter-subject variability, which is typically high in pERG. In order to avoid variable target fixations, a

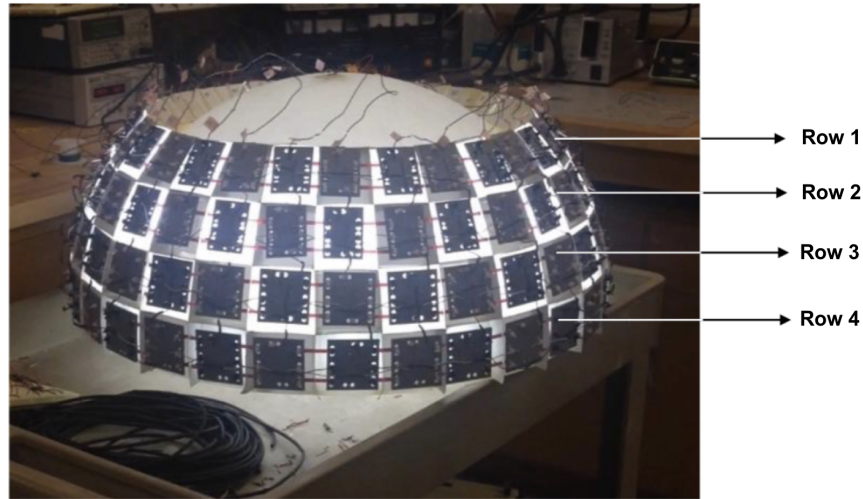


Figure 16: Distal view of the improved pattern stimulus source. Labeling of rows is shown. Adopted from^[7], the permission to reprint this copyright material is in the Appendix D.

cylindrical steel post was mounted onto the table. This ensured 30 cm of distance between the chin rest and the center of the hemisphere, and the chin rest height was fixed in order to have the recording eye of the subject tangential to the plane of the dome apex.^[7]

The chosen LEDs allowed to provide luminances $\sim 15X$ higher than the ones given by conventional monitors, resulting in higher signal amplitude and signal to noise ratio. The ISCEV-recommended minimum for luminance is 80 ph cd m^{-2} ^[5] (photopic candela per meter squared), and the mean ON-luminances used to measure the ppERG signal were 90 ph cd m^{-2} , 160 ph cd m^{-2} , 840 ph cd m^{-2} and $1670 \text{ ph cd m}^{-2}$. For a transient pERG response the ISCEV recommended reversal rate is 4 RPS^[5], and the reversal rates chosen to investigate ppERG signals were 2.3 RPS, 4.6 RPS and 9.2 RPS.^[7]

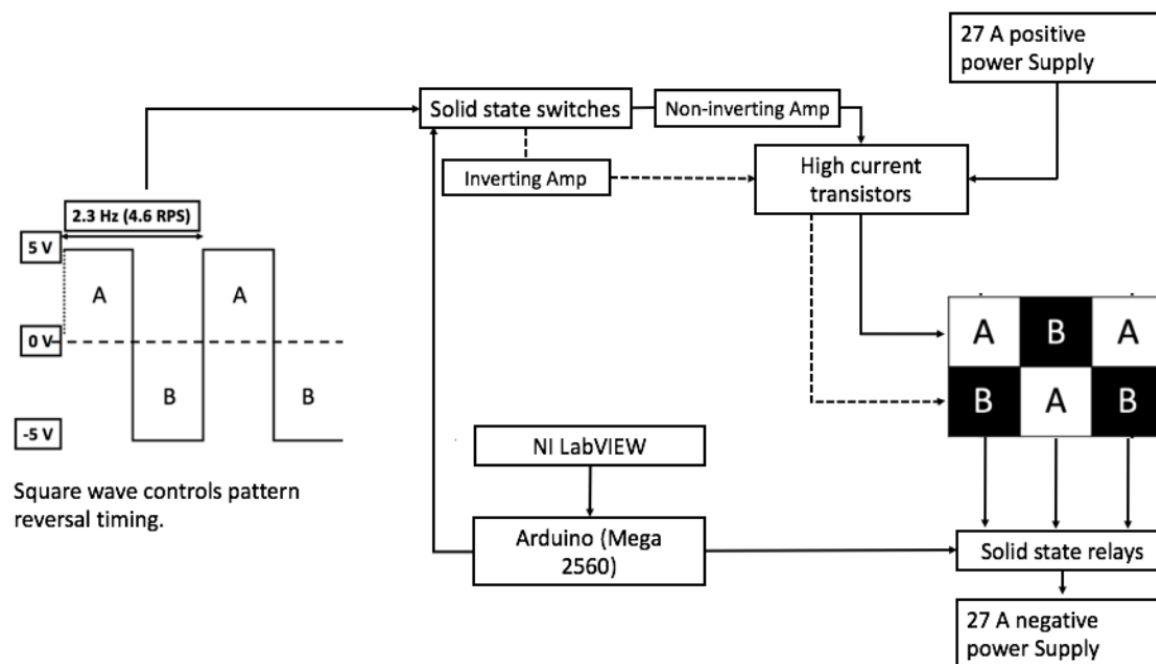


Figure 17: Flow of circuit connections in the second prototype, adopted from^[7].
The permission to reprint this copyright material is in the Appendix D.

In order to avoid luminance artifacts in the pERG response, the average ON-luminance should be the same in both phases, and their surface area should be equal. In order to achieve luminance uniformity, the gain of the operational amplifiers was adjusted in each phase and row and double diffusing layers were placed between each LED and the hemisphere surface. The IL 1800 photometer was used to measure mean ON-luminance between phases A and B and luminance across all checks. The difference in mean ON-luminance between the two phases was nearly constant (3.6%), while the standard deviation of luminance across checks was 32%. Luminance versus time measurements were

made between adjacent checks in order to confirm the absence of all-ON or all-OFF state during the transition between phases.^[7]

The electrodes chosen to record ppERG responses were DTL fiber electrodes (LKC Technologies, Gaithersburg, MD) while adhesive skin electrodes (Ultratrace, #1690-001, Medtronic, Minneapolis, MN) were used for reference (ipsilateral temple) and ground (neck). After 10000X signals amplification, LabVIEW data acquisition hardware (USB 6009, National Instruments, Austin, TX) was used for data acquisition (1-1000 Hz pass-band, 5 kHz sampling rate). In order to reduce the uncertainty of the response quality during the test, online data processing was added. The number of clean pattern reversals averaged real time was at least 300, while responses with blink artefacts were excluded using a $\pm 0.4 V$ ($\pm 40 \mu V$) threshold post amplification (ISCEV recommends $\pm 100 \mu V$ as maximum range for the pERG recording). Consequently the time length of the test depended on subject compliance, with a minimum of $\sim 1.5 - 2.0$ minutes. This data processing module increased the quality of the stimulus, reduced the ppERG test duration, and avoided the subjective operator decision on the amount of data to collect for offline averaging.^[7]

In order to validate the device and to demonstrate that the new three dimensional stimulus source elicited a response that was consistent with that obtained with conventional flat monitors, similar stimulus settings were used for both sources. Mean ON-luminance (90 ph cd m^{-2}), check size (5°), reversal rate ($\sim 4 \text{ RPS}$) and signal filtering of the two systems were matched. The average pERG and ppERG waveforms obtained from six normally-sighted subjects are shown in Figure 18, and they look very similar. Inter-subject and test-

retest repeatabilities were also tested, giving encouraging results. In Figure 19 ppERG response waveforms from 11 normally-sighted subjects (11 right eyes) are shown in black (mean ON-luminance of $1670 \text{ ph cd m}^{-2}$, reversal rate of 4.6 RPS, viewing distance of 30 cm), while the red trace represents the average signal. The shape of the waveforms looks similar and the inter-subject repeatability is good. In order to examine the test-retest repeatability, ppERG retests have been done 5, 19, and 25 months after the first test. The resulting response waveforms from one subject are shown in Figure 20, and they are almost identical.^[7]

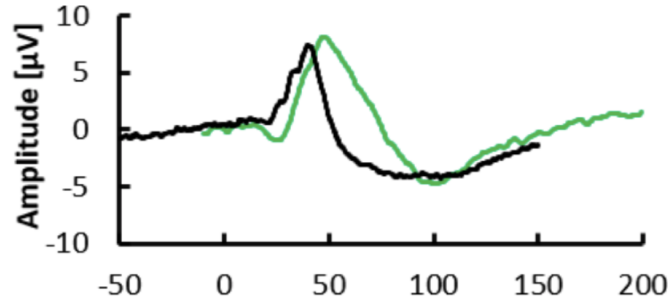


Figure 18: Improved ppERG system response matched with conventional pERG. Black trace: ppERG response waveform. Green trace: conventional pERG response waveform. Luminance (90 ph cd m^{-2}), reversal rate ($\sim 4 \text{ RPS}$) and passband (1-100 Hz) were matched. Adopted from^[7], the permission to reprint this copyright material is in the Appendix D.

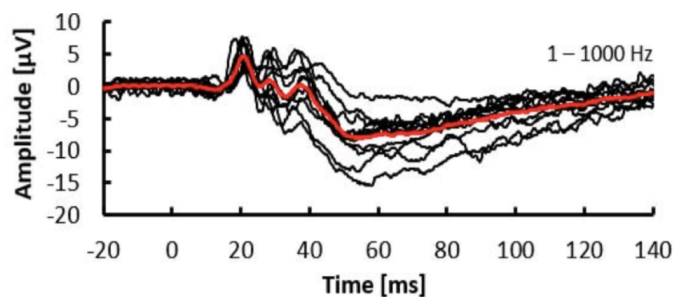


Figure 19: Improved ppERG system response.

Black traces: ppERG response waveforms from 11 right eyes ($1670 \text{ ph cd m}^{-2}$ mean ON-luminance, 4.6 RPS, 30 cm viewing distance). Red trace: black waveforms average. Adopted from^[7], the permission to reprint this copyright material is in the the Appendix D.

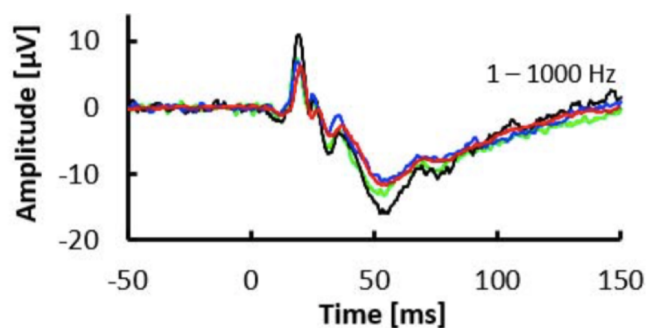


Figure 20: Test-retest repeatability of ppERG system.

Black trace: ppERG response waveform of the first test. Blue, green and red traces: ppERG response waveforms recorded 5, 19, and 25 months, respectively, after the first test ($1670 \text{ ph cd m}^{-2}$ mean ON-luminance, 30 cm viewing distance). Adopted from^[7], the permission to reprint this copyright material is in the Appendix D.

CHAPTER 2

SPECIFIC AIM

The aim of this project is the design, fabrication and testing of a highly-configurable full-field stimulus source for electroretinography, such that a physiologically and psychophysically reasonable arrangement of pixels is presented to the entire visual field of a test subject, thus bringing together the functionalities of Ganzfeld stimulators, standard monitors and ppERG stimulus source. The previous device developed by the Neural Engineering Vision Laboratory at University of Illinois at Chicago gave the possibility to perform only ppERG protocol and its central part was not tilted with LEDs, limiting the probing to the peripheral regions of the retina. The pattern of pixels shall be configurable to present stimuli for flash ERG, pERG, and mfERG protocols to any arbitrary sector of the visual field, giving also the possibility to use different colours. Representing almost ideal light sources^[24], red, green, blue and white (RGBW) LEDs were used to give the possibility to use stimuli of different wavelengths. In order to overcome the previous prototype concern about the standard deviation across checks of 32%^[7], their structure was redesigned to obtain more uniform luminance and minimal light reflection. The design of the new stimulus source focused on mechanical (dimensions and material selection) and optical components. Moreover, the square wave which controlled the ON-OFF pattern and the circuits organization adopted in the previous prototype limited the flexibility of the pattern style. Consequently, programming and control of the device was also explored, in order to

propose an electronic design flexible enough to allow the implementation of such different protocols. Figure 21 shows the renderings of how the full-field stimulus source should look during different protocol examples.

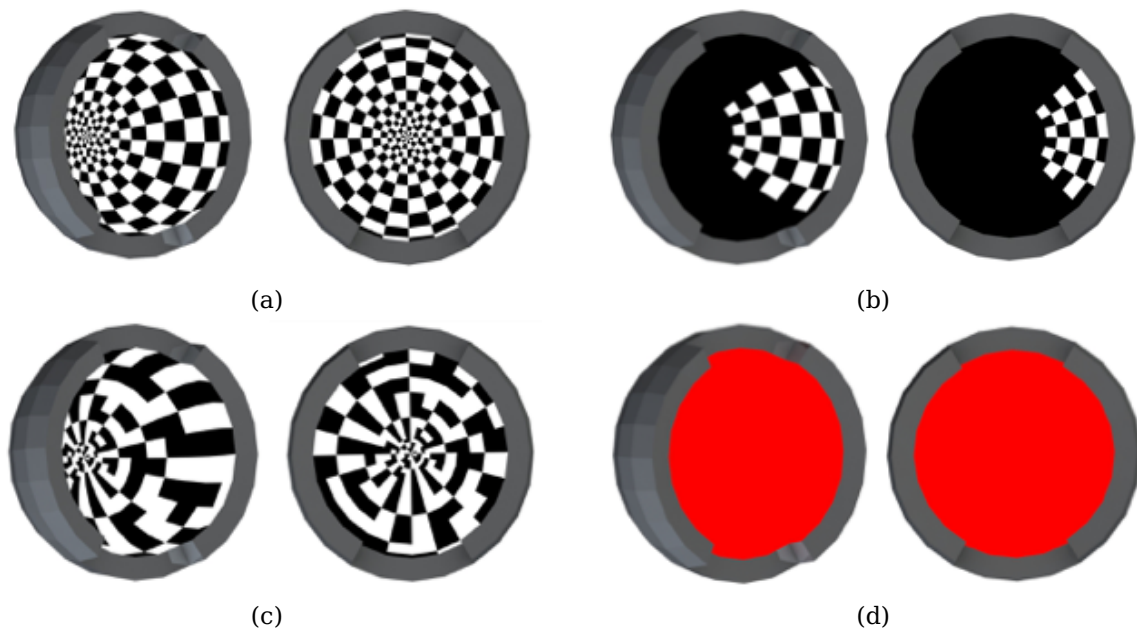


Figure 21: Renders of possible ERG patterns.

(a) Full-field pERG (b) Sectoral pERG (c) Full-field MfERG(d) Dark-adapted red full-field flash ERG.

CHAPTER 3

SPECIFIC AIM 1

The first specific aim is the design of the full-field stimulus source in terms of mechanical, optical and electronic components.

3.1 Methods

The geometry of the source was chosen taking into account both the physiology of the eye and the optical properties of the device components. In order to make possible the implementation of different ERG protocols with the same stimulus source, ISCEV standards requirements for ERG were considered. The mechanical design was developed in Solidworks, a solid modeling computer-aided design (CAD) and computer-aided engineering (CAE) software. The device geometry consists of an hemisphere composed by four concentric layers, respectively with a radius of 40, 43, 46 and 49 cm. The first layer (or shell) is made of glass, while the second and the third ones are made of two different diffusive materials. The fourth layer is made of Delrin and had LEDs mounted on PCBs, which were designed with Kicad, a software suited for the development of PCB designs. The electronic layout for the LEDs control consists of a microcontroller, shift registers, solid-state relays and resistances. The layers are composed of a set of flat faces, of which those of the same size and shape constitute a "row". In particular, each layer is composed by 12 flat faces in the rows A, B and C, 24 flat faces in the rows from D to L, and 16 flat faces in the row M.

Such formal subdivision is shown in Figure 22. The set of four faces (one for each layer) concentric to each other plus the side walls form three chambers and constitute a pixel (or check). in Figure 23 a representative lateral section of it is shown. Thus, in each row from A to C there were 12 pixels, in each row from D to L there were 24 pixels and in row M there were 16 pixels. In this chapter, the design choices made are motivated and described in detail.

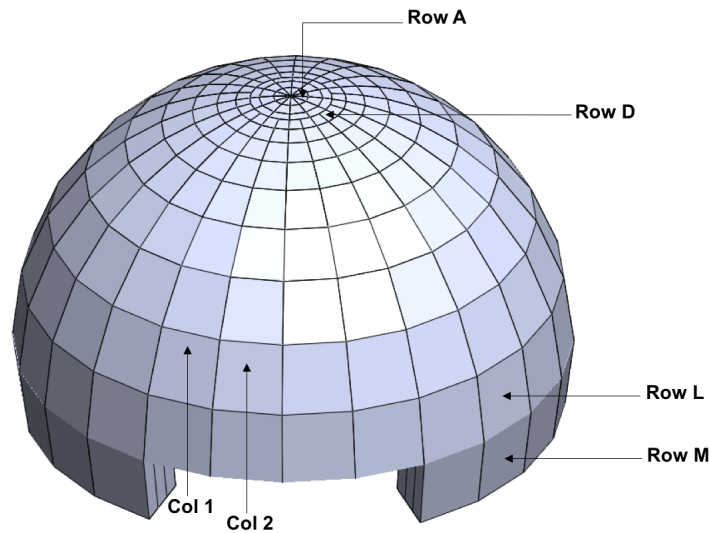


Figure 22: Organization of rows and columns of the dome.
 Rows A, B, and C are composed by 12 pixels, rows from D to L are composed by 24 pixels
 and row M is composed by 16 pixels.

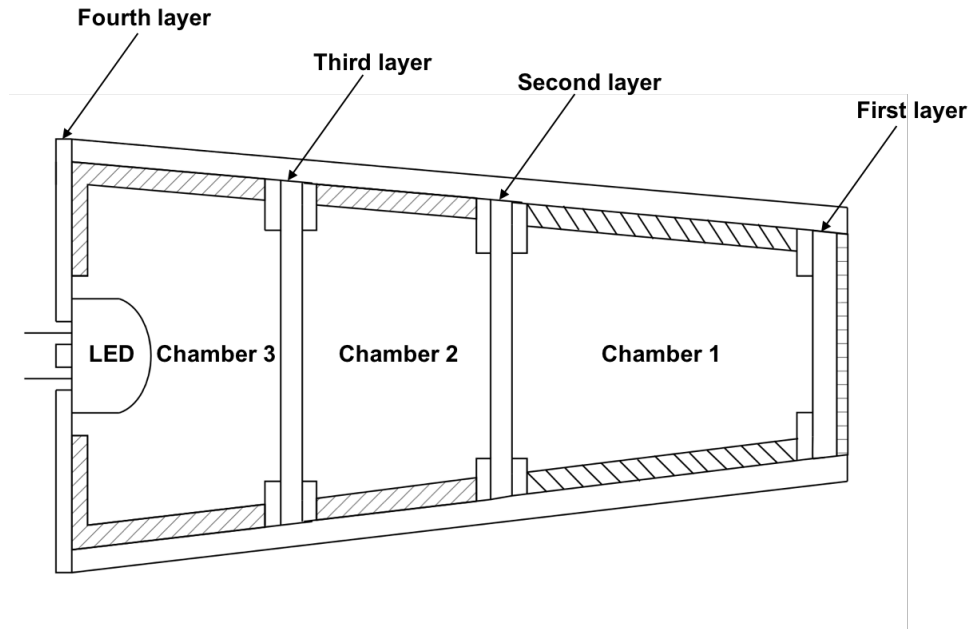


Figure 23: Representative lateral section of one redesigned pixel.

3.2 Design requirements

3.2.1 Visual field

In full-field clinical ERG the entire visual field needs to be stimulated by light, usually using a dome or sphere^[13]. In clinical mfERG, the stimulus field radius from the fixation point has to be $20^\circ - 25^\circ$ ^[4]. In clinical pERG the source field needs to be $15^\circ (\pm 3^\circ)$ (half angle) and its aspect ratio should be between 4:3 and 1:1^[5]. Classically, the visual field of a normal human eye is approximately quoted 60° superiorly from the horizontal meridian, 75° inferiorly from the horizontal meridian, 60° nasally from the vertical meridian and 90° temporally from the vertical meridian. In Figure 24 the red curve shows the visual field

subtended by a healthy right eye, while the numbers represent the half angles considering the center of the grid as fixation point. However, starting from the 19th century some studies report a temporal visual field extension considerably larger than the classical quotation of 90°, from 100° to approximately 107°.^[41,42]

The visual field subtended by the three dimensional stimulus source needs to extend enough to cover the limits of the entire human visual field, allowing the access to the peripheral glaucomatous degeneration using ppERG test, which appears particularly suited to detect the peripheral onset of this disease.

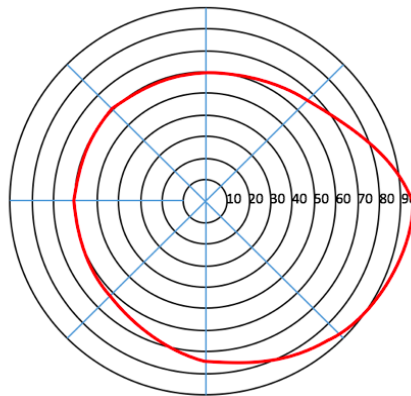


Figure 24: Red curve: human visual field limits for a healthy right eye. The numbers represent the visual half angles considering the center of the grid as fixation point. Adopted from^[7], the permission to reprint this copyright material is in the Appendix D.

3.2.2 Check shape, size and number

Conventional stimulus for pERG is a black and white reversing grating pattern. In IS-CEV standard for pERG, the individual checks shape has to be square ($\pm 5\%$ error) and their width needs to be 0.8° ($\pm 0.2^\circ$)^[5]. However, according to experimental findings both pERG components P50 and N95 remain constant varying check size from 1° to 15° (field size $32^\circ \times 27^\circ$, full angle), and the attenuation of pERG due to large-check size is minimal^[43]. Additionally, check size in ppERG may be larger than check size in conventional pERG because peripheral ganglion cells have larger average receptive fields. The average apparent check size used in the previous prototype was 10° at a viewing distance of 30 cm (distance from eye to dome apex), giving satisfactory results in terms of test robustness and repeatability. However, there is still no method to systematically determine the optimal check size in peripheral patterns.^[7]

In order to probe the entire retina and not only the central or the peripheral part, all the three dimensional stimulus source needs to be tilted with LEDs. Different design options need to be evaluated to decide the number of rows and the number of checks in each row, taking into account all the optimal design requirements.

3.2.3 Optical properties

The main optical requirements that the pixels of the stimulus source need to satisfy are listed below.

- **Reflectance requirements.** The reflectance of each pixel front viewing window needs ideally to be 0%, as well as the reflectance of the high absorbance coating on

the walls of the each chamber. In fact, the light that comes from outside the pixel does not have to be reflected towards the patient. Moreover, in order to maximize LED light reflection, the reflectance of the walls of each second and third chamber needs ideally to be 100%. The pixels materials have to be chosen in order to get as close as possible to these ideal values.

- **Chromatic stimuli.** In order to perform multiple ERG protocols in addition to conventional pERG and ppERG, different chromatic stimuli are needed. In particular, dark-adapted red flash ERG uses a red flash stimulus (red LEDs, 635-655 nm) to probe the functionality of generalized rod and cone system^[15]. PhNR of the light-adapted flash ERG uses a red flash stimulus (red LEDs, 630–660 nm) on a steady blue background (blue LEDs, 450–485 nm) to assess RGCs function and to monitor glaucomatous progression^[16]. In photopic On-Off ERG green wavelength (560 nm) has been used for the background together with orange stimuli in order to suppress rods and S-cones, thus stimulating L- and M-cones^[17]. Additionally, green colour may be useful in tests where a monochromatic high luminance source is required, for example to quantify number of photons that reach the retina. In fact, human eye is most sensitive to green light because cones and rods sensitivities coincide at a wavelength of 555 nm (green), which is also the peak of photopic vision (daylight vision) sensitivity^[44].
- **Stimulus luminance and strength.** In full-field electroretinography, the standard white background luminance is 30 photopic cd m^{-2} with a scotopic strength of 75

scotopic cd m^{-2} , and the recommended white stimulus strength goes from 0.01 photopic cd s m^{-2} and 0.025 scotopic cd s m^{-2} for dark-adapted 0.01 ERG to 10 photopic cd s m^{-2} and 25 scotopic cd s m^{-2} for dark-adapted 10 ERG^[13] (strong flash ERG). In dark-adapted red flash ERG the minimum flash strength needs to be 0.3 (photopic or scotopic?) cd s m^{-2} ^[15]. In PhNR of the light-adapted flash ERG the blue background luminance needs to be $\sim 10 \text{ ph cd m}^{-2}$, while the red flash strength needs to be higher than $2.0 \text{ ph cd s m}^{-2}$ ^[16]. In photopic On-Off ERG, white stimuli need to be $150\text{-}350 \text{ ph cd m}^{-2}$, and the background luminance recommended is 30 cd m^{-2} ^[17]. In clinical mfERG, the stimulus luminance of elements in the white light state needs to be greater or equal to 100 ph cd m^{-2} ^[4]. In clinical pERG, the required stimulus luminance in white areas (white LEDs) needs to be greater than 80 ph cd m^{-2} ^[5].

- **Stability of LEDs.** In order to consistently stimulate the retina, the luminance provided by the LEDs has to be as stable as possible in time.
- **Uniform luminance.** The viewing surface luminance of each pixel needs to be as uniform as possible.

3.2.4 Electronic layout

In order to have a stimulus source able to perform different protocols among ERG standards, an electronic design extremely flexible is required. The user should be able to choose among the available protocols, and to set several parameters (e.g. colour, luminous intensity and frequency of the stimulus, test duration).

3.3 Design results

3.3.1 Visual field

Considering an half angle of 25° , rows from A to G of the new stimulus source can be used to perform mfERG recordings, and considering an half angle of 15° , rows from A to E can be used to perform pERG recordings. The aspect ratio of the stimulus field is 1:1 because of the circular geometry, and therefore it complies with pERG requirements. The conventional pERG is limited to the central 30° (full angle) of the visual field, not allowing the access to any peripheral glaucomatous degeneration and limiting the sensitivity of the test^[7]. The visual field subtended by the second prototype considering 30 cm viewing distance is shown in Figure 25, with visual field limits superimposed (red curve). The visual field subtended by the source extends from 35° to 85° (half angles), which is more than human visual field superior limits for nasal, superior and inferior regions, but not for the lateral one^[7]. Because of this uncovered region the peripheral stimulation is not complete and therefore the response of the most peripheral retina may be affected. Thus, an additional row (M) with 16 lateral checks (8 on the right side and 8 on the left side) was added to the new three dimensional stimulus source. As shown in Figure 26, the lateral angle subtended thanks to the new design is $\sim 105^\circ$ (half angle), overcoming the prototype and almost completely covering the human visual field limits, as also required by the full-field clinical ERG Standard.

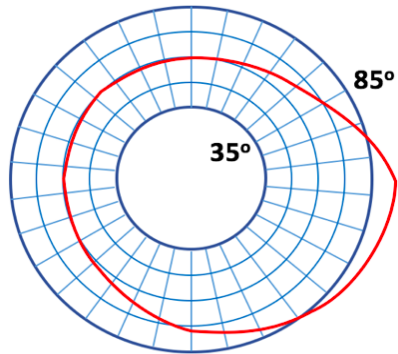


Figure 25: Visual field subtended by ppERG prototype.
 The viewing distance is 30 cm, and the visual field limits are superimposed (red curve).
 Adopted from^[7], the permission to reprint this copyright material is in the Appendix D.

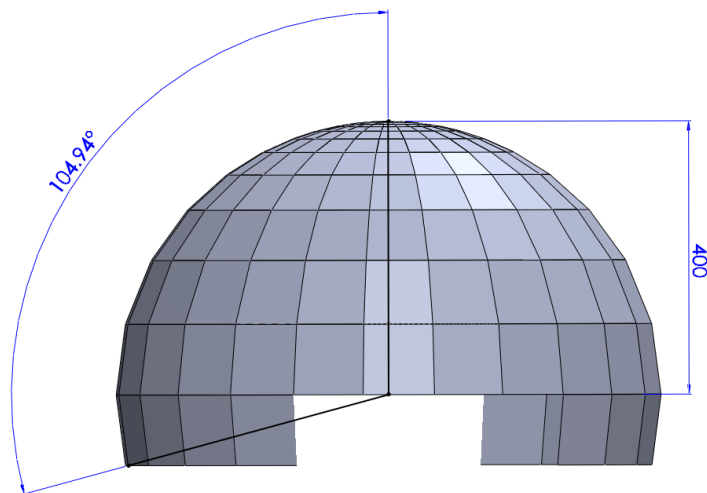


Figure 26: Lateral angle subtended by the new three dimensional stimulus source.
 Viewing distance: 400 mm.

3.3.2 Check shape, size and number

The shape chosen for the checks in rows from B to M is the trapezoidal one. In fact it allows to increase pixels dimensions from the center to the periphery of the device, at the same maintaining time an overall hemispherical geometry. Square pixels would form empty spaces between them because of the tridimensional design, while triangular pixels should have all the same dimensions, not taking into account the larger receptive fields of the peripheral RGCs^[7]. More complex shapes may be adopted (e.g. pentagons, hexagons) but the complexity of such a geometry is neither convenient nor necessary for the purpose. Moreover, the trapezoidal geometry of the pixels was able to elicit robust and repeatable pERG responses from the peripheral retina^[7]. The checks in row A are triangles in order to close the hemisphere and therefore to stimulate the entire visual field.

The apparent check size [degrees] in each row was calculated by averaging the apparent width and height of each check, considering a viewing distance of 40 cm (radius of the innermost shell). Considering rows from A to E for the stimulation of the central retina (0° to 15° , half angles), average apparent check size goes from 2.6° (row A) to 3.6° (row E). Considering rows from I to M for the stimulation of the peripheral retina (35° to 105° , half angles), average apparent check size goes from 10.5° (row I) to 14.9° (row M). All the average apparent check sizes are shown in Table II.

In each row from D to M there are 24 pixels. This choice has been made in order to achieve a balance between device complexity, components costs and checks requirements.

TABLE II: CHECK SIZES FOR EACH ROW.

Row	Width [mm]	Height [mm]	Apparent width [degrees]	Apparent height [degrees]	Average apparent size [degrees]
A	12.56	23.93	1.80	3.43	2.62
B	17.95	19.57	2.57	2.80	2.69
C	26.57	14.05	3.81	2.01	2.91
D	17.54	20.02	2.51	2.87	2.69
E	23.69	27.01	3.40	3.87	3.64
F	31.77	36.08	4.56	5.17	5.32
G	42.09	47.53	6.04	6.82	6.43
H	54.71	61.22	7.87	8.80	8.34
I	69.05	76.18	9.95	11.03	10.49
J	83.50	90.21	12.06	13.02	12.54
K	95.47	100.33	13.82	14.57	14.20
L	102.24	104.01	14.81	15.06	14.94
M	102.24	104.01	14.81	15.06	14.94

From row C to row A pixels number needed to be decreased to 12 in order to have surfaces large enough to mount PCBs on them. The procedure used to design the pixels in Solidworks begins by individually sketching each of the four shells, using the same workflow. Considering one layer, 13 planes parallel to the Top Plane were created and in each of them a circumference with an inscribed polygon was sketched. For the first 11 planes (rows M-D) the vertexes of polygons of two successive planes were jointed with the 3D Sketch tool, and then surfaces were created by filling each 3D Sketch face obtained.

In order to calculate the height of the planes and the radius of the circumferences for the rows D-M, an algorithm was implemented in Matlab. Referring to the figures 28 and 29, γ_1 is computed knowing that in the row L (the largest row of the dome together with

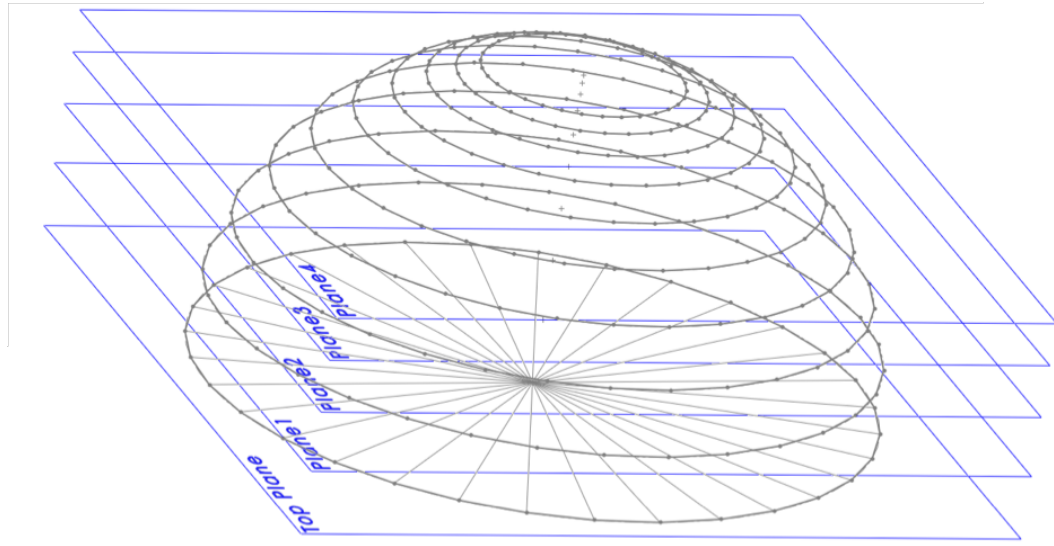


Figure 27: Partial Solidworks design procedure.

Considering the first shell (40 cm radius), the figure shows some of the planes, circumferences and polygons that have been created to design the flat faces in each row. The procedure is the same for each of the four layers, since only the radius changes (40 cm, 43 cm, 46 cm and 49 cm, respectively).

row M) there must be 24 isosceles trapezoids. Consequently γ_1 is given by dividing 360° for 24 times. The length of the chord w_1 can be found by applying the formula $2R_1 \sin\left(\frac{\gamma_1}{2}\right)$, with $R_1 = 40\text{cm}$ in the case of the first shell. For the rows D-M, the major base of each trapezoid has the same length of the oblique side, and so $h_1 = w_1$. This choice was made in order to have pixels as similar as possible to squares. Then α_1 is computed by subtracting γ_1 to 180° and dividing for 2 the result. In the largest row β_1 coincides with α_1 , R_2 is found by subtracting $h_1 \cos(\beta_1)$ to R_1 and a_1 corresponds to $h_1 \sin(\beta_1)$. From now on, the following procedure is repeated until h_i is greater than 1.5 cm using a for loop. This value

has been chosen in order to allow the design of appropriate PCBs, considering that the LEDs have size 5 mm x 5 mm. w_2 is found by applying the same formula applied for w_1 and by using the same angle, but now the radius is R_2 . $h_2 = w_2$, γ_2 is given by $2\arcsin\left(\frac{h_2}{2R_2}\right)$ and α_2 is computed by subtracting γ_2 to 180° and dividing for 2 the result. The angle δ_1 is the $\arccos\left(\frac{R_2}{R_1}\right)$ and β_2 is the difference between α_2 and δ_1 . The new radius R_3 is found by subtracting $h_2\cos(\beta_2)$ to R_2 , and a_2 is given by $h_2\sin(\beta_2)$. The Matlab code of the algorithm is shown in the Listing A.1 in the Appendix A. Row M is equal to mirrored row L in terms of height and trapezoids dimensions, but it has only 16 pixels sketched instead of 24.

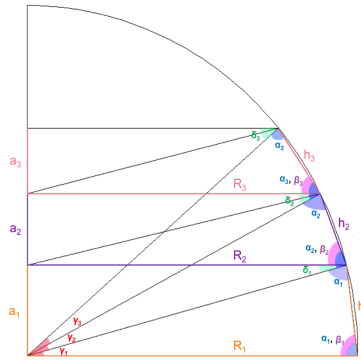


Figure 28: Frontal view of the first shell.

Since oblique sides and major basis of row D trapezoids measure 1.53 cm, it was the the last one designed using the algorithm. Row B and row C were build so that all isosceles trapezoids almost had the same area, and as already mentioned the number of faces in

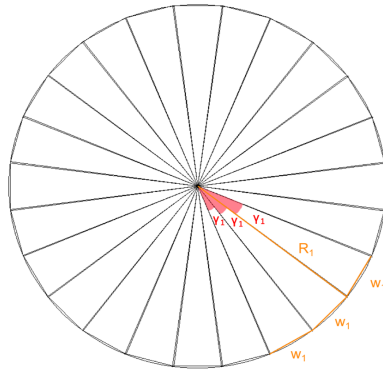


Figure 29: Top view of the circumference with radius 40 cm of the first shell.

each of these rows was halved to 12. Finally, the last row was made up of 12 isosceles triangles which close the hemisphere. During the sketching of all surfaces, the thickness of the aluminium walls was also taken into account. The complete design of the first layer is shown in Figure 30. The entire dome both with the four shells and with the sidewalls, which were sketched at the end of the explained procedure, is shown from different views in Figure 31.

3.3.3 Optical properties

- Reflectance requirements.** The material used for the front viewing window of the pixels was Anti-reflection (AR) Coated High Efficiency Window (#63217, Edmund Optics), which has a reflectance $\leq 0.5\%$ thanks to a broadband coating on both sides. The latter virtually eliminates back reflections, and the transmission at 0 degrees is 93-94%.^[45] The absorbance coating used on the walls of each first chamber was Adhesive Back Flock Paper (#54577, Edmund Optics), a black-out light absorbing mate-

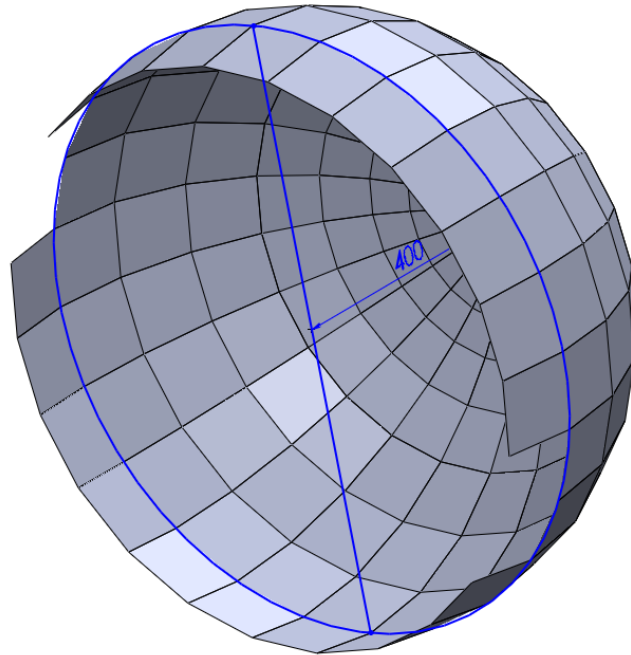


Figure 30: The first shell (400 mm radius) obtained with the explained procedure.

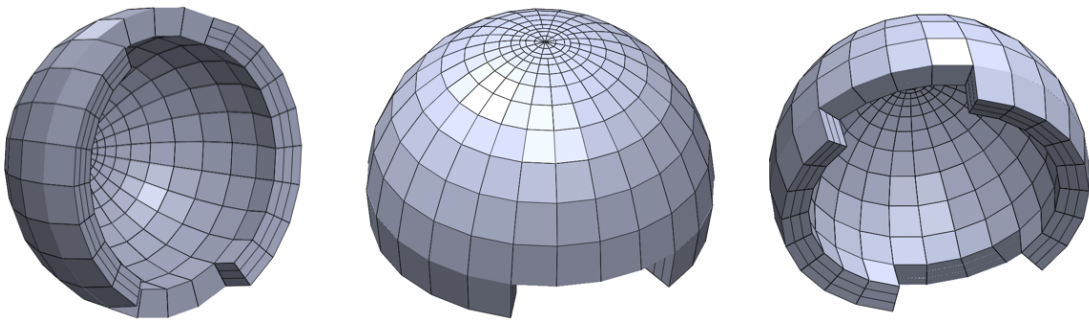


Figure 31: Complete design of the dome.
It is composed by the four shells (13 rows each) plus the sidewalls.

rial^[46]. Finally, the walls of each second and third chamber were covered by White98 Film (#F16A-98, White Optics). It helps to maximize the available Lumens per Watt to minimize LEDs 'hotspots' and it has a reflectance of 98%^[47]. In order to increase the diffusion of light coming from each LED and thus improve luminance uniformity on the front windows, two diffusive surfaces were placed inside each check, respectively one between the first and the second chamber (layer 2) and the other between the second and the third chamber (layer 3). The material chosen for layer 2 was a clear colorless plexiglass (acrylic). The material chosen for layer 3 was Optix 95 LD (Delvie's Plastic Inc.), another clear acrylic plexiglass. This rigid thermoplastic material is a good choice for LED lighting applications since it has a light transmittance of 92% and excellent diffusing properties^[48].

- **Chromatic stimuli.** The LED chosen for the device is the Cree XLamp MC-E LED. It is extremely small, it has an high performance and quality of light, and there is the possibility to choose the color among RGBW. In the typical spectral output of the XLamp MC-E Color LED with each LED on independently^[8], the red radiant power peak is at 630-635 nm and the blue one is at 450-460 nm, thus conforming to the standards. The maximum DC Forward Current is 700 mA for each color, and the maximum Forward Voltage for this amount of current is 2.3 V for the red, 3.7 V for the green, 3.5 V for the blue and 3.5 V for the white.

In order to control each check individually, a PCB for each LED was developed. The tool used for the electronic design was KiCad, a free software suite for the creation

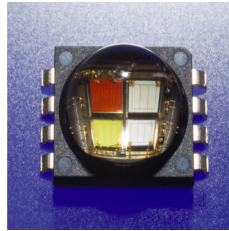


Figure 32: The Cree®XLamp MC-E LED, adopted from^[8].

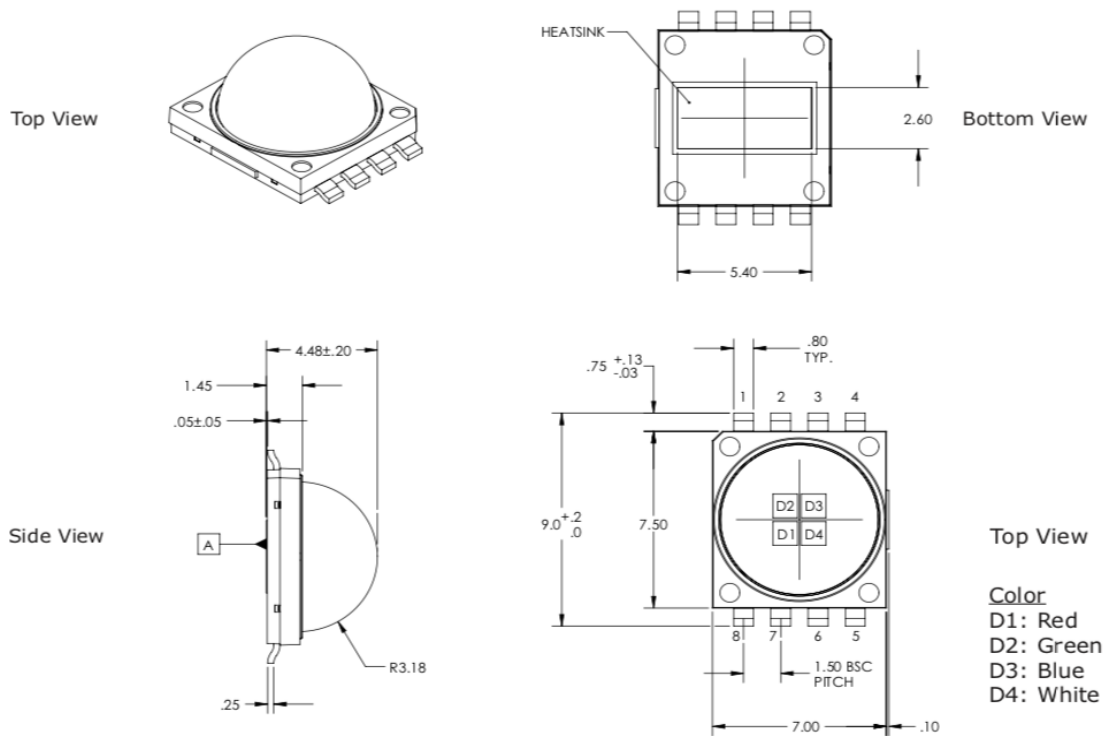


Figure 33: Mechanical dimensions of XLamp MC-E LED, adopted from^[8].

of electronic schematics and for their conversion to PCB designs. The schematic was created with the schematic capture editor of KiCad (Eeschema) and is reported in Figure 34. The LED has four positive poles and four negative poles, one for each color, plus the thermal pad, that is not actually connected. The negative poles were connected to ground (GND), while each of the positive ones was connected to a female connector. A fifth female connector was connected to GND. The connectors were used in order to create plated through-holes (PTHs) in which wires can be welded.

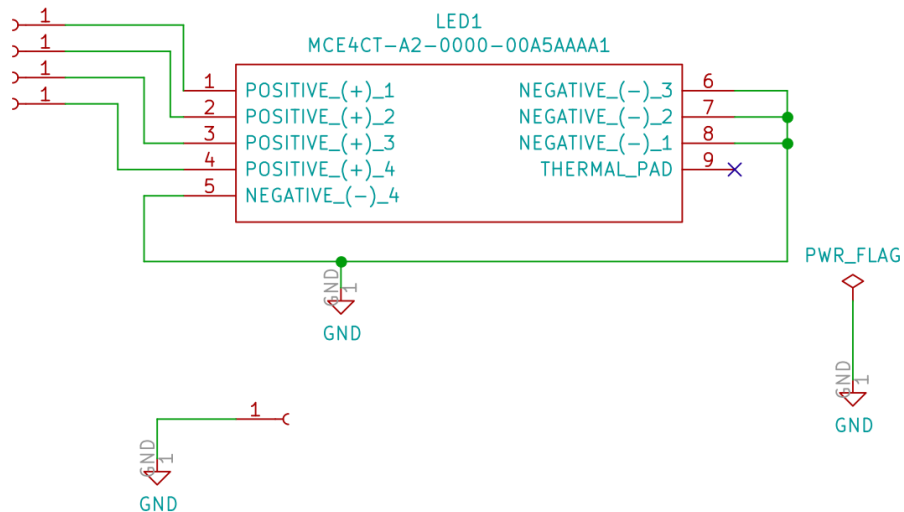


Figure 34: Eeschema Schematic of the PCB.

In the next step each component was associated with its fingerprint. For each female connector, a circular pad of PTH type was created and it is shown in Figure 36a.

The fingerprint for the LED was composed by eleven rectangular pads of surface-mount device (SMD) type, placed according to the mechanical dimensions of the package. The most common material used for the dielectric part of a PCB is FR-4, a glass fiber composite reinforced with epoxy resin which is characterized by low thermal conductivity. However, the LED package has a thermal contact electronically isolated both at the anode and at the cathode, and needs to be mounted on a appropriate sink. Adding plated through-holes between the conductive layers is a good economic way to increase the thermal transfer, and this technique is sustained by Cree^[9]. The cross section of the PCB with thermal vias is shown in Figure 35. Thus, in order to increase the thermal resistance of the PCB, two columns of seven circular pads of PTH type were added to the LED fingerprint, which is shown in Figure 36b.

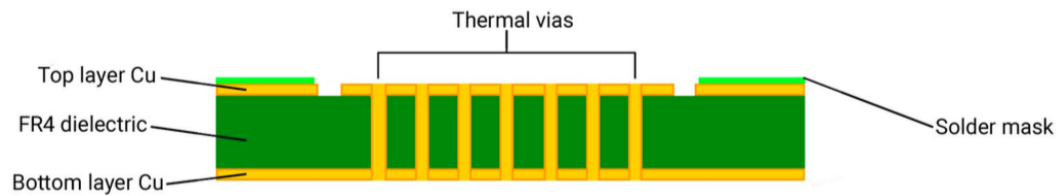
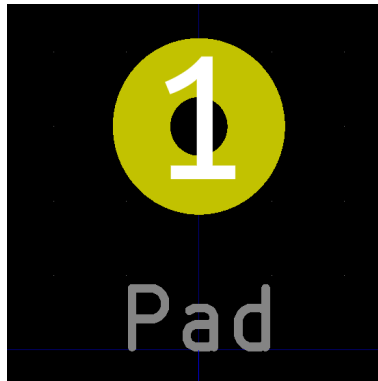
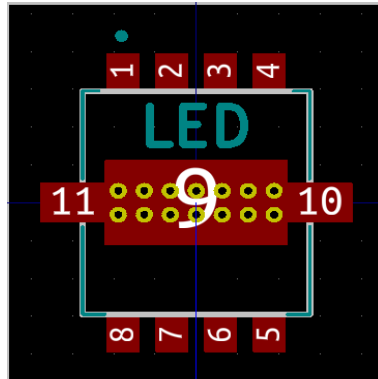


Figure 35: FR-4 cross-sectional geometry with thermal vias, adopted from^[9].



(a) Fingerprint linked to each female connector.



(b) Fingerprint linked to MC-E LED.

Figure 36: Fingerprints used in the designed PCB.

The next step was the generation of the netlist file. It describes the PCB components and their pin connections. Then Pcbnew tool was used to lay out the PCB through the netlist file created. After the definition of the edge of the PCB, tracks were added to the top copper layer and a ground plane connected to all GND pins was created. Finally, due to the concern about thermal dissipation previously stated, a thermal plane was added to the bottom copper layer. The final 3D appearance of the PCB is shown in Figure 38.

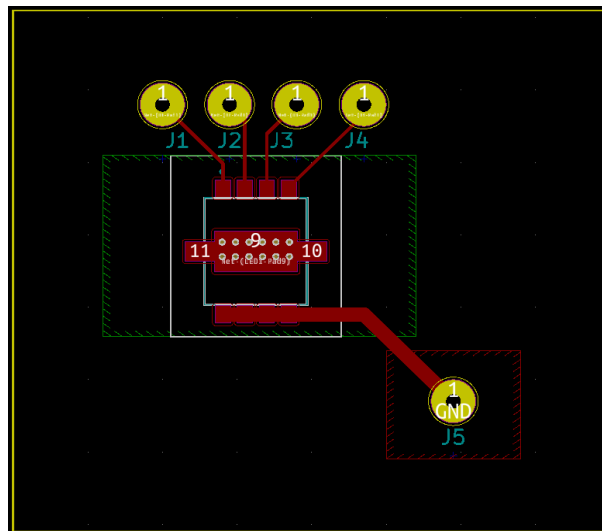


Figure 37: Final PCB in the Kicad tool Pcbnew.

Before placing the orders for all the needed PCBs, a prototype was developed in the laboratory using photoengraving technique. It was used to test both Kicad design and

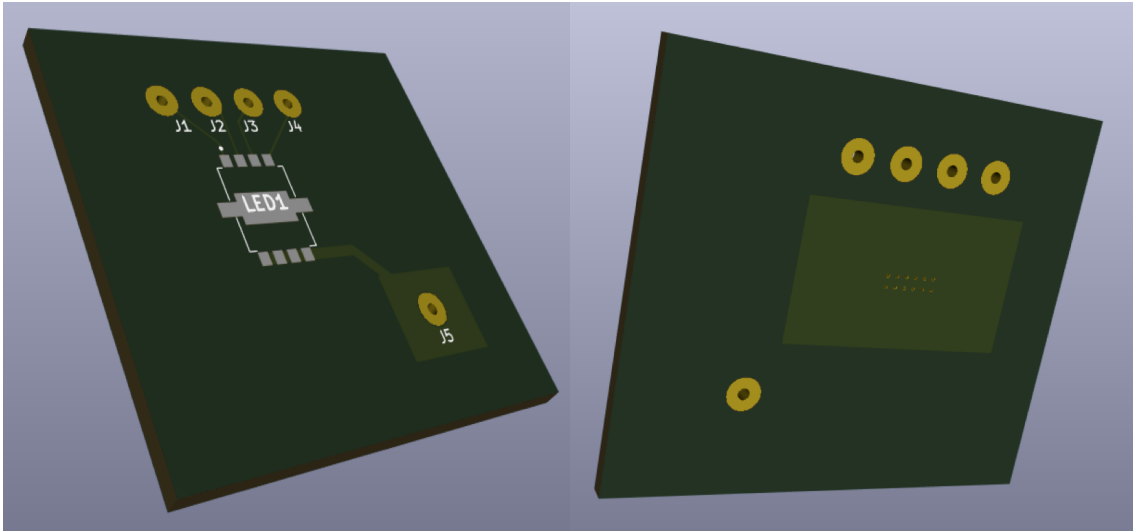


Figure 38: Final PCB shown with 3D Viewer.

luminance and stability of the LED. The design obtained in KiCad was printed on a transparency film for laser printers, leaving in black all the parts which corresponded to copper. A photo frame was used to keep the film pressed against the sensitized side of the board, which was covered by a positive PR. A positive PR becomes soluble when exposed to light because of the breaking of the main or side chains in the polymer. The presensitized board had a protective film to avoid accidental exposure and it was peeled off while a red light source was on.

A 100 Watt light bulb at seven inches away was used for the exposure, that lasted fifteen minutes. Then one part of concentrated positive type developer was mixed to ten parts of distilled water in a pyrex dish, where in turn the board was put in. As

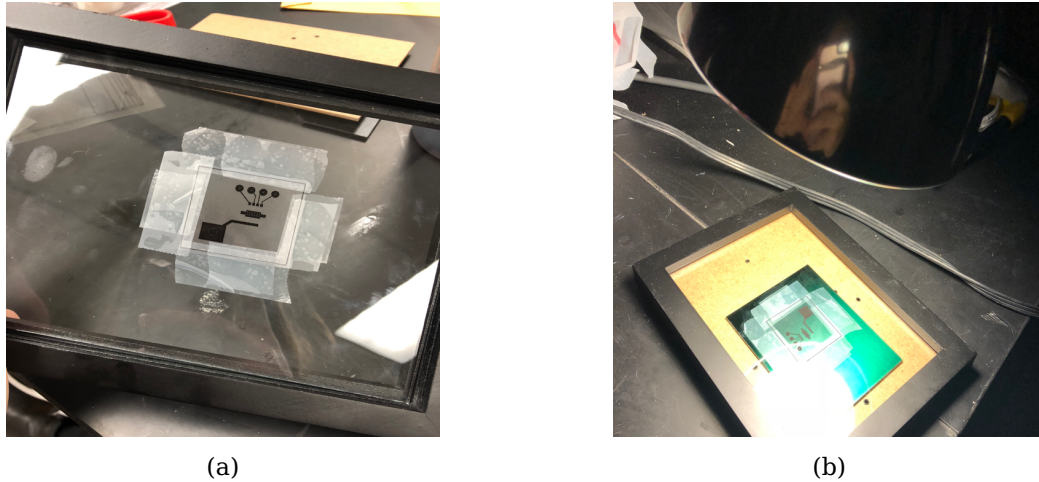


Figure 39: First phase of the photoengraving technique.
(a) Printed transparency film stuck to the frame. (b) Transparency film pressed against the sensitized side of the board.

shown in Figure 40, the developer removed areas of the photoresist exposed to white light, while maintained areas of PR that were not exposed.

After a quick rinsing in cold water the board was etched using a mixture of one part concentrated ferric chloride and one part of water. The process took about twenty minutes, and in Figure 41a the result is shown. Then a mini drill press was used to create holes of around 1.5 mm of diameter, and finally acetone was used to wipe off the resist.

The LED was adhered in place using a sticky solder paste which was deposited on the board through a syringe. Then heat was used to melt the past and to form conductive

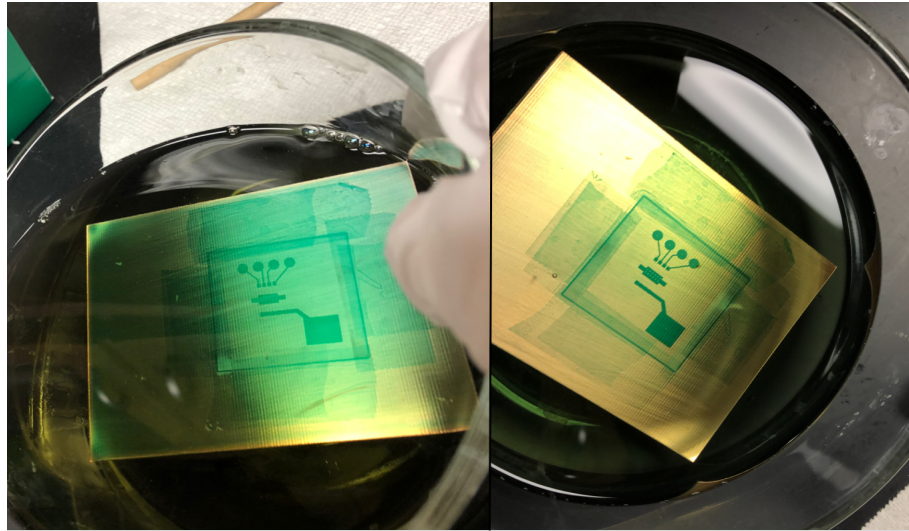


Figure 40: Development of the positive PR

connections between LED pads and PCB copper layer. One wire for each color were soldered to each circular pad, and a fifth wire was soldered to the GND plane.

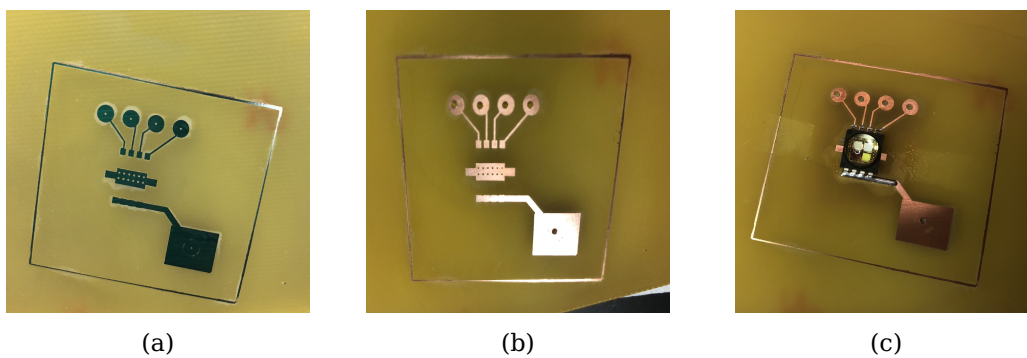


Figure 41: Last phases of the photoengraving technique.
 (a) PCB after the etching. (b) PCB after the removal of the residual PR. (c) PCB with the assembled MC-E LED.

- **Stimulus luminance and strength.** In order to analyse photopic luminance and stimulus strength given by the LED mounted on the customized PCB and by the chosen materials, a triangular check prototype was used. The measurement instrumentation consisted in a photometer (IL 1800, International Light, Peabody, MA), a SED100 photodiode detector, a R485 radiance barrel and a filter, Y#19474 photopic or ZCIE#19555 scotopic, respectively used for photopic (ph, day vision) or scotopic (sc, night vision) measurements. These correction filters weighed the incoming light in order to simulate the response of the human eye. The photodetector was firmly placed in front of the pixel surface using an appropriate holder, and the radiance barrel was used to let the photodetector (half visual angle 1.5°) be close enough to subtend a visual field which included only the surface of the pixel. The tests were performed in a dark environment where the LED was the only light source on, the 5V bias button of the photometer was always kept off and a surface completely black was used to take zero measurements during instrument calibration.

With regard to the main full-field ERG protocols, a summary of the stimulus strength and duration requirements is shown in Table III. The LED color channel of interest was powered with 350 mA (DC power supply), half of its maximum forward current. A digital pin of Arduino AtMega 2560 was programmed via software to generate a square wave (1Hz, 5V) with a different stimulus duration in each experiment (4 ms, 3 ms, 2 ms, 1 ms, 0.5 ms, 0.1 ms, 50 μ s and 20 μ s). The square wave powered a solid-state relay (VO14642, Vishay Semiconductors), whose two outputs were con-

TABLE III: STIMULUS STRENGTH AND DURATION REQUIREMENTS OF MAIN FULL-FIELD ERG PROTOCOLS

ERG test	Stimulus strength [ph cd s m ⁻²]	Stimulus strength [sc cd s m ⁻²]	Stimulus duration [ms]
Dark-adapted 0.01 ERG	0.010	0.025	≤ 5
Dark-adapted 3.0 ERG	3.0	7.5	≤ 5
Dark-adapted 10 ERG	10	25	≤ 5
Dark-adapted OPs	3.0	7.5	≤ 5
Light-adapted 3.0 ERG	3.0	7.5	≤ 5
Light-adapted 30 Hz flicker ERG	3.0	7.5	≤ 5
Dark-adapted red flash ERG	0.3	0.3	≤ 5
PhNR of the light-adapted flash ERG	> 2.0	/	< 5

nected to the positive and to the negative pins (GND) of the LED, respectively. The relay used as a switch to turn ON and OFF the check, also allowed the low forward current input to be used to control the high forward current LED. For each stimulus duration and for each color channel, the mean stimulus strength was calculated by averaging 10 consecutive photopic and then scotopic ON-luminance strength measurements, and the results are shown in Table IV.

The minimum required value of 0.01 ph cd s m⁻² was reached by white, red and blue channels, while for green channel the lowest photopic value was 0.03 ph cd s m⁻².

TABLE IV: MEAN STIMULUS STRENGTH FOR EACH LED CHANNEL AND FOR EACH STIMULUS DURATION

LED channel	Stimulus duration [ms]	Stimulus strength [ph cd s m ⁻²]	Stimulus strength [sc cd s m ⁻²]
White	4.00	14.98	25.100
	3.00	11.18	17.850
	2.00	7.32	12.400
	1.00	3.77	6.465
	0.50	1.87	3.130
	0.10	0.37	0.695
	0.05	0.31	0.532
	0.02	0.01	0.009
Red	4.00	12.57	0.939
	3.00	9.56	0.797
	2.00	6.50	0.553
	1.00	3.24	0.264
	0.50	1.66	0.079
	0.10	0.38	0.011
	0.05	0.27	0.005
	0.02	0.01	0.002
Green	4.00	26.50	63.000
	3.00	20.10	47.950
	2.00	13.84	31.650
	1.00	6.25	16.050
	0.50	3.41	5.710
	0.10	0.79	1.290
	0.05	0.58	0.987
	0.02	0.03	0.081
Blue	4.00	2.48	72.400
	3.00	2.06	53.450
	2.00	1.35	29.600
	1.00	0.68	13.900
	0.50	0.34	7.020
	0.10	0.08	1.595
	0.05	0.05	0.121
	0.02	0.01	0.068

The minimum required value of $0.025 \text{ sc cd s m}^{-2}$ was reached by white and red channels, while the lowest scotopic values for green and blue channels were 0.081 and $0.068 \text{ sc cd s m}^{-2}$, respectively. The values obtained with the green channel were high using both the photopic and scotopic filters, since cones and rods sensitivities coincide at green wavelength. Moreover, the highest values of photopic stimulus strength were obtained with this color since its wavelength is the peak of photopic vision sensitivity.^[44] The maximum required value of $10 \text{ ph cd s m}^{-2}$ was reached by white, red and green channel, while for blue channel the highest photopic value was $2.48 \text{ ph cd s m}^{-2}$. The values obtained with blue light were the greatest using the scotopic filter, while were the lowest among photopic stimulus strengths. In fact, scotopic sensitivity peaks sharply in the blue range, in which photopic vision is weaker^[1]. The maximum required value of $25 \text{ sc cd s m}^{-2}$ was reached by white, green and blue channels, while the highest scotopic value for red channel was $0.939 \text{ sc cd s m}^{-2}$. Scotopic stimulus strengths corresponding to red channel were the lowest, due to the fact that scotopic vision is almost insensitive to red light^[1]. Higher values of stimulus strength can be obtained by powering the LED with higher currents, as the results in Table V show. The electronic and the luminance measurements configurations were the same of the experiments described above, but the stimulus duration was always 3 ms, and the current provided to each LED channel by the DC power supply was 500 mA.

TABLE V: MEAN STIMULUS STRENGTH FOR EACH LED CHANNEL USING HIGHER CURRENT (500 mA)

LED channel	Stimulus duration [ms]	Stimulus strength [ph cd s m ⁻²]	Stimulus strength [sc cd s m ⁻²]
White	3	31.20	122.00
Red	3	38.86	6.38
Green	3	32.00	132.40
Blue	3	15.94	138.40

Moreover, each LED color channel was powered for fifteen minutes with lower currents (DC power supply, 1.2 and 2.0 mA) in order to match the background photopic and scotopic low luminances required by the standards. A measure was taken each five minutes, and the mean luminances for each color channel are shown in Table VI. The values obtained proved that by powering the LED with a fairly low current, it is possible to obtain background luminances that comply with the standards requirements.

Finally, for mfERG and pERG protocols the white channel photopic luminance was measured for fifteen minutes powering the channel with 350 mA (DC power supply), half of its maximum forward current. A measure was taken each five minutes, and the mean photopic luminance was 2130 ph cd m⁻², much higher than the minimum value recommended by the standards. For the sake of completeness the same test was also performed for the other colour channels, and all the results are shown in Table VII.

TABLE VI: MEAN LUMINANCE (TOTAL TIME PERIOD 15 MIN) OF EACH CHECK COLOUR USING LOW CURRENTS (1.2 AND 2 mA) TO POWER EACH LED CHANNEL

LED channel	Current provided [mA]	Stimulus strength [ph cd m ⁻²]	Stimulus strength [sc cd m ⁻²]
White	1.2	32.20	34.50
	2.0	55.30	83.30
Red	1.2	14.45	0.41
	2.0	30.40	2.40
Green	1.2	48.40	84.90
	2.0	91.00	176.20
Blue	1.2	3.67	73.80
	2.0	7.94	101.60

TABLE VII: MEAN ON-LUMINANCE (350 mA, TOTAL TIME PERIOD 15 MIN) OF EACH LED COLOUR CHANNEL

LED channel	White	Red	Green	Blue
Mean ON- luminance [ph cd m ⁻²]	2130.00	1266.33	2163.33	512.33

- Stability of LEDs.** A common behaviour of LEDs is to become stable when they reach thermal equilibrium, after a starting peak of intensity when they are switched on^[49]. In order to determine the amount of time needed to reach thermal equilibrium, a thermocouple (52 II Thermometer, Fluke) was placed at the bottom of the PCB prototype, under the LED, and the temperature was measured starting when it was switched on (350 mA). in Figure 42 the temperature variation over time for each color channel is shown, and it can be observed that after five minutes it starts to be

more constant for all channels. Consequently, all the measurements done to analyse the LED stability were made at least 5 minutes after turning it on.

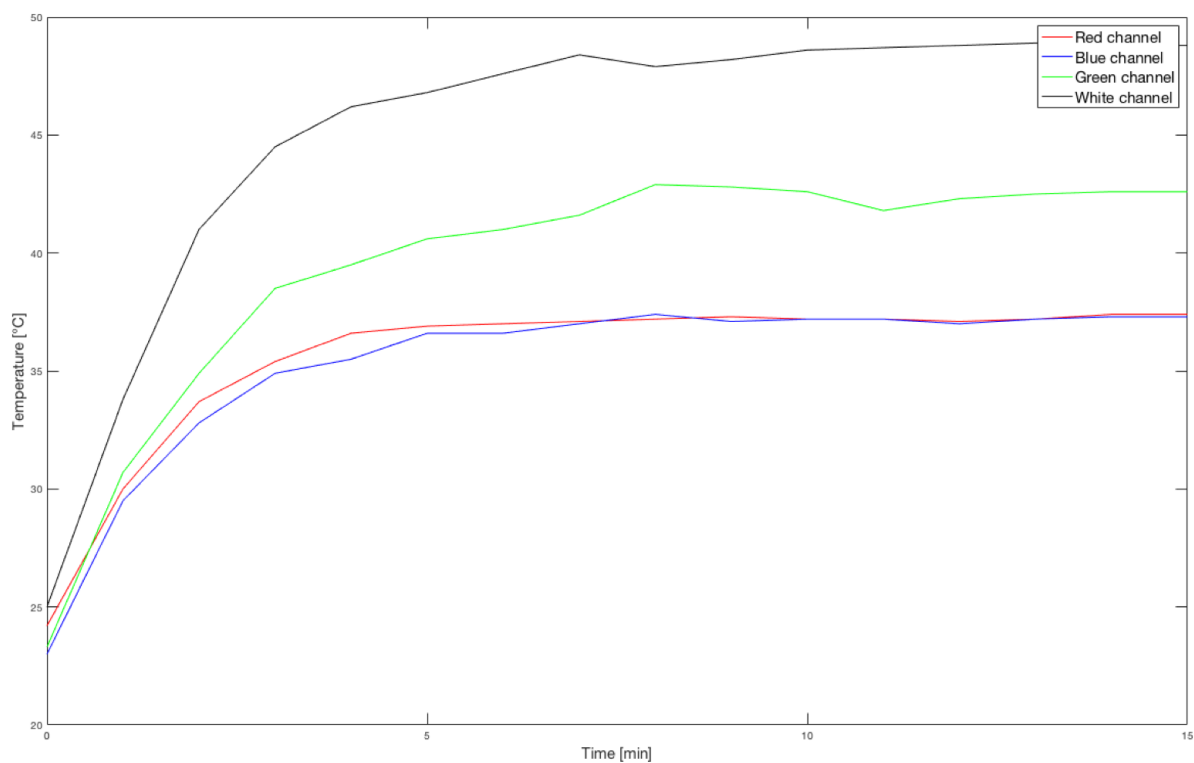


Figure 42: Temperature variation over time for each LED color channel.

In order to analyse the stability of each LED color channel (red, green, blue and white), two different luminance measurements were made. The photodiode detector together with the radiance barrel and the scotopic filter was firmly placed in front

of the pixel surface using an appropriate holder. The tests were performed in a dark environment where the LED was the only light source on, the 5V bias button of the photometer was always kept off and a surface completely black was used to take zero measurements during instrument calibration.

In the first measurement, each LED die was powered for one consecutive hour with 350 mA (DC power supply), half of the maximum LED DC forward current, and luminance readings were made every 10 minutes. For all data of each LED color, the mean μ and the standard deviation σ were computed and then used to find the coefficient of variation % :

$$CV\% = \frac{\sigma}{\mu} \cdot 100 \quad (3.1)$$

In the second luminance measurement, each LED die was powered for 30 minutes using the DC power supply (350 mA) again, but its switching on and off were controlled by a solid-state relay (VO14642, Vishay Semiconductors), which was in turn powered by a square wave (4 ms stimulus duration, 5V, 1 Hz) generated by a digital pin of Arduino AtMega 2560, programmed via software. Scotopic ON-luminance readings were made every 5 minutes, and also in this case the coefficient of variation % was calculated for each color channel. The results of both experiments are shown in Table VIII. The variation is always less than 1 % except for the red colour channel in the first measurement (1.56 %), which, however, remains low.

TABLE VIII: COEFFICIENT OF VARIATION % GIVEN BY THE TWO LUMINANCE MEASUREMENTS MADE IN ORDER TO ANALYSE STABILITY IN TIME OF MC-E LED CHANNELS

LED channel	White	Red	Green	Blue
CV given by the first measurement [%]	0.11	1.56	0.26	0.45
CV given by the second measurement [%]	0.59	0.41	0.45	0.15

- **Uniform luminance.** In order to analyze luminance uniformity across a check given by the new chosen LED and materials, the triangular prototype was used. A photograph of the check for each LED color was opened in ImageJ (National Institute of Health, Bethesda, Maryland), drawing one line across the frontal surface width and one line across the frontal surface height, as shown in Figure 44. The greyscale intensity level of the pixels along each of the two red lines was plotted, and the plots for each color channel are shown in Figure 45 .

For all data of each LED color the coefficient of variation % was computed using Equation 3.1. The results are shown in Table IX and according to them the luminance uniformity is higher in blue channel (CV=0.17%) and lower in the red one (CV=3.51%). In Section 5 luminance uniformity across checks of each row will be similarly analyzed and compared to the results given by the previous prototype.

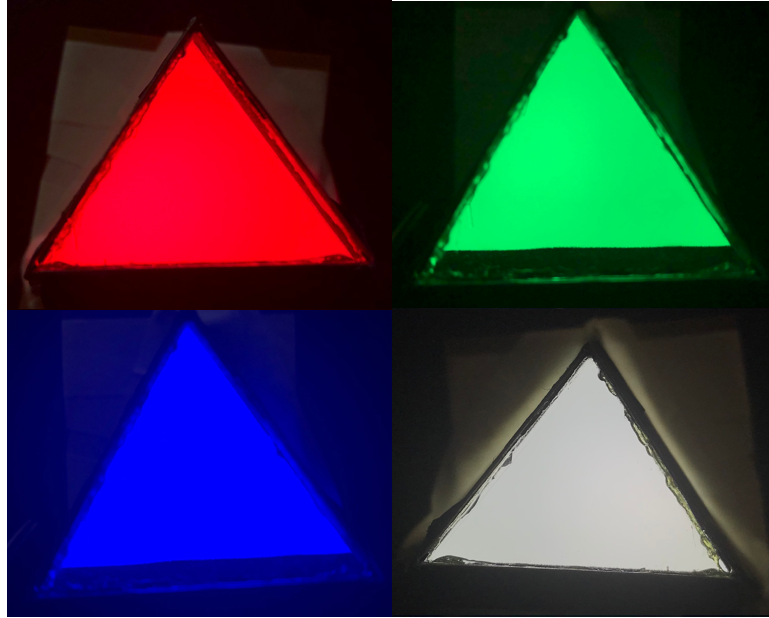


Figure 43: The photographs used, one for each LED color.

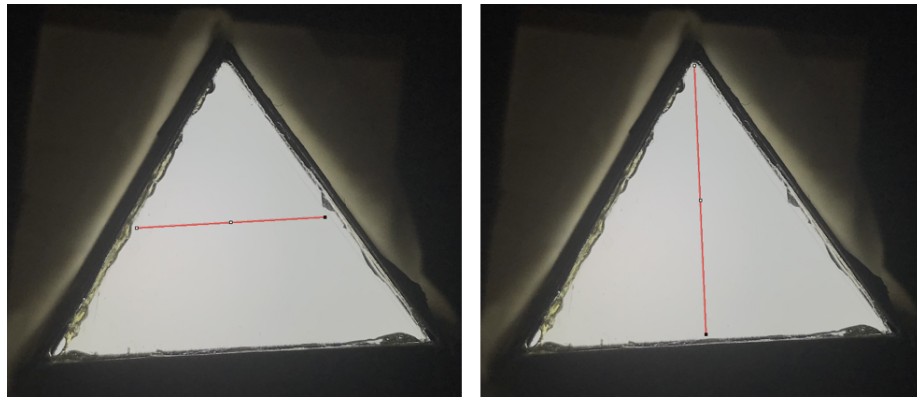


Figure 44: Lines along which grayscale intensity levels were evaluated.

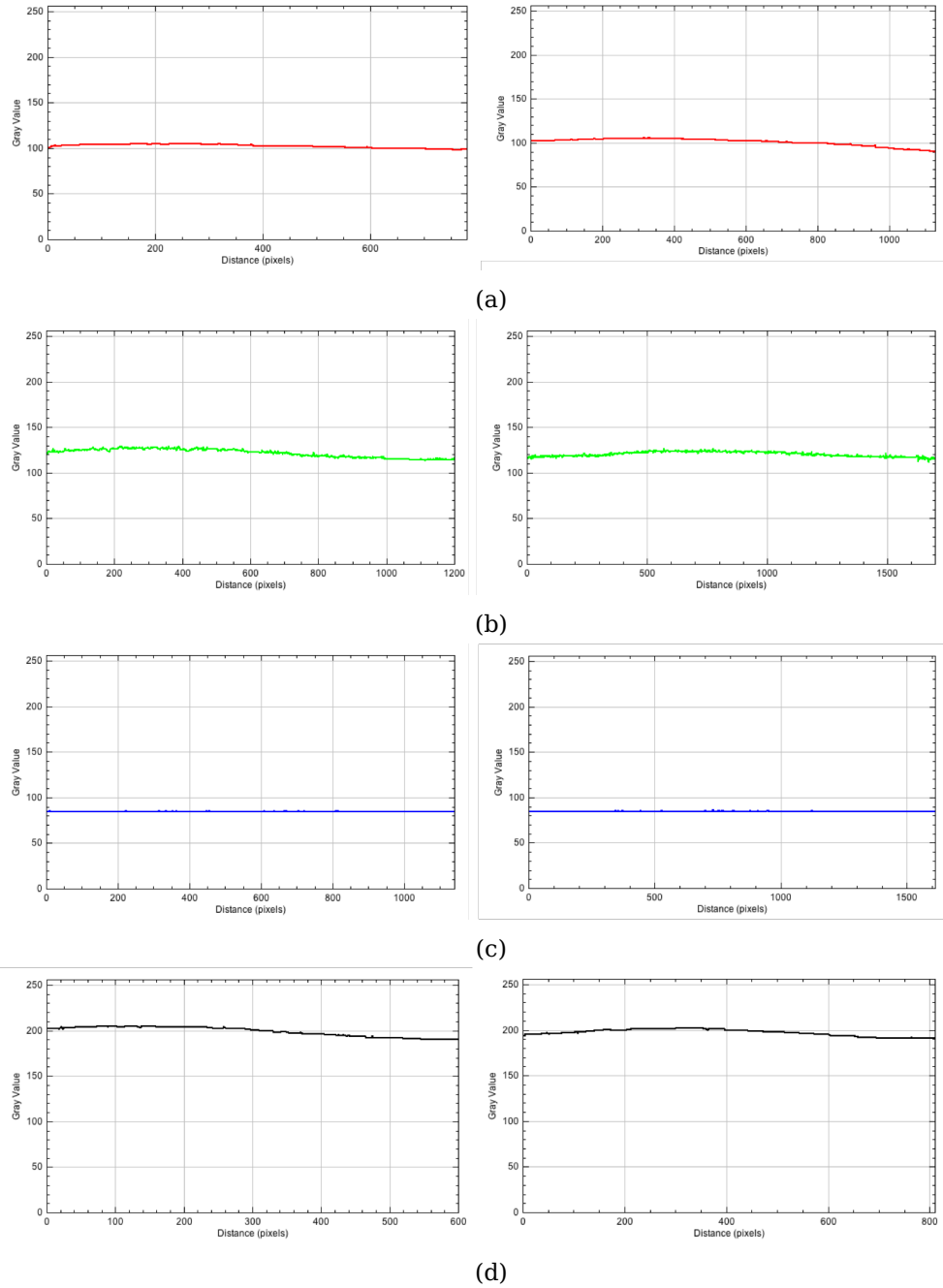


Figure 45: Greyscale intensity level of the pixels along the lines. Horizontal line (left column) and vertical line (right column) for red (a), green (b), blue (c) and white (d) channel photographs.

TABLE IX: COEFFICIENT OF VARIATION % OF GRAYSCALE INTENSITY LEVEL OF THE PIXELS ALONG THE TWO LINES, FOR EACH COLOUR CHANNEL.

LED channel	White	Red	Green	Blue
CV [%]	2.25	3.51	3.01	0.17

3.3.4 Electronic layout

Arduino AtMega 2560 was the microcontroller used in the project, programmed through the open-source Arduino integrated development environment (IDE), and LabVIEW (National Instruments, Austin TX) was the graphical IDE. As a proof of concepts, the electronic layout developed controlled only the first 36 LEDs (rows A-C of the stimulus source), but the approach chosen can be appropriately adapted to control all 268 LEDs.

The protocols chosen for implementation were the pERG and the flicker ERG. The first one was implemented using 4.6 RPS (2.3 Hz), and thus a time delay between the reversals of ~ 217 ms, and the total protocol duration was ~ 65 s, which corresponds to 300 pattern reversals. The second one was implemented using a frequency of 30 Hz, and thus a time delay between the flickers of ~ 33 ms, in which the LEDs were turned on for the first 2 ms and turned off for the remaining 31 ms. The total protocol duration in this case was set to 3.3 s, which corresponds to 100 repetitions of the stimulus. For both protocols the user has the possibility to choose the LEDs colour among red, green, blue and white.

- **Hardware configuration**

In the Figure 62 in the Appendix B.1 the schematic of the partial electronic circuitry is shown. In all five 8-bit serial-in, serial or parallel-out shift registers (SN74HC595, Texas Instrument), the output-enable pin (OE) (pin 13) input, active low, was grounded, while the direct overriding clear (SRCLR) (pin 10) input, active low, was connected to 5V Arduino's pin. Thus, the output pins are enabled and their bits reset is not performed. Between each shift register's Vcc pin and 5V Arduino's pin, a decoupling capacitance of $10\ \mu F$ was placed. Shift register clock (SRCLK) input (pin 11) and storage register (RCLK) input (pin 12) were respectively connected to Arduino's digital pins 12 and 8, for all shift registers. Serial (SER) input (pin 14) of the first shift register was directly connected to Arduino's digital pin 11. Pin Q_H' (pin 9) of the first shift register was connected to SER input of the second shift register, pin Q_H' of the second shift register to SER input of the third, and so on until the fifth. As shown by the SN74HC595 timing diagram in Figure 46, when the voltage on SRCLK is changed from low to high, shift register bits move one step to the left: bit 7 gets the value of bit 6, bit 5 gets the value of bit 4, etc. until bit 0, which accepts the value present on SER input. In each SN74HC595 a second register (storage register) is connected to the output pins (from Q_A to Q_H), and when RCLK voltage changes from low to high each bit gets moved from the shift register to the storage register, and so to the parallel output pins. The output pin Q_H' is used to output bit 7 of the shift register to the SER input of another shift register, and since the five shift registers have the

same SRCLK and RCLK signals, the setting of this configuration for all of them gives 40 parallel outputs.

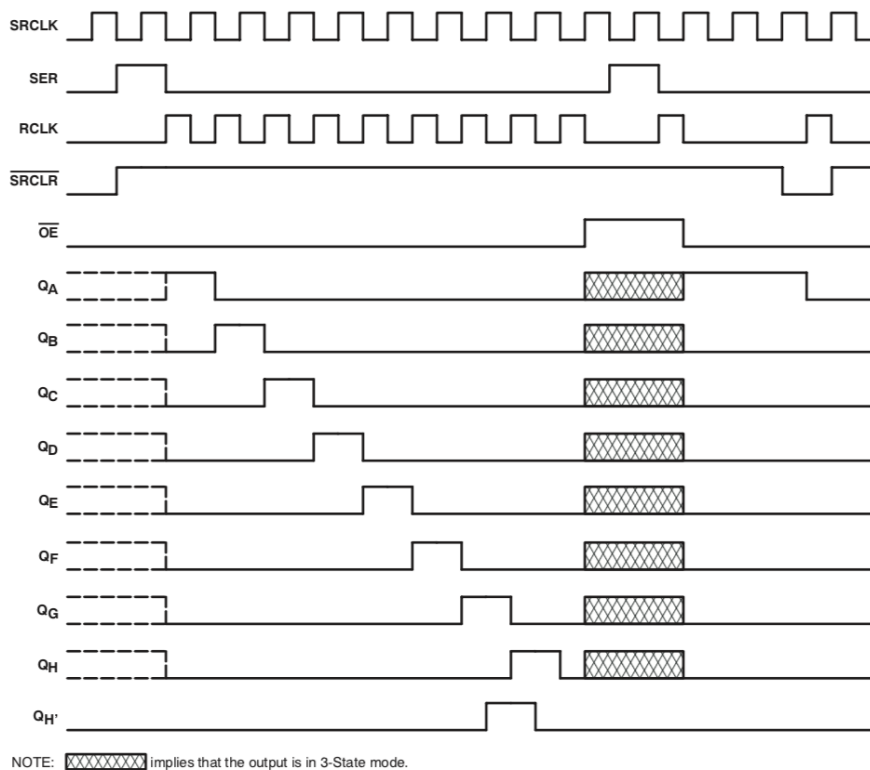


Figure 46: Timing diagram of SN74HC595, taken from^[10].

Considering the first four shift registers, each output pin (from Q_A to Q_H) is connected to the input pin 1 (anode) of a solid-state relay (VO14642AT-ND, Vishay Intertechnology, Malvern, PA), for a total of 36 relays. Considering the last shift reg-

ister, only the first four outputs are connected, each to the input pin 1 of a different relay. For simplicity, in the schematic in the Figure 62 only the first relay connected to the first shift register output is shown. Each of these normally open relays uses optical connection between the input and the output, being completely insulated electrically. When low forward current passes through an infrared LED on the input side (50 mA), it enables the passage of high current on the output side through MOSFET switches (peak load current 3.6 A) ^[50]. The output pin 6 of each of these relays was connected to a resistance (10 Ω), which in turns was connected to the negative pins (from pin 5 to 8) of a LED. Each positive pin (from pin 1 to 4) of the LED was connected to the output pin 4 of another relay, whose input pin 1 in turns was connected to one Arduino's digital pin. In particular, Arduino's digital pins 2, 3, 4 and 5 are connected through four different relays to LED pins 1 (red diode), 2 (green diode), 3 (blue diode) and 4 (white diode), respectively. The output pin 6 of each of these four relays was connected to the same power source. The same configuration was used for all LEDs, using one relay for each LED to control its state, and other four relays each eight LEDs to select their colour. This was done to allow the selection of all LEDs color channel through only four Arduino's digital pins. For simplicity, in the schematic in Figure 62 only the first four relays used for the first eight LEDs are shown. All the components were inserted in five different breadboards. Each of the first four breadboards was composed by one shift register, 12 relays, 8 resistances and 8 LEDs, and the last one was composed by one shift register, 8 relays, 4

resistances and 4 LEDs. Each group of LEDs was powered with a DC power supply which provided a maximum current of 10 A. The groups of 4 relays (normally open) connected the power supply with the chosen colour channel, allowing the current to flow through the LEDs. The division of the current was carried out connecting the power supply to each breadboard, in particular to the column from which the LEDs were powered. The wires size used to connect LEDs to the breadboards had to be less than 0.5 mm, which was the diameter of the PTHs of the PCBs on which the LEDs were mounted. Thus, the chosen wires had 26 American Wire Gauge (AWG) size, with a diameter of 0.40386 mm and a maximum current of 0.361 A. For all the other connections the wires used had 22 AWG size, with a diameter of 0.64516 mm and a maximum current of 0.92 A.

- **Software**

In order to establish a serial communication between LabVIEW interface and Arduino AtMega 2560, the package LabVIEW Interface for Arduino (LIFA) was used. The template `LIFA_base.ino` which allows serial communication between LabVIEW and Arduino was suitably modified to execute the protocols chosen for the device validation. If data is stored in Arduino serial receive buffer and is available from the serial port, it is read:

```
1 // send data
2 if (Serial.available()) {
3     // read data:
4     char labview = Serial.read();
```

Depending on its value, a switch case structure sets the variable `PIN` to the Arduino's digital pin corresponding to one of the available colours and the two bytes of `Arraydata` to `0b10101010` and `0b01010101` (pERG protocol case), or `0b11111111` and `0b00000000` (flicker ERG protocol case), respectively. The setting of `PIN` allows to close one relay out of four on each breadboard, and thus to power the LEDs so that the same color is selected in all of them. In the selected switch case the delay between the loading of the two bytes and the number of times that they have to be loaded are also set. Two examples of the switch cases are shown in the Listings below, the first for pERG protocol and the second for flicker ERG protocol:

```

1  switch (labview) {
2      case 'R':
3          PIN=2; //Controls red LEDs
4          Arraydata[0] = 0b10101010; //first phase of pERG
5          Arraydata[1] = 0b01010101; //second phase of pERG
6          interval[0]=217; //time duration of the first phase [ms]
7          interval[1]=217; //time duration of the second phase [ms]
8          iter=150; //number of times that the above sequence is
9                  //repeated (300 total reversals)
10         break;

1  case 'r':
2          PIN=2; //Controls red LEDs
3          Arraydata[0] = 0b11111111; //first phase of flicker ERG
4          Arraydata[1] = 0b00000000; //second phase of flicker ERG
5          interval[0]=2; //time duration of the first phase [ms]
6          interval[1]=31; //time duration of the second phase [ms]
7          iter=100; //number of times that the above sequence is
8                  //repeated (100 repetitions of the stimulus)
9         break;

```

After the switch cases, the voltage of the selected colour pin is set high and the first element of `Arraydata` is loaded into the five shift registers through the function

shiftOut, maintaining low their storage register input pins. As shown in the Listing below, this function uses a bitmask to determine the value of each bit of the first Arraydata element, and then sends it to the first shift register through the serial input pin (insDataPin), giving a clock stroke:

```

1 void shiftOut(int insDataPin, int insClockPin, byte insDataOut) {
2
3   int i=0;
4   int State;
5   pinMode(insClockPin, OUTPUT);
6   pinMode(insDataPin, OUTPUT);
7   digitalWrite(insDataPin, 0);
8   digitalWrite(insClockPin, 0);
9
10  for (i=7; i>=0; i--) {
11    digitalWrite(insClockPin, 0);
12    if ( insDataOut & (1<<i) ) {
13      State= 1;
14    }
15    else {
16      State= 0;
17    }
18
19    digitalWrite(insDataPin, State);
20    digitalWrite(insClockPin, 1);
21    digitalWrite(insDataPin, 0);
22  }
23  //stop shifting
24  digitalWrite(insClockPin, 0);
25 }

```

The function is called five consecutive times, so that the first byte of Arraydata is loaded into each of the five shift registers. Then the storage register input pins (Pinlatch) are set high to move the bits to the parallel output pins of the shift registers, each of them connected to a relay which in turn is connected to a LED.

Thus the relays are set open or closed according to the shift registers output values, consequently turning off or on the LEDs, respectively.

```

1   for (int j = 0; j < 2; j++) {
2       datashift1 = Arraydata[j];
3       datashift2 = Arraydata[j];
4       datashift3 = Arraydata[j];
5       datashift4 = Arraydata[j];
6       datashift5 = Arraydata[j];
7       digitalWrite(Pinlatch, 0);
8       shiftOut(Pindata, Pinclock, datashift1);
9       shiftOut(Pindata, Pinclock, datashift2);
10      shiftOut(Pindata, Pinclock, datashift3);
11      shiftOut(Pindata, Pinclock, datashift4);
12      shiftOut(Pindata, Pinclock, datashift5);
13      digitalWrite(Pinlatch, 1);
14      delay(interval[j]);
15  }

```

After a certain delay previously set in the selected switch case (`interval[0]`), also the second byte of `Arraydata` is likewise sent to the shift registers outputs, and its values are maintained at the shift registers outputs for the number of ms specified in `interval[1]`. This procedure is repeated a number of times (`iter`) which depends on the chosen protocol, previously set in the switch case. The complete Arduino's firmware is shown in the Listing A.2 in the Section A.2 of the Appendix A. For the shift registers control one of the tutorials from the official Arduino's website was readapted^[51].

- **Graphical interface**

LabVIEW was the graphical programming environment used to develop a user-friendly interface through which the ERG protocol of interest can be selected and its parame-

ters can be set. As already mentioned above, as proof of concepts two protocols were developed, the pERG (4.6 RPS, \sim 65 s total duration) and the flicker ERG (30 Hz, 3.3 s total duration). The user has the possibility to choose one of the available protocols and he can also set the colour of the light stimuli among red, green, blue and white.

LabVIEW programs are called VIs, and each of them consists of the user interface (front panel) and of the graphic source code (block diagram). In the front panel controls represent the inputs, while indicators represent the outputs. The front panel of the VI developed is shown in Figure 47. It contains two radio buttons controls, four boolean LEDs indicators and a boolean control button. The first radio button control (on the left) is used to select a protocol between pERG and flicker ERG, while the second radio button control (on the right) is used to select the colour among red, green, blue and white. The coloured LEDs indicators turn on when the corresponding colour is selected. Radio buttons are mutually exclusive, meaning that in each of them only one case at a time can be selected, avoiding users errors such as the simultaneous selection of multiple protocols or colours. When the *START* button is pressed, it becomes green and the selected protocol starts, using the chosen LEDs colour. Immediately after pressing the button, from green it returns to gray and the execution of the VI is aborted in order to avoid possible user errors during the protocol execution. In order to start a new protocol, the VI needs to be run again.

The block diagram of the VI developed is showed in Figure 48. The radio button through which one of the two protocols is selected was wired to a case structure,

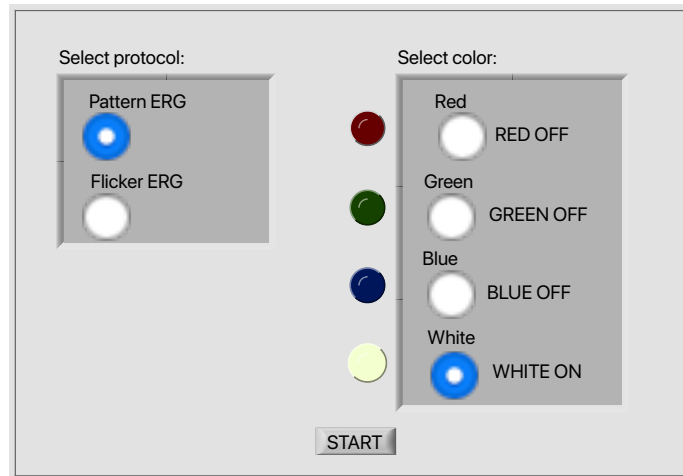


Figure 47: Front panel of the LabVIEW VI developed.

which executes one different subdiagram according to the input value. Inside each of the two cases, another case structure was created and wired to the radio button through which the colour is selected. Inside each colour case, a third case structure was placed and wired to the boolean control button `START`.

National Instruments VISA (NI-VISA) is the National Instruments implementation of the Virtual Instrument Software Architecture (VISA) input/output standard, which provides the programming interface between LabVIEW and hardware such as Arduino^[52]. For this application, the serial port connected to Arduino via USB was initialized through the VISA Configure Serial Port VI. Then the VISA resource name out (purple wire) and the error out (yellow wire) were both wired to a while cycle which contains all the case structures mentioned above. Given a protocol and a colour, if the

boolean control button `START` is true, the VISA Write Function sends the character wired to the write buffer (input of VISA Write Function) to Arduino, via serial communication. Each character corresponds to a different switch case in the firmware implemented in the Arduino IDE, in which variables are set in order to execute the desired protocol using the chosen LEDs colour, as already explained above. At the same time, the true boolean control button stops the while loop because it is connected to the loop conditional terminal (red button at the bottom right), which is set to `'Stop if True'`. At this point, if there are no errors the device session is closed through the VISA Close Function, which is outside the while loop. If the boolean control button is false, the while loop continues the execution without sending any character until the boolean button is pressed.

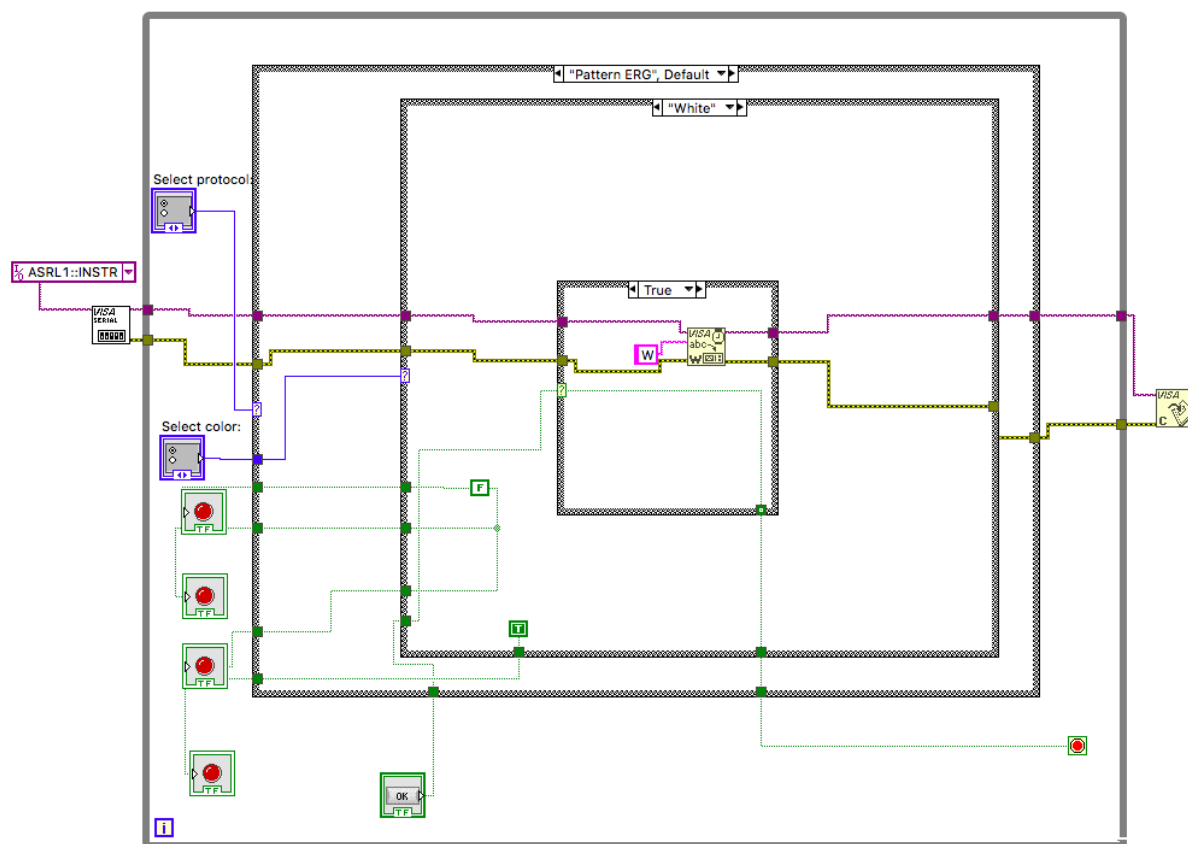


Figure 48: The block diagram of the LabVIEW VI developed.

CHAPTER 4

SPECIFIC AIM 2

As proof of concepts, the first three rows A, B and C of the three dimensional stimulus source were assembled. Each row is made by 12 pixels and the visual field subtended by them at a viewing distance of 40 cm is 8.5° (half angle). This chapter includes the description of all the materials used, the CAD files provided to the vendors and the description of the assembling procedure.

4.1 Materials

4.1.1 First layer

The flat faces of the first layer of each pixel were made of an AR Coated High Efficiency Window, as already mentioned in the Subsection 3.3.3. The reflectance of this glass is $\leq 0.5\%$ thanks to a broadband coating on both sides which eliminates back reflections, resulting in a light transmission at 0 degrees of 93-94%^[45]. The sheets of material (1 mm thick) were ordered from Edmund Optics and were cut by the Glass Shop of the UIC Department of Chemistry. The number of pieces needed was 12 for each row. In Figure 49 three of the pieces obtained after the cutting are shown, one for each row. The Solidworks files used for cutting pieces for each of the three rows are shown in the Figures in Section C.1 of the Appendix C. For completeness, a drawing of the first surface shape for one pixel of each row is also shown in the same section.

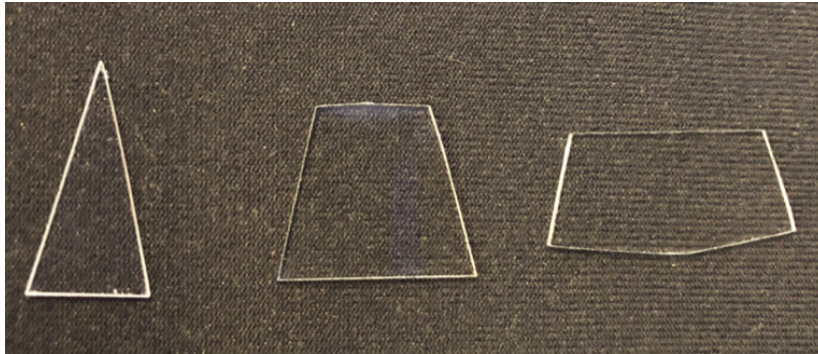


Figure 49: From the left, the first layer piece for one pixel of rows A, B and C.

4.1.2 Second layer

The flat faces of the second layer of each pixel were made of clear plexiglass (acrylic). This material has a smooth side and a rough side, and the latter was positioned towards the front glass window in order to maximize the diffusive effect. The sheets of material (3.17 mm thick) were ordered from Estreetplastics and were cut by the LAS Physical Sciences Machine Shop at UIC. The number of pieces needed was 12 for each row. In Figure 50 three of the pieces obtained after the cutting are shown, one for each row. The Solidworks files used for cutting pieces for each of the three rows are shown in the Figures in Section C.2 of the Appendix C. For completeness, a drawing of the second surface shape for one pixel of each row is also shown in the same section.

4.1.3 Third layer

The flat faces of the third layer of each pixel were made of Optix 95 LD, as already mentioned in the Subsection 3.3.3. The material is a colorless acrylic plexiglass particu-

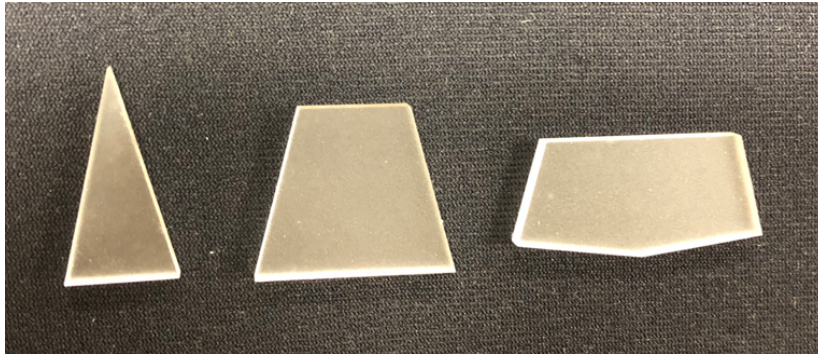


Figure 50: From the left, the second layer piece for one pixel of rows A, B and C.

larly suitable for LED lighting applications thanks to its excellent diffusing properties and a light transmittance of 92%^[48]. As the plexiglass described for the second layer, Optix 95 LD has a smooth side and a rough side, and also in this case the latter was positioned towards the front glass window in order to maximize the diffusive effect. The sheets of material (3.17 mm thick) were ordered from Delvie's Plastic Inc. and were laser cut at UIC Engineering Makerspace. The number of pieces needed was 12 for each row. In Figure 51 three of the pieces obtained after the cutting are shown, one for each row. The Solidworks files used for cutting pieces for each of the three rows are shown in the Figures in Section C.3 of the Appendix C. For completeness, a drawing of the third surface shape for one pixel of each row is also shown in the same section.

4.1.4 Fourth layer

The flat faces of the fourth layer of each pixel were made of white Delrin. The sheets of material (3.17 mm thick) were cut by the LAS Physical Sciences Machine Shop at UIC. A

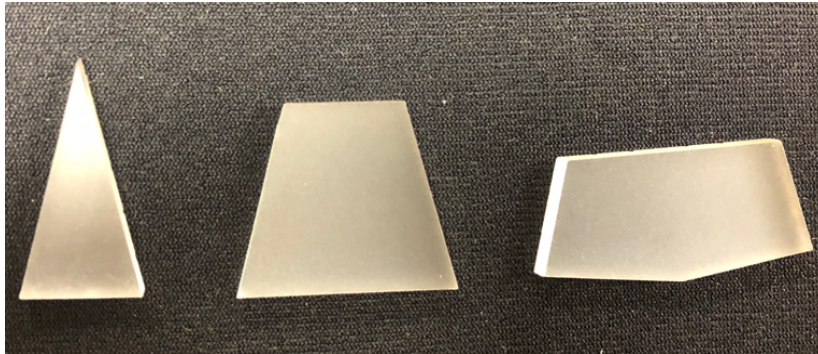


Figure 51: From the left, the third layer piece for one pixel of rows A, B and C.

hole was designed in each piece to allow the PCB of the LED to be mounted on the back of the surface. The number of pieces needed was 12 for each row. In Figure 52 three of the pieces obtained after the cutting are shown, one for each row. The Solidworks files used for cutting pieces for each of the three rows are shown in the Figures in Section C.4 of the Appendix C. For completeness, a drawing of the fourth surface shape for one pixel of each row is also shown in the same section. From row E to row M two circular holes were added to each piece in order to mount the PCB with screws.

4.1.5 PCB

The LEDs (MCE4CT-A2-0000-00A5AAAA1) were ordered on *www.digikey.com* and shipped to Imagineering Inc., which provided both the manufacturing of the PCBs and the assembly of the LEDs. Despite the choice to assemble only the rows from A to C, the PCBs were ordered for the rows from A to D because they have the same layout and ordering them all at once was convenient in terms of price. The number of PCBs needed was 60 (12 for each

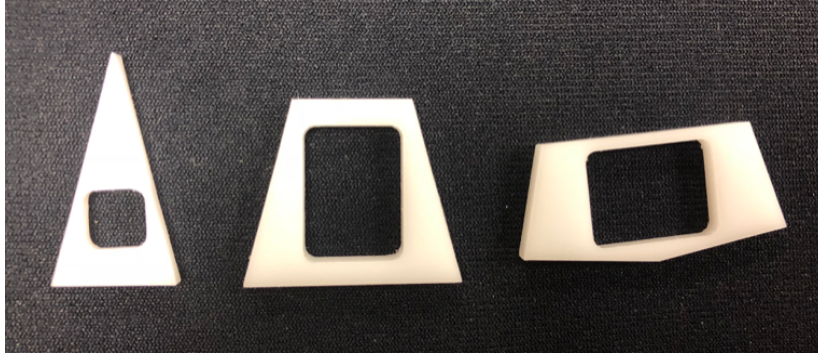


Figure 52: From the left, the fourth layer piece for one pixel of rows A, B and C.

of the rows from A to C and 24 for row D), but the actual order consisted of 65 PCBs and 85 LEDs in order to have extra components in case of attrition. The PCBs were made of FR-4 (1.57 mm thick, 21.44 mm x 13 mm board size) and more details about their specifications and requirements are shown in Table X . Figure 53 shows one of the obtained PCBs.

TABLE X: SPECIFICATIONS AND REQUIREMENTS OF THE ORDERED PCBs

Part number: Board A-D	Testing: yes
Layers: 2	Smallest hole: 0.25 mm
Material: FR-4	Minimum line: 0.25 mm
Thickness: 1.57 mm	Minimum spacing: 0.25 mm
Board size: 21.44 mm x 13 mm	Surface-mount technology sides: top side
Finish type: leaded finish	Surface-mount technology pitch: 0.64 mm

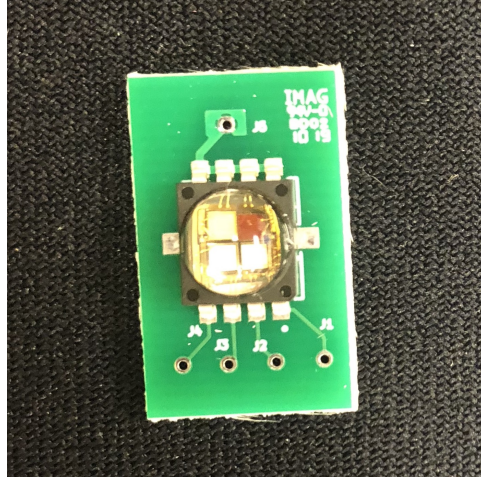
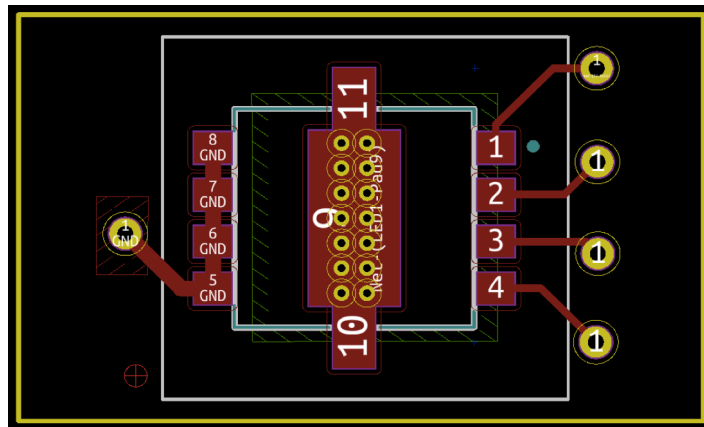
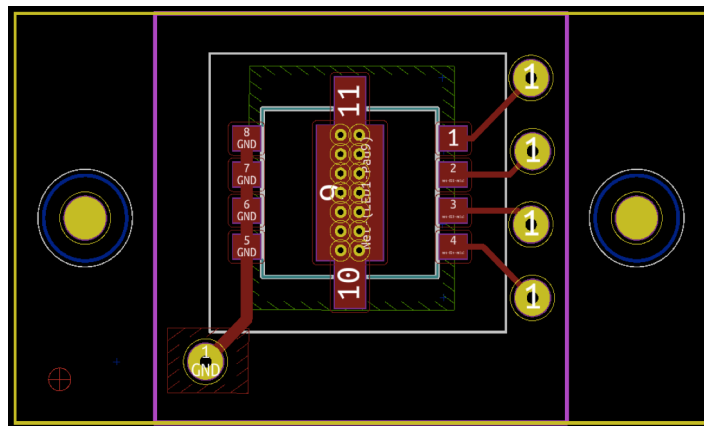


Figure 53: One of the PCBs with the LED mounted on it.

Using the same layout of traces and fingerprints described in the Subsection 3.3.3, the PCBs for the LEDs were designed in two different shapes, one for rows from A to D and another one for rows from E to M, and for completeness the Kicad tool Pcbnew view of both of them is shown in Figure 54. The PCB for the rows from A to D was designed to be placed on the back of the fourth surface by gluing its side ends to the Delrin surface, and the board size was 21.44 mm x13 mm. The 12 PCBs for the row A were grinded with an appropriate tool in order to match the triangular shape of these pixels. The PCBs for the rows from E to M were designed to be mounted by using two screws, and thus two non plated through-holes (NPTHs) (diameter of 1.78 mm) were added in the Kicad file. In this case the board size was 29.67 mm x 17.04 mm. In the PCBs for the rows from A to D the holes for the screws were not inserted due to the smaller dimensions of these pixels.



(a)



(b)

Figure 54: Final PCBs.

(a) Final PCB for rows from A to D in the Kicad tool Pcbnew. (b) Final PCB for rows from E to M in the Kicad tool Pcbnew.

4.1.6 Base and side walls

The flat faces of the base and side walls of each pixel were made of aluminum. The sheets of material (0.4064 mm thick) were ordered from McMaster-Carr and were cut by the LAS Physical Sciences Machine Shop at UIC. The number of base walls needed was 12 for rows A and B, and 24 for row C. The number of side walls needed was 12 for each row. The Solidworks files used for cutting pieces for each of the three rows are shown in the Figures in Section C.5 of the Appendix C. For completeness, a drawing of the base and side walls shape for one pixel of each row is also shown in the same section.

4.1.7 Black coating

The aluminum walls of the first chamber of each pixel were coated with a black adhesive back flock paper meant to absorb light, as already mentioned in the Subsection 3.3.3. The sheets of this light absorbing material (0.51 mm thick) were ordered from Edmund Optics and were cut using a custom-made cardboard tool to help get the required shape.

4.1.8 White coating

The aluminum walls of the second and the third chamber of each pixel were coated with a white reflective film, as already mentioned in the Subsection 3.3.3. It improves light diffusion of LEDs and it provides a reflectance of 98%^[47]. The sheets of this light absorbing material (0.23 mm thick) were ordered from White Optics in their version with adhesive and removable liner, and were laser cut at UIC Engineering Makerspace.

4.2 Assembling

Each aluminum base wall was joined to an aluminum side wall using Foil HVAC Tape (McMaster-Carr), an aluminum tape (25.4 mm wide, 0.08 mm thick) with acrylic adhesive. Then the black and the white adhesive coatings were applied, the former to the first chamber aluminum walls, and the latter to the second and third chamber aluminum walls. in Figure 55 three of the pieces obtained after this procedure are shown, one for each row. An acrylic glue was used to stick each of the four surfaces to the aluminium areas not covered by the coatings. Afterwards, the same acrylic glue was used to attach the pixels of each row together, starting from row A and ending with row C. At the beginning each pixel is composed of one base wall and one side wall, but when they are all put together the right sidewall of a pixel becomes also the left sidewall of the right neighbor, and the base wall forms also the top wall of the corresponding pixel in the following row. In order to reinforce the structure, very narrow elastic tapes wrapped around the rows were also used. Finally the PCBs were hot glued to the back of the Delrin surfaces after having soldered the wires in their PTHs. Each wire was connected to its appropriate hole in the breadboards, which contained the electronic control circuit previously described in the Subsection 3.3.4. Figure 56 shows the prototype during the hot gluing of the PCBs.

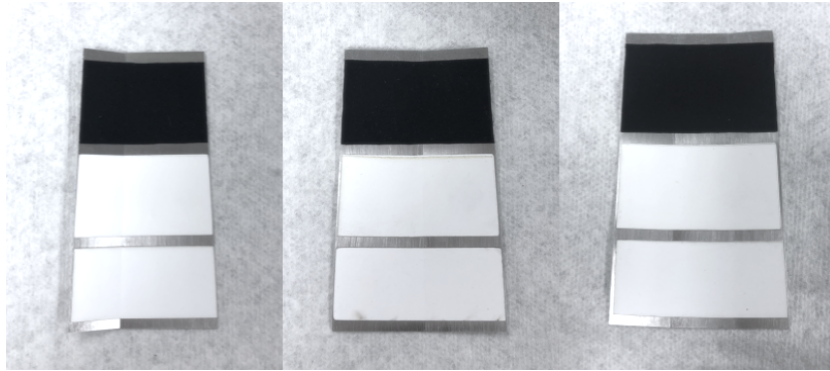


Figure 55: From the left, the aluminum walls for one pixel of rows A, B and C. Black and white coatings are also shown.

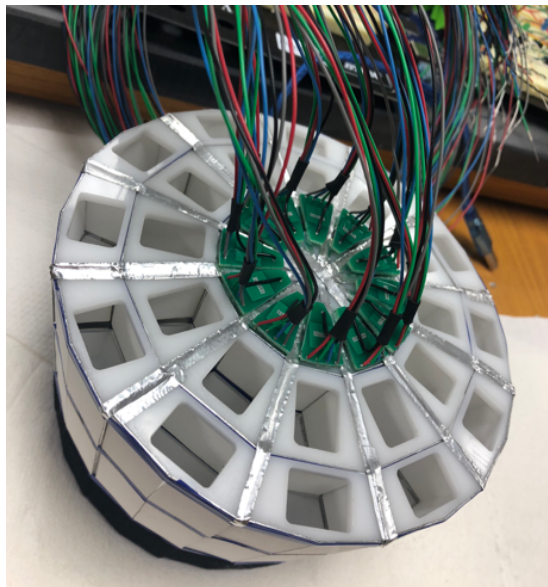


Figure 56: The assembled prototype during the hot gluing of the PCBs.

4.3 Results

Figure 57 shows different views of the stimulus source first three rows assembled.

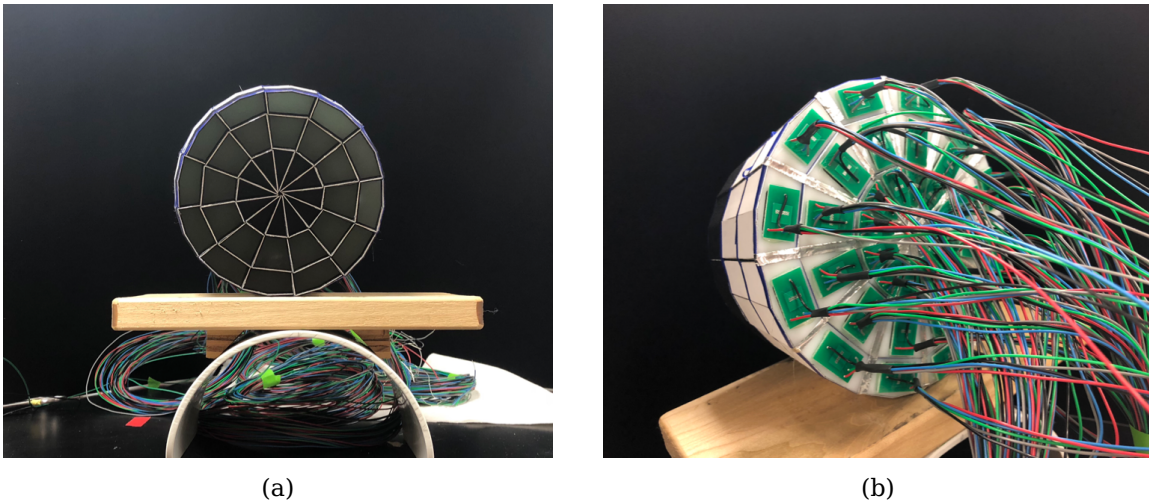


Figure 57: Different views of the prototype assembled.

(a) Front view of the prototype assembled. (b) Back view of the prototype assembled.

CHAPTER 5

SPECIFIC AIM 3

In this chapter the characterization and the testing of the novel stimulus source prototype are presented. First, luminance and its uniformity between pixels were measured and analysed. Then, the contrast obtained in pERG protocol was evaluated. Every experiment and evaluation were done for every LED color channel.

5.1 Methods

5.1.1 Luminance measurements

The photometer IL 1800, the photodiode detector SED100, the radiance barrel R485 and the photopic filter Y#19474 used for the triangular check prototype testing (as described in the Subsection 3.3.3) were used also to measure the luminance across all checks in the previous prototype, obtaining a coefficient of variation of 32%^[7]. Thus, the same apparatus was used to analyse photopic luminance given by the assembled pixels. The photodetector was firmly placed in front of each pixel surface using an appropriate holder, and the radiance barrel was used to let the photodetector be close enough to subtend as far as possible a visual field which included only the surface of the pixel. The tests were performed in a dark environment where the LED was the only light source on, the 5V bias button of the photometer was always kept off and a surface completely black was used to take zero measurements during instrument calibration. The current provided to each

LED was 200 mA (DC power supply), the same that will be used for ERG recordings, and luminance readings were made for each LED color of each pixel, for each of the three rows assembled. The mean μ , the standard deviation σ and then the coefficient of variation % were computed considering each time the luminance measures obtained from the twelve pixels of a row using one of the available colors, for all three rows and for each of the four colors.

5.1.2 Uniformity measurements

In order to analyse luminance uniformity across the viewing window of each pixel, one photograph of the device was taken for each color channel, with all the LEDs turned on and at 40 cm of distance from the device's center (fixation point). The current provided to each LED was 200 mA (DC power supply), the same that will be used for ERG recordings. Nikon Digital SLR D5100 was the camera used to take the photos. It allows the control of several parameters such as shutter speed, sensitivity and aperture, which can be adjusted to get a good exposure^[53]. The shutter speed represents the amount of time during which the shutter is open, and since slower shutter speed is needed to get more light into the sensor^[54], 1/100th of a second was the value chosen for the experiments. Furthermore, the human eye can detect light flashes about 1/100th of a second^[55]. The sensitivity of the image sensor is expressed in the standard International Organization of Standard (ISO) and it has a normal range of about 100 to 3200, in which lower numbers make the camera less sensitive to light and increase the grain of the picture^[56]. In order to prevent blown-out images because of the chosen shutter speed, the ISO needs to be set low^[54] and the

chosen value was 100. The camera aperture is usually written as a fraction called f-stop, and when a lower shutter speed is used it needs to be increased in order to prevent over-exposed photos^[54]. Since the highest f-stop number available on the camera was f/25, it was the value chosen for the experiments.

in the Subsection 3.3.3 the luminance uniformity across the triangular check prototype was estimated drawing two lines across the photograph of every check frontal viewing window in ImageJ, and then computing the coefficient of variation % of the grayscale intensity levels along each of the two lines. In order to obtain a more precise uniformity indicator, in this subsection the coefficient of variation % has been computed in Matlab, considering the entire area of the frontal viewing window of each check, for each row and for each colour. Each photograph was read using its `.tiff` file, which is a lossless compression file format. Then each file was reshaped in order to obtain a 3D image matrix, and converted to a 16-bit grayscale image, eliminating information about the hue and the saturation, but retaining information about luminance^[57]. In order to create a mask for each check to isolate it from the rest of the image and analyze it individually, the grayscale image was then converted to a binary image using a threshold of 0.15, 0.35, 0.09 and 0.6, for red, green, blue and white, respectively. At this point, the function `bwconncomp()` was used to return the components connected in terms of pixels found in the binary image. In fact, they represent the objects that populate the image, which in this case were the frontal viewing windows of the checks. Objects containing less than 1000 pixels were deleted as they were too small to represent a check. So, for each of the 36 objects thus obtained, a zeroes

matrix was filled with ones in the positions corresponding to the object itself, and then it was saved in a structure array, which after this procedure contained the binary masks for all the checks of an image. In Figure 58a an example of binary image containing all 36 checks is shown, while figure 58b shows an example of mask for one of the checks. Finally, each mask is multiplied for the grayscale image of the protograph analysed, making zero all elements of it except for the pixels corresponding to the object contained in the mask, which in turn corresponds to one of the checks. For each of the 36 images thus obtained, the average and the standard deviation were computed considering only the image area in which pixels had a value greater than 0. Then the coefficient of variation % of each check was obtained according to the Equation 3.1. The same Matlab algorithm was used for each of the four photographs taken, and the main code is reported in the Listing A.3 in the Section A.3 of the Appendix A.



Figure 58: Binary images obtained.

(a) An example of binary image containing all 36 checks. (b) An example of binary mask for one of the checks.

5.1.3 Contrast measurements

In the standard pERG, the contrast between black and white checks should be 80-100 %^[5]. In order to analyse contrast between the assembled checks, one photograph of the device was taken for each pERG phase at 40 cm of distance from the device's center (fixation point). The current provided to each LED was 200 mA (DC power supply), the same that will be used for ERG recordings. The color of greatest interest for pERG protocol is white, but for completeness then the same analysis was performed for each color channel. The camera used to take the photographs and the parameters chosen for its setting are identical to those already mentioned in Section 5.1.2. The `.tiff` file of each photo was read in Matlab, was reshaped in order to obtain a 3D image matrix, and then was converted to a 16-bit grayscale image.

First, the contrast was analysed computing the contrast ratio, a widely used contrast indicator:

$$\text{Contrast Ratio} = \frac{Lum_1 + 0.05}{Lum_2 + 0.05} \quad (5.1)$$

Lum_1 is the maximum relative luminance of the image and L_2 is the minimum one, with relative luminance normalized to 0 for darkest black and to 1 for lightest white. Contrast ratios range goes from 1 (contrast of 0 %) to 21 (contrast of 100 %).^[58]

However, the contrast ratio is not very suitable to represent the human perception of contrast. Matković et al. developed a method to compute an improved contrast factor in grayscale images, which is called GCF. The GCF is given by a weighted average of lo-

cal contrasts at various resolutions, since human vision sensitivity changes at different spatial frequencies. By applying a gamma correction and by scaling the pixels of the original grayscale image to the [0,1] range, linear luminance values are obtained and their square root gives approximated perceptual luminance values. In order to find the local contrast at the finest resolution (original grayscale image), local contrast of each pixel is computed by doing the average difference in terms of perceptual luminance between the considered pixel and its four neighbours. Then the average local contrast for the resolution considered is found by averaging the local contrast of each pixel. The average local contrast is computed for different resolutions, combining more pixels into one super pixel, using a different number of pixels for each resolution. The process stops when the pixels are so large that they are very few in the image. The weighting function was developed from the results of user experiments, in which the subjects had to order images according to the perceived contrast. After having assigned values to each image according to the experimental results of each user, the average relation number was computed for each image. Weight values were determined generating quasi-random numbers for some free parameters, and after sorting the GCF computed for every image, GCF values were compared with the experimental ones, already sorted. Finally, the optimum approximation was found by considering the correlation between the two ordered series.^[59] A version of this algorithm implemented in Matlab was found on GitHub (<https://gist.github.com/zabela/8539136>) and was used to compute the GCF of the taken photographs.

Since the GCF depends on the number of pixels of the image, an absolute maximum value cannot be determined. Thus, the binary images (threshold 0.6) of the two pERG phases using the white channel were converted into 16-bit grayscale images (shown in Figure 59) and used as reference to evaluate contrast in the photographs. Thus, their pixels are either 0 (black) or 65535 (white) and the GCF is 8.43 for the image 59a (phase A image), and 8.37 for the image 59b (phase B image). These two values are considered the optimum ones for phase A and phase B, respectively, resulting in a contrast of 100 %. The contrast ratio of these two images was computed as well (Equation 5.1), and as expected it was 21 in both cases, corresponding to a contrast of 100 %.

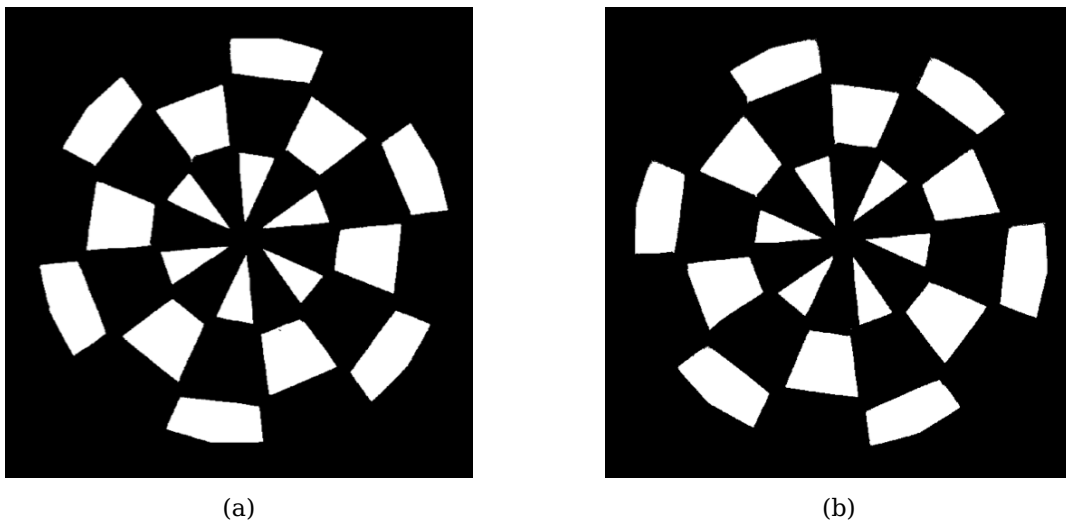


Figure 59: Binaryzed version of the images of pERG protocol phases. They were used as references to evaluate the photographs taken. (a) Reference for phase A. (b) Reference for phase B.

5.2 Results

5.2.1 Luminance measurements

According to the Equation 3.1, the coefficient of variation % of the measured luminance was found for each row and colour, and the results are shown in Table XI. Differently from the triangular check prototype mentioned in the Subsection 3.3.3, the pixels of rows A, B and C have a front window area smaller than the minimum area subtended by the sensor. The dimensions (width and height) of the pixels viewing window of the rows A, B and C are 12.56 mm x 23.93 mm, 17.95 mm x 19.57 mm and 26.57 mm x 14.05 mm, respectively. Consequently, the luminance measured is lower than that which would be obtained using a field of view that includes only the surface of the pixel. Indeed, the table XI shows that the luminance measured in pixels of row A is lower than luminance measured in pixels of row B and C. Instead, with the same current used to power the LEDs, the smaller pixels should have a higher luminance in the front window because the same amount of photons is distributed over a smaller area, increasing the candles per square meter. It should be noted that although the measured luminance is lower than expected due to the sensor not suitable for probing such small areas, it is much higher than the minimum required in protocols such as pERG (80 ph cd m⁻² [5]) and mfERG (100 cd m⁻² [4]).

However, the sensor used allowed to establish the maximum luminance uniformity across pixels which have the same shape, and therefore which belong to the same row. In fact, each luminance reading was made considering the maximum value obtainable by adequately positioning the sensor in front of each pixel surface. The results show that for

each row and for each colour the coefficient of variation is less than 4%, with a minimum of 0.79% for the white channel in row B and a maximum of 3.94% for the blue channel in row A.

TABLE XI: COEFFICIENT OF VARIATION % GIVEN BY THE LUMINANCE MEASUREMENTS MADE IN ORDER TO ANALYSE MAXIMUM LUMINANCE UNIFORMITY OF PIXELS BELONGING TO THE SAME ROW, FOR EACH COLOUR, POWERING EACH LED WITH 200 mA.

	Row A	Row B	Row C
Red channel mean luminance [ph cd m ⁻²]	5493.33	10958.33	10848.33
Red channel CV [%]	3.31	2.52	2.41
Green channel mean luminance [ph cd m ⁻²]	11196.67	22200.00	21504.17
Green channel CV [%]	3.56	1.18	3.28
Blue channel mean luminance [ph cd m ⁻²]	2015.25	4376.67	4069.17
Blue channel CV [%]	3.94	2.75	3.63
White channel mean luminance [ph cd m ⁻²]	12799.17	25975.00	24334.17
White channel CV [%]	3.65	0.79	2.87

5.2.2 Uniformity measurements

in Figure 60 the photographs used to analyse luminance uniformity across the checks are shown, one for each LED colour channel. As already mentioned in the Subsection 5.1.2,

the coefficient of variation % of each check was computed according to the Equation 3.1, for each 16-bit grayscale version of the four images. The tables XII, XIV, XIII and XV show the results for red, green, blue and white colour channel, respectively. Considering the individual pixels, the maximum coefficient of variation % was 11.72 for pixel 9 of the row A, using the blue LED colour channel, and the minimum was 6.50 for pixel 9 of the row B, using the white LED colour channel. Considering the rows, the maximum coefficient of variation % was 10.84 for row A using the blue LED colour channel, and the minimum was 7.19 for row B using the white LED colour channel. The minimum variation in luminance intensity considering all the checks was obtained using the white channel (8.18 %). Considering red, green and blue channels the coefficient of variation % was 9.77, 9.56 and 10.75, respectively. Therefore, all the results are more than halved compared to the luminance variation across checks measured in the previous prototype, which overall was 32 %. These results prove that the diffusive layers, the white reflective coating, the black absorbent coating and the glass front window used to build the new prototype have improved LED light diffusion, thus increasing luminance uniformity. In addition to this, it should be noted that the measurements of luminance uniformity made in the previous prototype did not take into account the entire area of a check, but only two lines drawn along its dimensions, as was done in the luminance uniformity experiments described in the Subsection 3.3.3. Therefore, the variation of 32 % obtained could increase considerably if the whole checks areas were considered. The experiment reported in this subsection does not have this limitation, since the algorithm used calculate the variation of luminance uniformity

across checks takes into account the whole area of each of them. Finally, each experiment was made using the same setting of the camera parameters, thus guaranteeing its reproducibility, differently from the experiments made on the previous prototype.

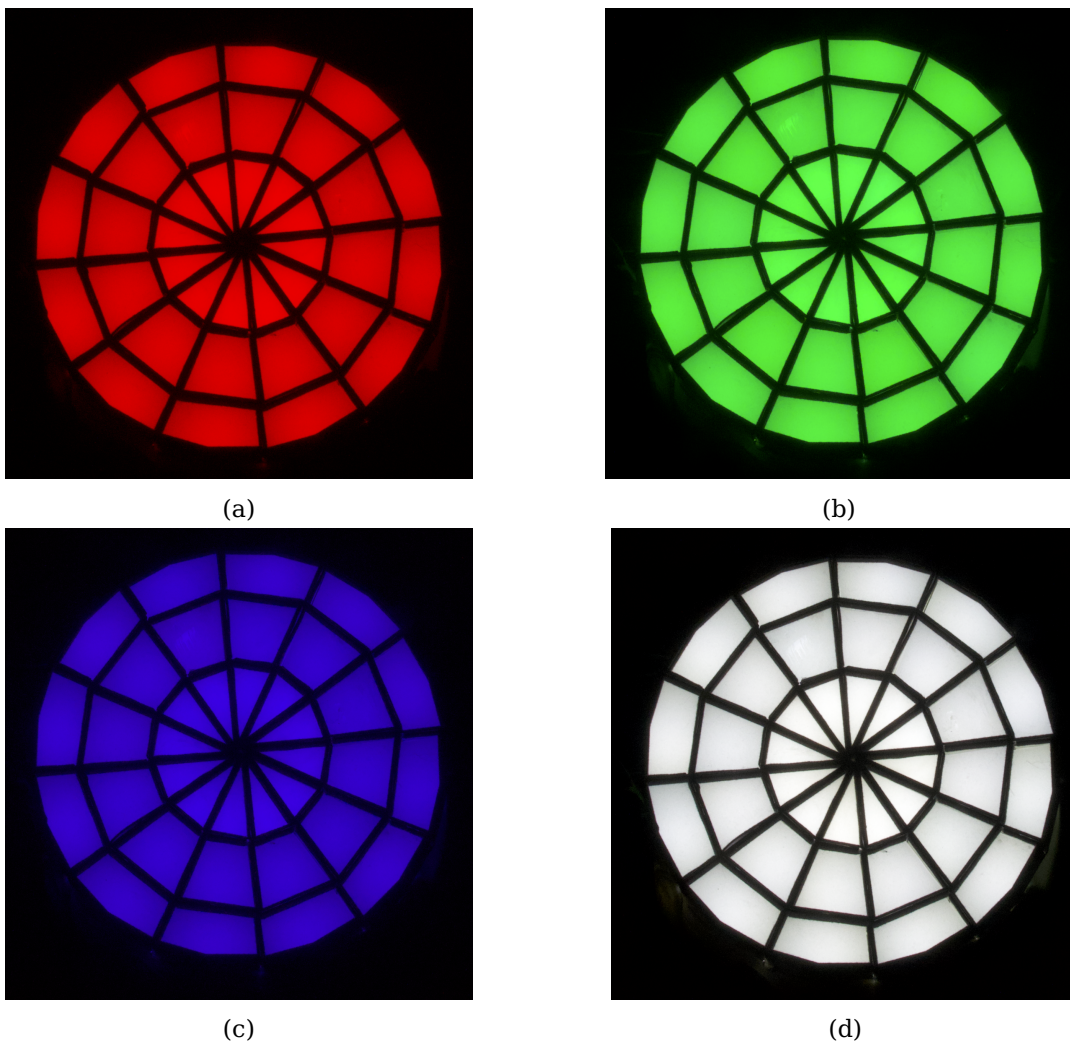


Figure 60: Original photographs of the assembled device with all LEDs on. For (a) red (b) green (c) blue and (d) white colour channel, they were used to analyse luminance uniformity.

TABLE XII: COEFFICIENT OF STANDARD DEVIATION % OF GREYSCAL INTENSITY LEVEL OF EACH PIXEL OF EACH ROW USING THE LED RED CHANNEL.

Red channel	Row A	Row B	Row C
Pixel 1 CV [%]	9.72	8.68	8.88
Pixel 2 CV [%]	9.43	9.11	9.20
Pixel 3 CV [%]	9.24	8.29	9.65
Pixel 4 CV [%]	10.14	8.06	9.95
Pixel 5 CV [%]	9.45	9.14	9.35
Pixel 6 CV [%]	9.90	7.84	9.08
Pixel 7 CV [%]	10.20	8.35	9.46
Pixel 8 CV [%]	9.46	7.93	9.52
Pixel 9 CV [%]	8.65	8.31	9.46
Pixel 10 CV [%]	9.46	8.65	9.24
Pixel 11 CV [%]	9.27	9.14	9.39
Pixel 12 CV [%]	9.11	8.62	9.76
12 pixels CV [%]	9.62	8.57	9.48
36 pixels CV [%]	9.77		

TABLE XIII: COEFFICIENT OF STANDARD DEVIATION % OF GREYSCAL INTENSITY LEVEL OF EACH PIXEL OF EACH ROW USING THE LED GREEN CHANNEL.

Green channel	Row A	Row B	Row C
Pixel 1 CV [%]	9.84	8.54	9.13
Pixel 2 CV [%]	10.90	8.68	8.66
Pixel 3 CV [%]	10.37	8.30	9.13
Pixel 4 CV [%]	10.54	8.91	8.37
Pixel 5 CV [%]	10.46	8.71	8.91
Pixel 6 CV [%]	10.06	8.59	8.94
Pixel 7 CV [%]	11.05	8.01	9.06
Pixel 8 CV [%]	10.06	9.25	9.43
Pixel 9 CV [%]	10.86	7.85	8.97
Pixel 10 CV [%]	10.25	8.22	9.22
Pixel 11 CV [%]	10.27	7.94	8.80
Pixel 12 CV [%]	10.12	8.23	9.62
12 pixels CV [%]	10.53	8.50	9.06
36 pixels CV [%]	9.56		

TABLE XIV: COEFFICIENT OF STANDARD DEVIATION % OF GREYSCAL INTENSITY LEVEL OF EACH PIXEL OF EACH ROW USING THE LED BLUE CHANNEL.

Blue channel	Row A	Row B	Row C
Pixel 1 CV [%]	10.49	9.32	10.38
Pixel 2 CV [%]	11.36	9.03	9.83
Pixel 3 CV [%]	10.34	9.11	10.20
Pixel 4 CV [%]	10.59	9.94	9.46
Pixel 5 CV [%]	10.84	9.55	9.92
Pixel 6 CV [%]	10.01	10.00	10.43
Pixel 7 CV [%]	11.70	8.97	10.50
Pixel 8 CV [%]	10.34	10.72	10.41
Pixel 9 CV [%]	11.72	8.62	9.98
Pixel 10 CV [%]	10.20	9.23	10.46
Pixel 11 CV [%]	10.48	8.60	10.32
Pixel 12 CV [%]	10.61	9.05	10.91
12 pixels CV [%]	10.84	9.47	10.39
36 pixels CV [%]	10.75		

TABLE XV: COEFFICIENT OF STANDARD DEVIATION % OF GREYSCAL INTENSITY LEVEL OF EACH PIXEL OF EACH ROW USING THE LED WHITE CHANNEL.

White channel	Row A	Row B	Row C
Pixel 1 CV [%]	7.40	7.19	8.17
Pixel 2 CV [%]	8.02	7.19	8.00
Pixel 3 CV [%]	7.23	7.04	7.81
Pixel 4 CV [%]	7.52	7.75	7.38
Pixel 5 CV [%]	7.79	7.25	7.76
Pixel 6 CV [%]	7.16	7.64	8.21
Pixel 7 CV [%]	8.38	6.66	8.00
Pixel 8 CV [%]	7.25	7.93	8.45
Pixel 9 CV [%]	8.62	6.50	7.76
Pixel 10 CV [%]	7.54	6.90	8.01
Pixel 11 CV [%]	7.66	6.66	8.20
Pixel 12 CV [%]	7.63	6.79	8.24
12 pixels CV [%]	7.76	7.19	8.04
36 pixels CV [%]	8.18		

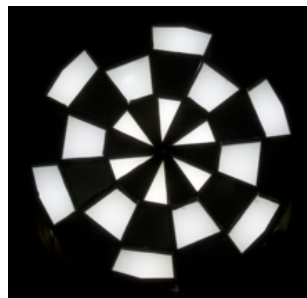
5.2.3 Contrast measurements

in Figure 61 the photographs used to analyse contrast between the assembled checks are shown, one for each phase, for each LED colour channel. Although the colour required by the ISCEV Standard pERG is white^[5] and coloured LEDs are not currently part of it, they may be used in versions of pERG different from the standard one, for example in order to separate cones and rods. Therefore, a contrast characterization was performed also for the other three LED colour channels.

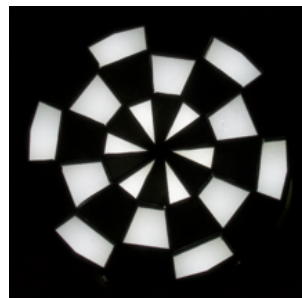
After the normalization to 0 for darkest black and to 1 for lightest white of every 16-bit grayscale version of the original images, the contrast ratio was computed according to Equation 5.1, and the results for each image are shown in the Table XVI. The contrast % was obtained considering to have a contrast of 100 % for a contrast ratio of 21. Then, GCF was computed for every image using the algorithm already mentioned in the Subsection 5.1.3, and the results are shown in the Table XVII. In this case the contrast % was obtained considering to have a contrast of 100 % for a GCF of 8.43 in phase A cases, and for a GCF of 8.37 in phase B cases.

Considering the colour channel of greatest interest for pERG protocol, the contrast between black and white checks is much higher than the minimum 80 % required by the Standard^[5], both considering contrast ratio and GCF, resulting in an average contrast between the two phases of 91.90 % in the latter indicator case. Both green and blue colour channels result in an average GCF % of 75.34 %, approaching very close to the minimum contrast required, while the red channel has the lowest average GCF %, which is 50.00 %.

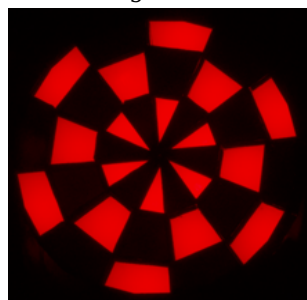
Finally, it can be observed that in the first experiment the % variation of contrast ratio between phase A and phase B is pretty high, with a maximum in red channel case (18.89 %). However, as already mentioned ppERGpERG 5.1.3, the contrast ratio only takes into account the maximum and minimum pixel values in each image, resulting in an unreliable contrast indicator. In fact, the contrast variation between the two phases decreases drastically when GCF values are considered (maximum variation of 0.82 % in red channel case), since this indicator better represents the human perception of contrast. The latter result also confirms the qualitative observation of the images, in which the perception that a person has during the observation of the two phases is that the contrast between checks is almost the same.



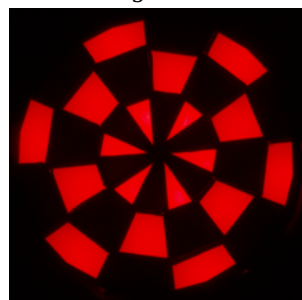
(a) Phase A using white LED channel



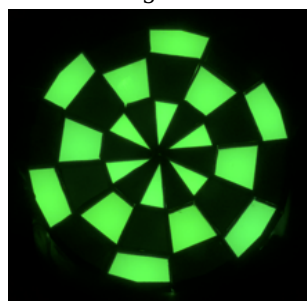
(b) Phase B using white LED channel



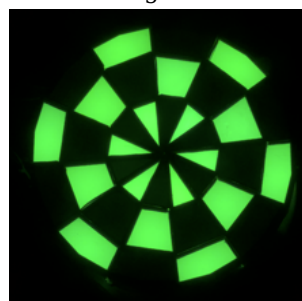
(c) Phase A using red LED channel



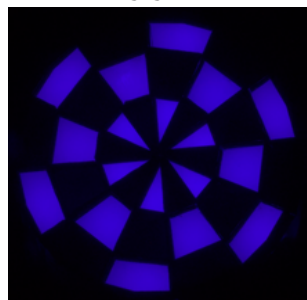
(d) Phase B using red LED channel



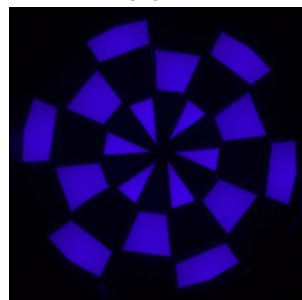
(e) Phase A using green LED channel



(f) Phase B using green LED channel



(g) Phase A using blue LED channel



(h) Phase B using blue LED channel

Figure 61: Photographs used to analyse contrast between the assembled checks.

TABLE XVI: CONTRAST RATIO AND RELATIVE CONTRAST % FOR EACH pERG PHASE 16-BIT GRAYSCALE IMAGE.

	Contrast ratio	Contrast %
White channel phase A	20.94	99.70
White channel phase B	20.58	97.99
Red channel phase A	8.36	39.79
Red channel phase B	9.93	47.30
Green channel phase A	16.39	78.05
Green channel phase B	16.50	78.58
Blue channel phase A	16.39	78.05
Blue channel phase B	16.50	78.58

TABLE XVII: GCF AND RELATIVE CONTRAST % FOR EACH pERG PHASE 16-BIT GRAYSCALE IMAGE.

	GCF	Contrast %
White channel phase A	7.73	91.66
White channel phase B	7.71	92.14
Red channel phase A	4.22	50.02
Red channel phase B	4.18	49.97
Green channel phase A	6.31	74.87
Green channel phase B	6.34	75.80
Blue channel phase A	6.31	74.87
Blue channel phase B	6.34	75.80

CHAPTER 6

DISCUSSION

6.1 Conclusions

The ERG is a functional test widely used in clinical practice to help diagnose retinal and optic nerve diseases^[18]. The most common stimulator in visual electrophysiology are Ganzfeld stimulators, spherical domes used to perform full-field ERG, and flat monitors, able to display patterns to perform standard central mfERG and pERG^[4,5,13]. Despite the conventional pERG testing is limited to the central retina resulting in a relatively low sensitivity^[7], it probes RGCs and it may be extremely useful in early detection of glaucoma, whose course begins with the damage of the peripheral RGCs^[20,21,32,33]. Since flat monitors are not really suited for the detection of peripheral dysfunctions, an hemispherical dome tilted with white LEDs in its peripheral part was developed and successfully validated by the Neural Engineering Vision Laboratory at UIC^[7]. The aim of this thesis is therefore the design, fabrication and testing of a highly-configurable full-field stimulus source for electroretinography, capable of presenting an arbitrary pattern of pixels to the entire visual field, bringing together the features of all the existing stimulators.

The design was done for the entire device, while only the central part of it was assembled and tested, as proof of concepts. The geometry chosen for the new full-field stimulus source was the hemispherical one. It consists of four concentric layers, each of which is

composed by flat faces and is made of different materials, which starting from the innermost layer are glass, two diffusive plastics, and Delrin. One face for each layer plus the side walls form three chambers and constitute a pixel. The coating chosen for the chambers between the glass and the first diffusive material was a light absorbing material, while the one chosen for the other chambers was an highly reflective film. 16 lateral pixels were added to the hemispherical geometry and this allowed to subtend an half angle of 105° , overcoming the 85° of the previous prototype^[7] and almost completely covering the human visual field limits. The shape chosen for the checks was the trapezoidal one, except for the most central one which was chosen to be triangular in order to close the dome. In fact, the trapezoidal shape was used also in the previous prototype and it allows to increase pixels dimensions from the center to the periphery of the device, maintaining at the same time an overall hemispherical geometry. This feature is consistent with the fact that peripheral ganglion cells have larger average receptive fields^[7].

The assembled part of the device consisted in 36 total pixels, each of which has one RGBW LED glued on its back side. LEDs were chosen because of their ideal features as light sources^[24], and each of them was mounted on a PCB properly designed. Preliminary experiments on a triangular prototype of the pixels have shown that simply by varying the duration of the stimulus or the intensity of the current, it is possible to obtain almost all luminance and stimulus strength values required by the ERG protocols Standards. The luminance stability of the chosen LED was also analyzed, obtaining satisfactory results. Regarding the electronic layout, despite it was developed to control only the 36 LEDs

constituting the assembled prototype, it has been made so that in future it can be easily expanded to the control of the entire device. The hardware part consisted in a microcontroller, five shift registers and several solid-state relays. The shift registers in cascade allowed to control the stimulus source pattern extremely easily via software, sending strings of bits to the shift registers and then connecting each of their output to one different LED. Four digital pins of the microcontroller were used to choose the colour of the LEDs. A user-friendly interface which allows protocol and colour selection was developed in LabVIEW. The protocols chosen as proof of concepts for the implementation were the pERG and the flicker ERG, but several different protocols can be easily added just changing the bits sequences sent to the shift registers.

Finally, the novel stimulus source prototype was characterized and tested. Maximum luminance measurements across each pixel were performed using a photodetector and a photometer, resulting in a coefficient of variation smaller than 4 % for each pixel shape and for each colour. Then, photographs of the prototype with all LEDs on were taken for each colour channel using fixed camera parameters. The coefficient of variation % of the grayscale intensity levels along the pixels area was computed and the maximum variation considering the individual pixels, all the pixels having the same shape and finally all the prototype pixels was 11.72 %, 10.84 % and 10.75 %, respectively. Considering all the pixels, the minimum variation of 8.18 % was obtained with the white channel. Therefore, the concern about the 32 % luminance variation across the pixels of the previous device^[7] was largely overcome, resulting in a percentage variation of less than half in each experiment

performed. Consequently, the results prove that the diffusive layers, the white reflective coating, the black absorbent coating and the glass front window used to build the new prototype have improved LED light diffusion, thus decreasing luminance variation. Since in pERG the contrast between ON- and OFF- pixels is an important parameter which has to be taken into account, photographs of the device running this protocol were taken for each pERG phase and for each colour channel. The contrast was evaluated using different definitions of it, in particular the contrast ratio^[58] and the global contrast factor^[59]. Considering the colour channel of greatest interest for pERG protocol, the contrast between black and white checks was much higher than the minimum 80 % required by the Standard^[5], for all the definitions of contrast used.

6.2 Limitations and future works

First of all, the black coating used in the first chamber is too much thick (0.51 mm) and therefore is visible to the subject, as it can be seen from the photographs shown in the Figure 60 . Ideally, a subject placed 40 cm away from the center of the dome should not see lines of separation between pixels. Hence, this material should be removed and replaced with a less thick one, such as Metal Velvet Adhesive Foil Sheet^[60] ($\sim 100 \mu m$ thick).

In addition, the dome should be completed by assembling the rows from D to M. Most of the materials for the whole device assembling have already been purchased, and therefore should be cut by the machine shops. To ensure stability to the structure, the dome should be mounted on a support, such as the wooden housing used in the previous prototype. The printed circuit boards for row D have already been purchased, while those for the other

rows have still to be ordered. The electronic circuit developed has to be extended, always using the same logic and the same types of components. In order to make the circuit more reliable, solderable perfboards could be used instead of breadboards for connections between the electronic components. Alternatively, a PCB or more PCBs for one or more parts of the electronic layout could be custom-designed.

When the device will be fully assembled, a calibration must be performed in order to adjust the current of each LED. In fact, the average luminance value of each pixel needs to be as close as possible. Thanks to the flexibility of the designed electronic circuit, it can be done simply by using a different value for the resistances of the LEDs, which instead in the proof of concepts presented is the same for each LED. The photodetector used is not suitable to measure an exact average luminance value because its size is too big to probe the smallest pixels. Thus, another optic probe such as a fiber optic cable may be used, which is particularly suitable for measuring luminance of small areas.

Moreover, after the calibration photopic luminance and stimulus strength should be explored in function of stimulus duration and current, similarly to what was already done with the triangular check prototype in the Subsection 3.3.3. This analysis will confirm whether the LEDs and the materials chosen allow to obtain all the minimum and maximum values required by the standards. Furthermore, it may also be useful to understand how luminance uniformity varies depending on the current supplied.

Finally, the ability to deliver effective and standards-compliant full-field flash and pattern stimuli needs to be evaluated using volunteer subjects. An Institutional Review Board

(IRB) approved human subjects protocol is in place for this work. Additionally, the possibility to deliver different full-field colour and pattern stimuli will allow the evaluation of the effectiveness of stimuli not present in the current standards. Other protocols needs to be added to the user-friendly LabVIEW interface, as well as the possibility to control other parameters such as frequency, stimulus duration and test duration.

APPENDICES

Appendix A

ALGORITHMS

A.1 Algorithm for Solidworks dome construction

The algorithm computes the heights and the radii of the circumferences circumscribed to the polygons which are then used to sketch the flat faces in each row of the dome, for each of the four shells. The algorithm was implemented in Matlab.

Listing A.1: Algorithm for Solidworks dome construction

```
1 %Radii are in centimeters and angles are in degrees
2 R=[40]; %The same algorithm is run for R=40, R=43, R=46, R=49
3 w=[];
4 a=[];
5 theta=360/24;
6 gamma=theta;
7 w=[w;2*R(1)*sind(theta/2)];
8 h=w(1);
9 alpha=(180-gamma)/2;
10 beta=alpha;
11 r=h*cosd(beta);
12 R=[R;R(1)-r];
13 a=[a;h*sind(beta)];
14
15 for i=2:100
16     if(h>=1.5)
17         w=[w;2*R(i)*sind(theta/2)];
18         h=w(i);
19         gamma=2*asind(h/(2*R(1)));
20         alpha=(180-gamma)/2;
21         delta=acosd(R(i)/R(1));
22         beta=alpha-delta;
23         r=h*cosd(beta);
24         R=[R;R(i)-r];
25         a=[a;h*sind(beta)];
```

Appendix A (Continued)

```
26     end
27 end
```

A.2 Algorithm for the electronic control of 36 LEDs

The algorithm controls 36 LEDs using serial communication between Arduino AtMega 2560 and LabVIEW, which is the graphical IDE. It was implemented in the open-source Arduino IDE.

Listing A.2: Algorithm for the electronic control of 36 LEDs

```
1 #include <Wire.h>
2 #include <SPI.h>
3 #include <Servo.h>
4 #include "LabVIEWInterface.h"
5
6 //RCLK
7 int Pinlatch = 8;
8 ////SER
9 int Pindata = 11;
10 //SRCLK
11 int Pinclock = 12;
12 int PIN;
13 byte datashift1;
14 byte datashift2;
15 byte datashift3;
16 byte datashift4;
17 byte datashift5;
18 byte Arraydata[2];
19 String labview;
20 unsigned int interval[2];
21 unsigned int iter;
22
23 void setup()
24 {
25     pinMode(Pinlatch, OUTPUT);
26     Serial.begin(9600);
27     pinMode(2, OUTPUT);
28     pinMode(3, OUTPUT);
29     pinMode(4, OUTPUT);
```

Appendix A (Continued)

```
30 pinMode(5,OUTPUT);
31 digitalWrite(2,LOW); //R
32 digitalWrite(3,LOW); //G
33 digitalWrite(4,LOW); //B
34 digitalWrite(5,LOW); //W
35
36 syncLV();
37
38 }
39
40 void loop() {
41     // send data
42     if (Serial.available()) {
43         // read data:
44         char labview = Serial.read();
45         switch (labview) {
46             case 'R':
47                 PIN=2; //Controls red LEDs
48                 Arraydata[0] = 0b10101010; //first phase of pERG
49                 Arraydata[1] = 0b01010101; //second phase of pERG
50                 interval[0]=217; //time duration of the first phase [ms]
51                 interval[1]=217; //time duration of the second phase [ms]
52                 iter=150; //number of times that the above sequence is
53                     //repeated (300 total reversals)
54                 break;
55             case 'G':
56                 PIN=3; //Controls green LEDs
57                 Arraydata[0] = 0b10101010;
58                 Arraydata[1] = 0b01010101;
59                 interval[0]=217;
60                 interval[1]=217;
61                 iter=150;
62                 break;
63             case 'B':
64                 PIN=4; //Controls blue LEDs
65                 Arraydata[0] = 0b10101010;
66                 Arraydata[1] = 0b01010101;
67                 interval[0]=217;
68                 interval[1]=217;
69                 iter=150;
70                 break;
71             case 'W':
72                 PIN=5; //Controls white LEDs
```

Appendix A (Continued)

```
73     Arraydata[0] = 0b10101010;
74     Arraydata[1] = 0b01010101;
75     interval[0]=217;
76     interval[1]=217;
77     iter=150;
78     break;
79
80     case 'r':
81     PIN=2; //Controls red LEDs
82     Arraydata[0] = 0b11111111; //first phase of flicker ERG
83     Arraydata[1] = 0b00000000; //second phase of flicker ERG
84     interval[0]=2; //time duration of the first phase [ms]
85     interval[1]=31; //time duration of the second phase [ms]
86     iter=100; //number of times that the above sequence is
87             //repeated (100 repetitions of the stimulus)
88     break;
89     case 'g':
90     PIN=3;
91     Arraydata[0] = 0b11111111;
92     Arraydata[1] = 0b00000000;
93     interval[0]=2;
94     interval[1]=31;
95     iter=100;
96     break;
97     case 'b':
98     PIN=4;
99     Arraydata[0] = 0b11111111;
100    Arraydata[1] = 0b00000000;
101    interval[0]=2;
102    interval[1]=31;
103    iter=100;
104    break;
105    case 'w':
106    PIN=5;
107    Arraydata[0] = 0b11111111;
108    Arraydata[1] = 0b00000000;
109    interval[0]=2;
110    interval[1]=31;
111    iter=100;
112    break;
113    }
114
115    pinMode(PIN, OUTPUT);
```

Appendix A (Continued)

```
116     digitalWrite(PIN,HIGH);
117     for (int i=0;i<iter;i++){
118         for (int j = 0; j < 2; j++) {
119             datashift1 = Arraydata[j];
120             datashift2 = Arraydata[j];
121             datashift3 = Arraydata[j];
122             datashift4 = Arraydata[j];
123             datashift5 = Arraydata[j];
124             digitalWrite(Pinlatch, 0);
125             shiftOut(Pindata, Pinclock, datashift1);
126             shiftOut(Pindata, Pinclock, datashift2);
127             shiftOut(Pindata, Pinclock, datashift3);
128             shiftOut(Pindata, Pinclock, datashift4);
129             shiftOut(Pindata, Pinclock, datashift5);
130             digitalWrite(Pinlatch, 1);
131             delay(interval[j]);
132         }
133     }
134     digitalWrite(PIN,LOW);
135 }
136 }
137
138 void shiftOut(int insDataPin, int insClockPin, byte insDataOut) {
139
140     int i=0;
141     int State;
142     pinMode(insClockPin, OUTPUT);
143     pinMode(insDataPin, OUTPUT);
144     digitalWrite(insDataPin, 0);
145     digitalWrite(insClockPin, 0);
146
147     for (i=7; i>=0; i--) {
148         digitalWrite(insClockPin, 0);
149         if ( insDataOut & (1<<i) ) {
150             State= 1;
151         }
152         else {
153             State= 0;
154         }
155
156         digitalWrite(insDataPin, State);
157         digitalWrite(insClockPin, 1);
158         digitalWrite(insDataPin, 0);
```

Appendix A (Continued)

```

159 }
160 //stop shifting
161 digitalWrite(insClockPin, 0);
162 }

```

A.3 Algorithm to analyse the luminance uniformity of checks

Listing A.3: Algorithm to analyse the luminance uniformity of checks

```

1 I = imread('red.tiff'); %the algorithm is applied to four files:
2                               %red.tiff, green.tiff, blue.tiff and white.tiff
3 I=I(:,:,1:3);%3D matrix
4 I_gray = rgb2gray(I);
5 BW = im2bw(I_gray,0.15); %red 0.15, %green 0.35, %blue 0.09, %white 0.6
6
7 objects = bwconncomp(BW);
8 numPixels = cellfun(@numel,objects.PixelIdxList);
9 for i=1:size(numPixels,2)
10     if numPixels(i)<1000
11         BW(objects.PixelIdxList{i}) = 0;
12     end
13 end
14
15 objects = bwconncomp(BW);
16 P={}; %structure array containing the masks
17 pixel = false(size(BW));
18 for i=1:36
19     pixel(objects.PixelIdxList{i}) = true;
20     figure
21     imshow(pixel)
22     P{i}=uint16(pixel);
23     pixel = false(size(BW));
24 end
25
26 %Apply the masks to the grayscale image
27 for i=1:36
28     P{i}=I_gray.*P{i};
29 end
30
31 %Create structure array containing only the values of interest
32 tot_pix={};
33 values=[];

```

Appendix A (Continued)

```
34 for k=1:36
35     pixel=P{k};
36     for i=1:size(pixel,1)
37         for j=1:size(pixel,2)
38             if pixel(i,j)>0
39                 values=[values;pixel(i,j)];
40             end
41         end
42     end
43     tot_pix{k}=values;
44     values=0;
45 end
46
47 %Compute the mean, the standard deviation and the CV %
48 mu=[];
49 sigma=[];
50 CV=[];
51 for i=1:36
52     data=double(tot_pix{i});
53     mu=[mu;mean(data)];
54     sigma=[sigma;sqrt(var(data))];
55     CV=[CV;(sigma(i)/mu(i))*100];
56 end
```


Appendix C

SOLIDWORKS DRAWINGS

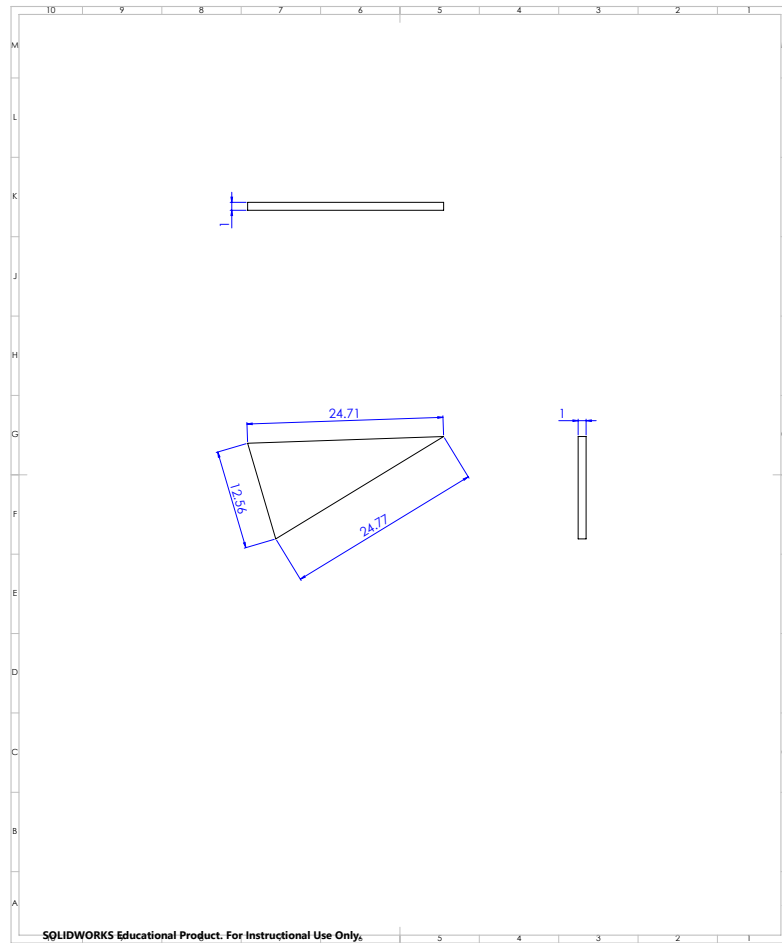
Appendix C (Continued)**C.1 First layer**

Figure 63: Surface 1 section of row A

Appendix C (Continued)

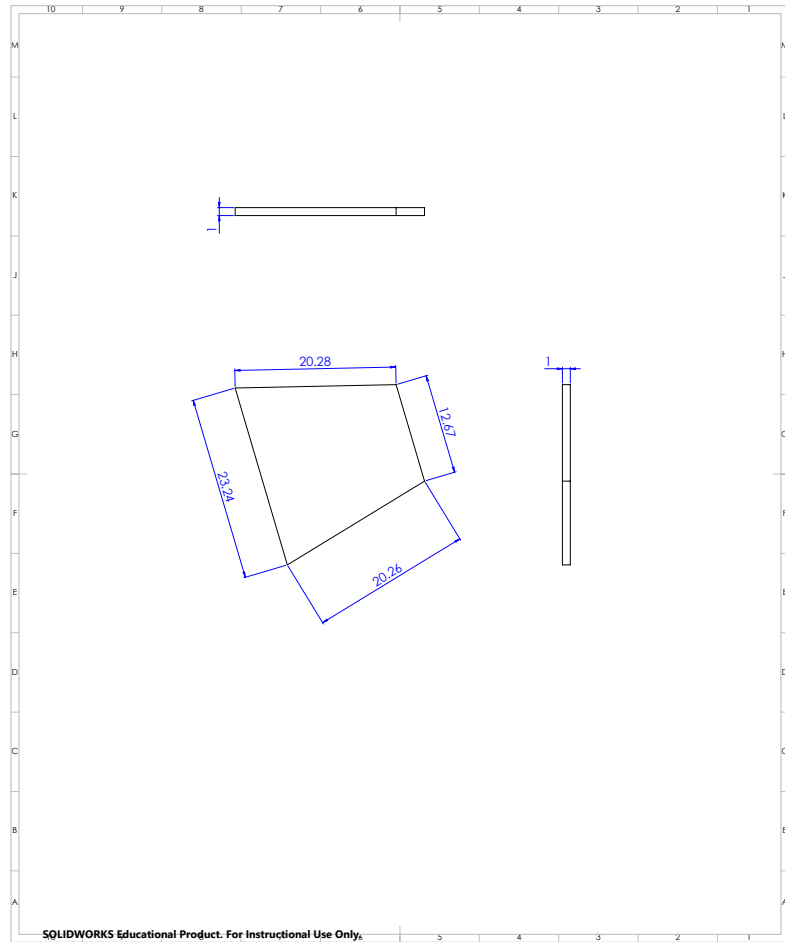


Figure 64: Surface 1 section of row B

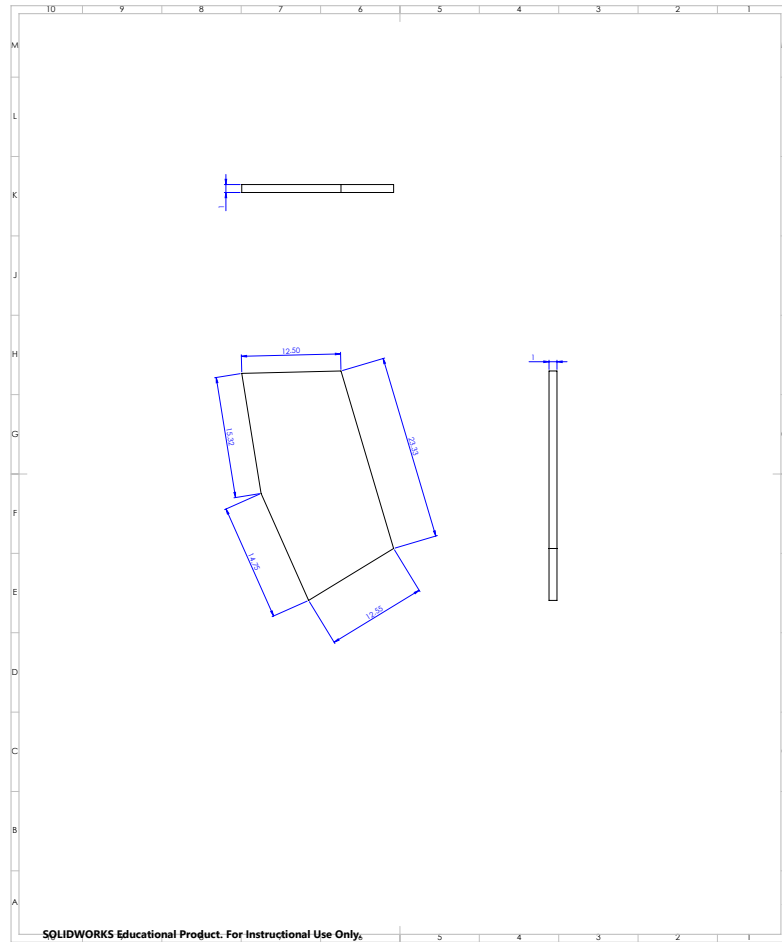
Appendix C (Continued)

Figure 65: Surface 1 section of row C

Appendix C (Continued)

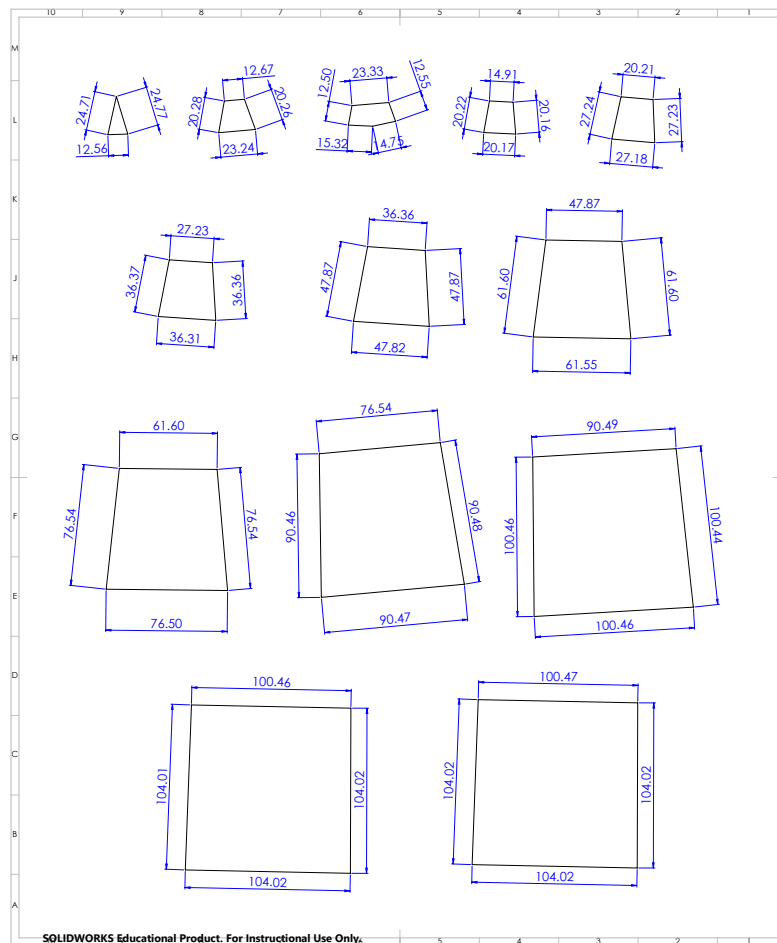


Figure 66: Surface 1 front view of each row (A-M)

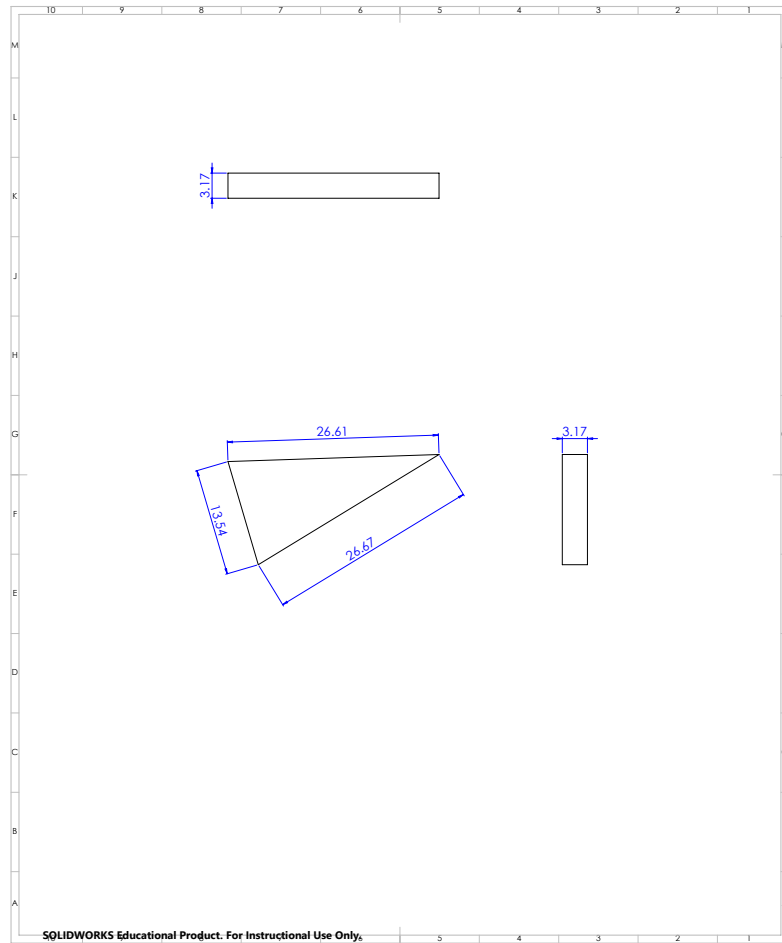
Appendix C (Continued)**C.2 Second layer**

Figure 67: Surface 2 section of row A

Appendix C (Continued)

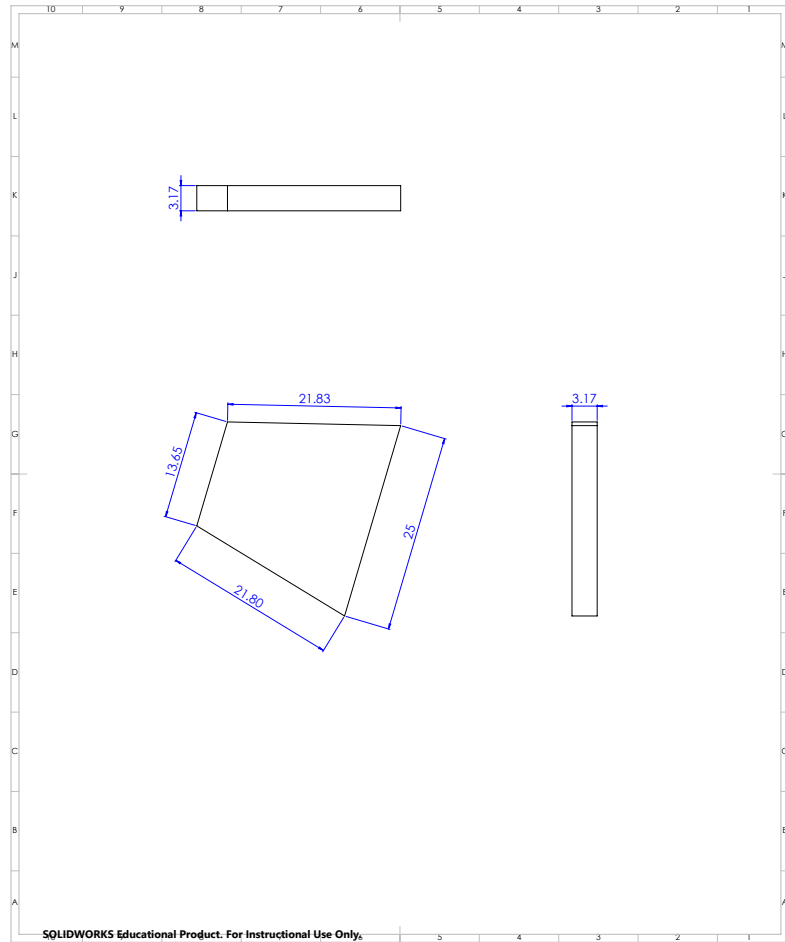


Figure 68: Surface 2 section of row B

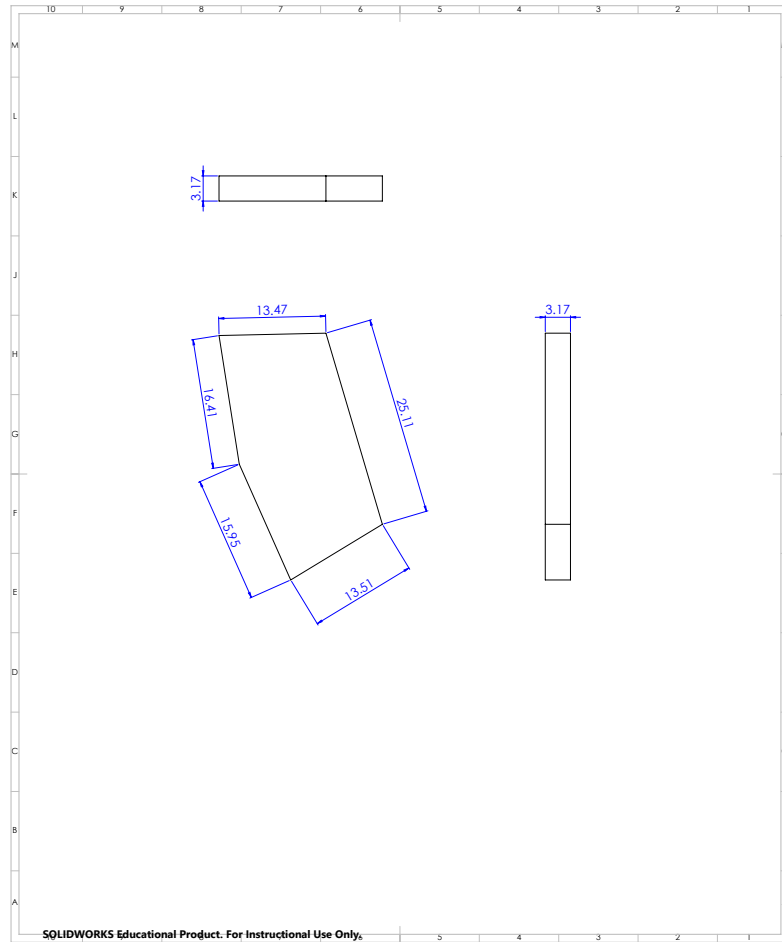
Appendix C (Continued)

Figure 69: Surface 2 section of row C

Appendix C (Continued)

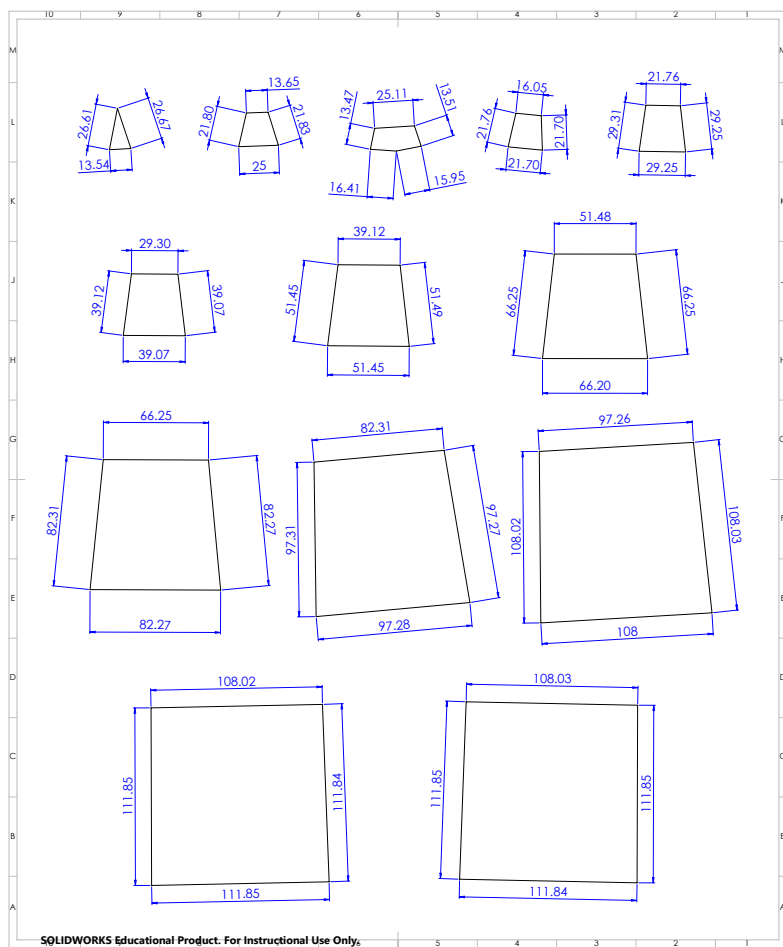


Figure 70: Surface 2 front view of each row (A-M)

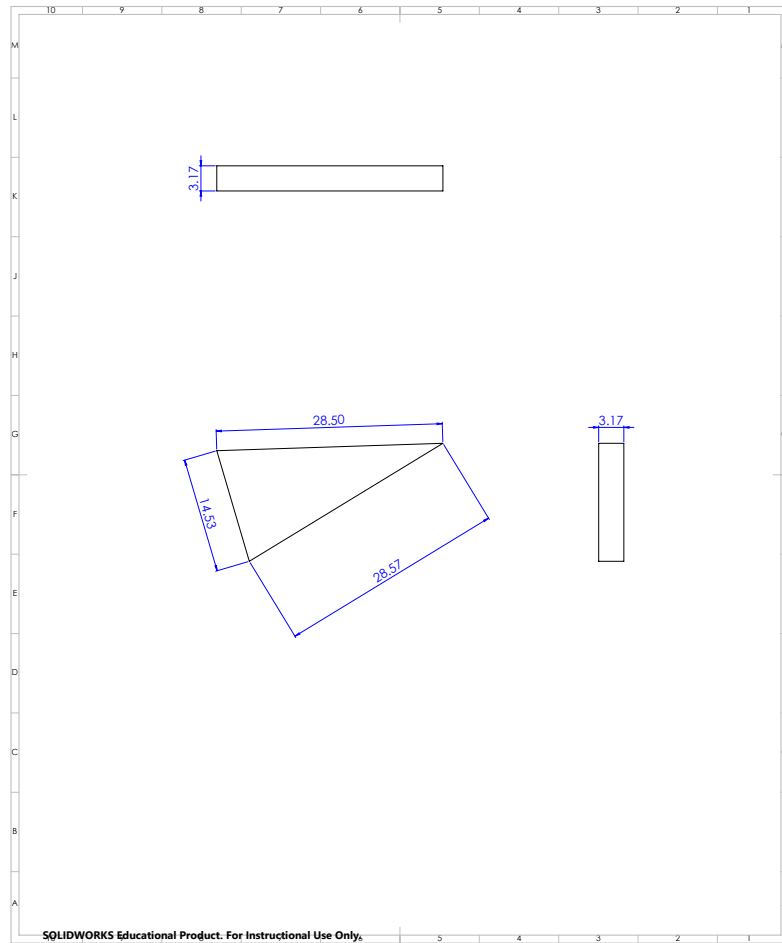
Appendix C (Continued)**C.3 Third layer**

Figure 71: Surface 3 section of row A

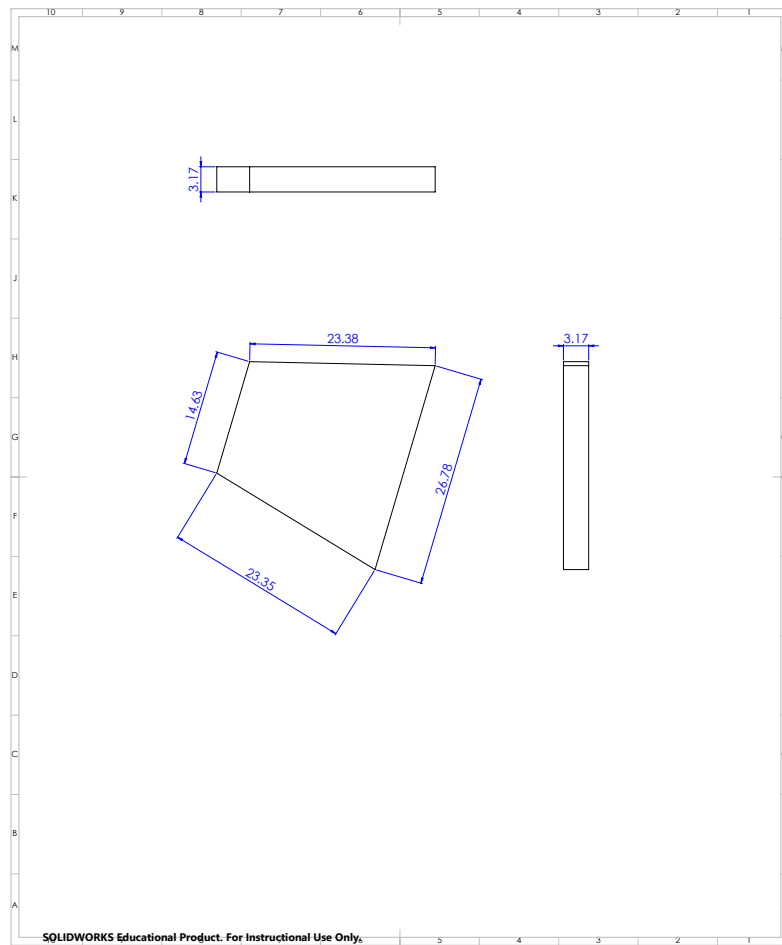
Appendix C (Continued)

Figure 72: Surface 3 section of row B

Appendix C (Continued)

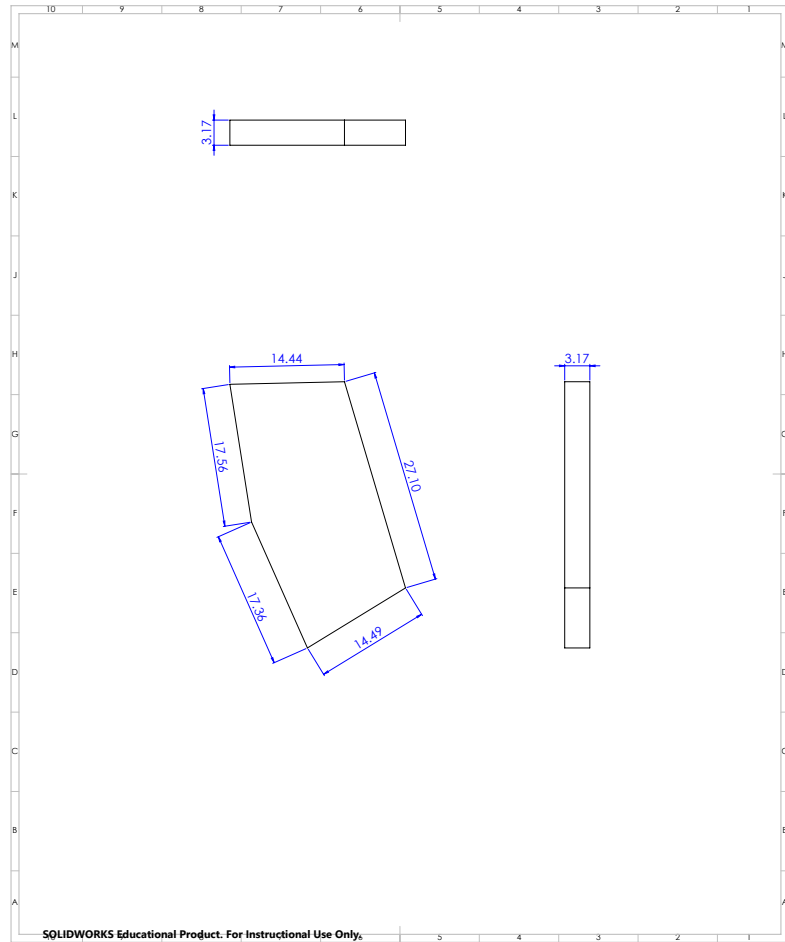


Figure 73: Surface 3 section of row C

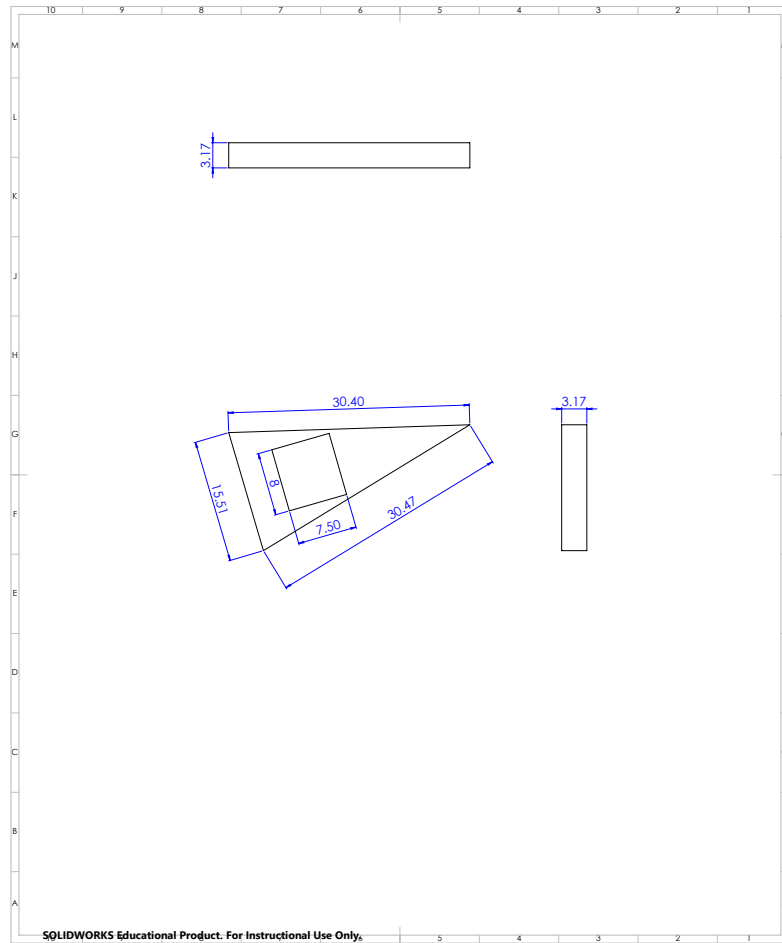
Appendix C (Continued)**C.4 Fourth layer**

Figure 75: Surface 4 section of row A

Appendix C (Continued)

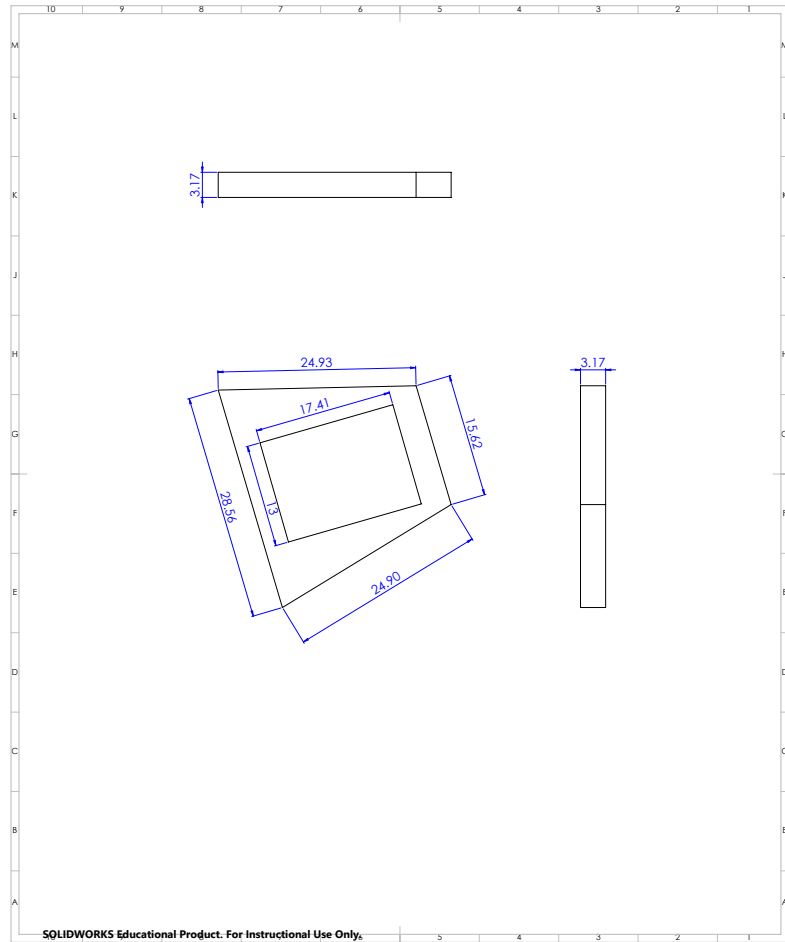


Figure 76: Surface 4 section of row B

Appendix C (Continued)

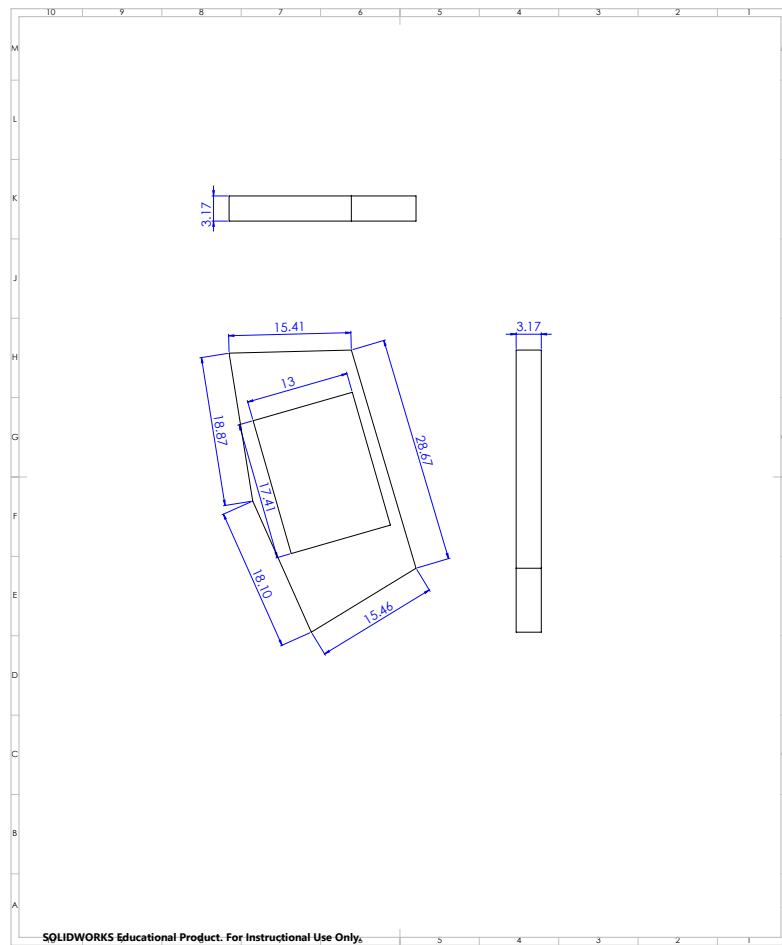


Figure 77: Surface 4 section of row C

Appendix C (Continued)

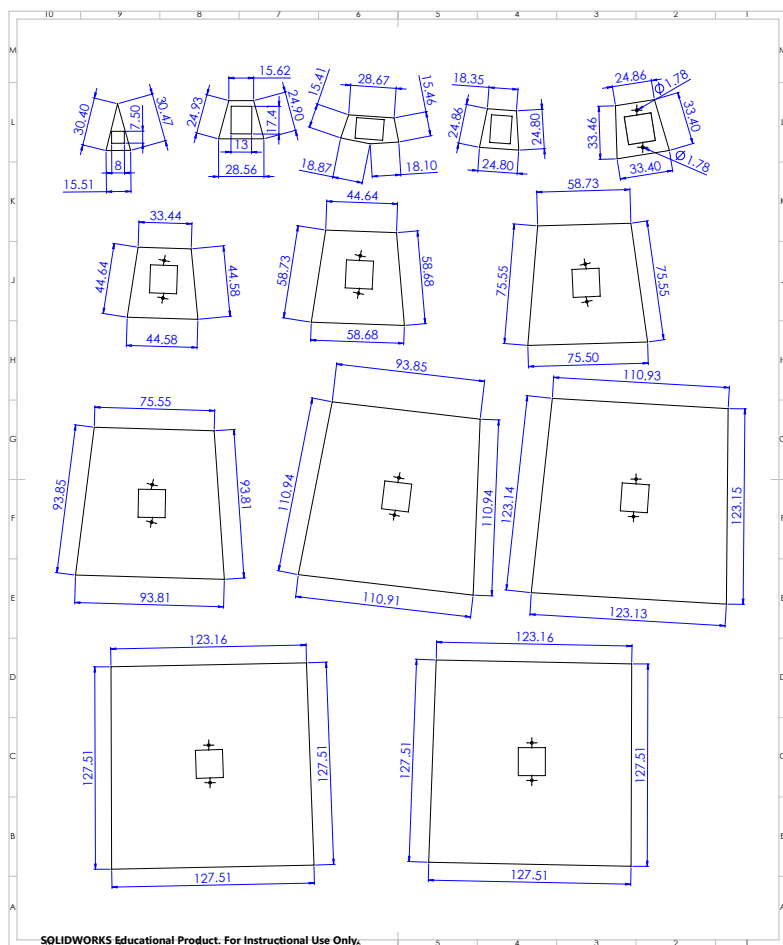


Figure 78: Surface 4 front view of each row (A-M)

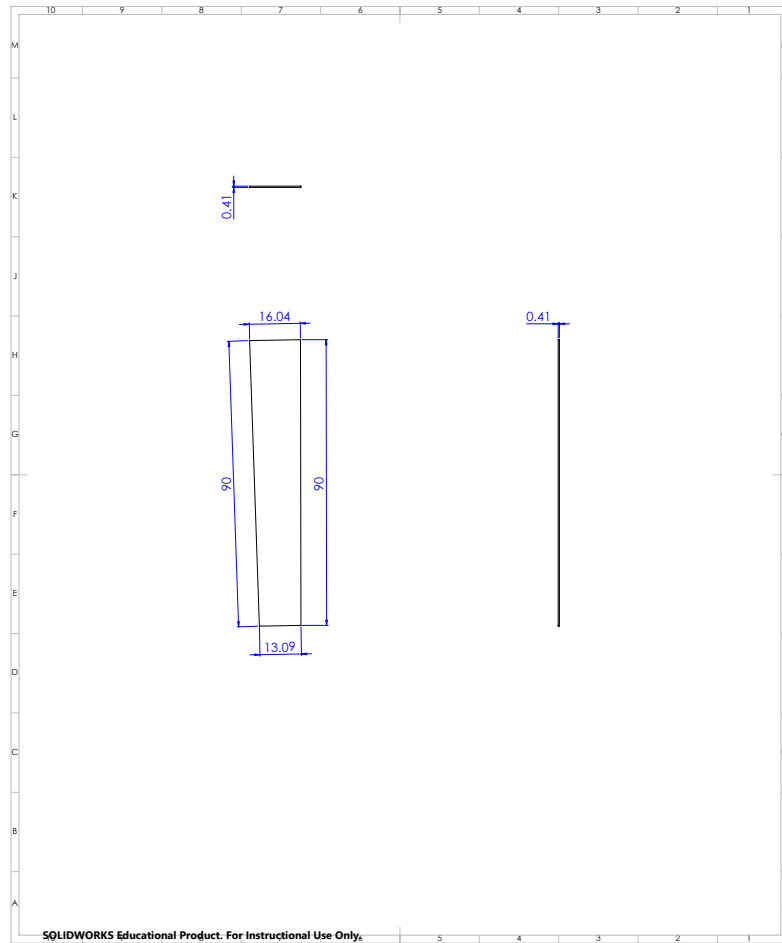
Appendix C (Continued)**C.5 Base and side walls**

Figure 79: Base wall section of row A

Appendix C (Continued)

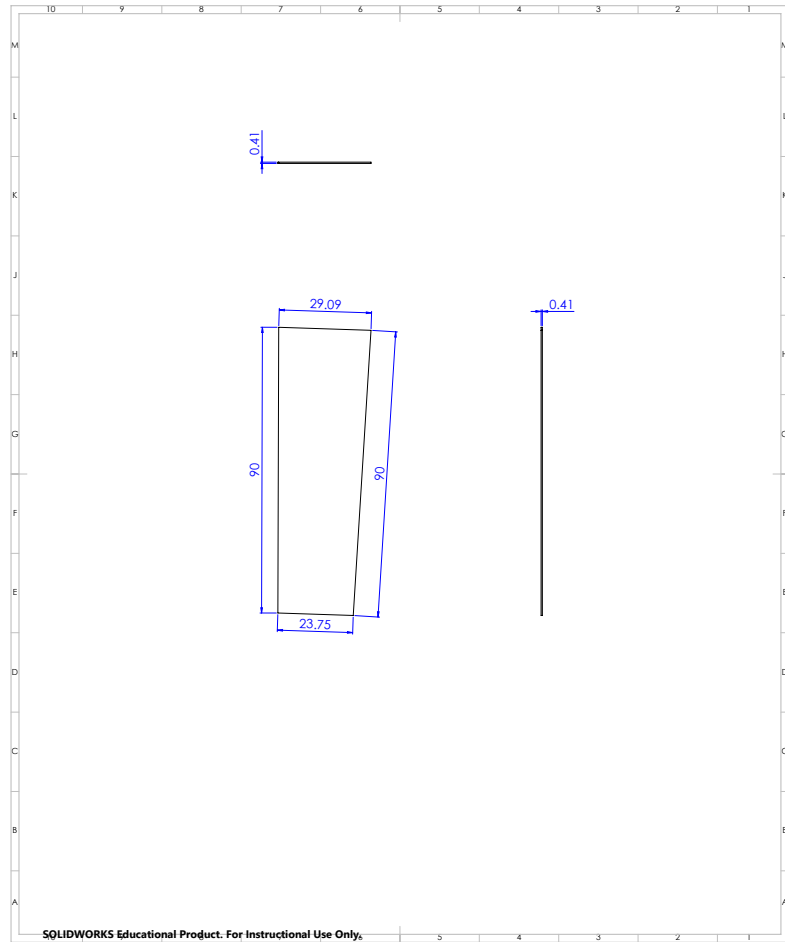


Figure 80: Base wall section of row B

Appendix C (Continued)

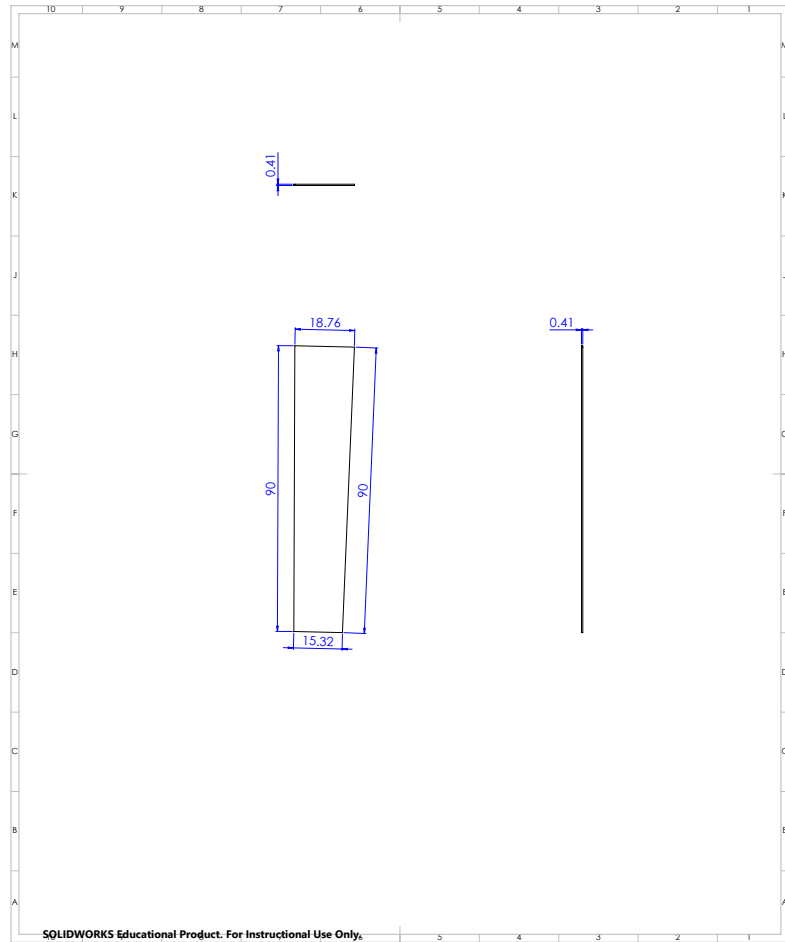


Figure 81: Base wall section of row C

Appendix C (Continued)

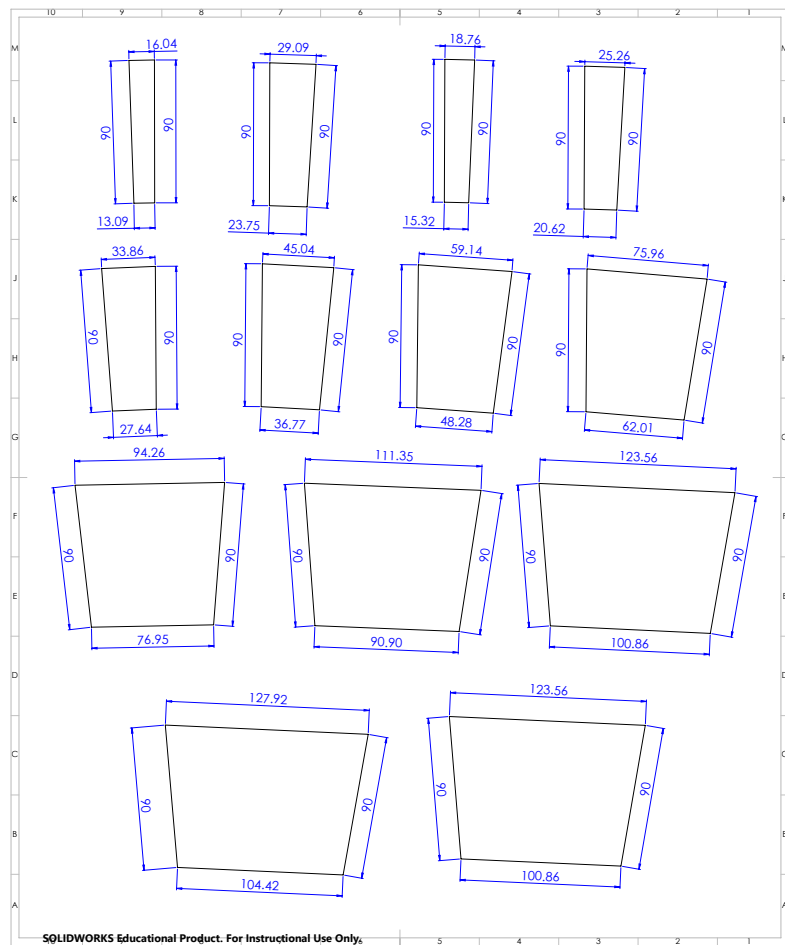


Figure 82: Base wall front view of each row (A-M)

Appendix C (Continued)

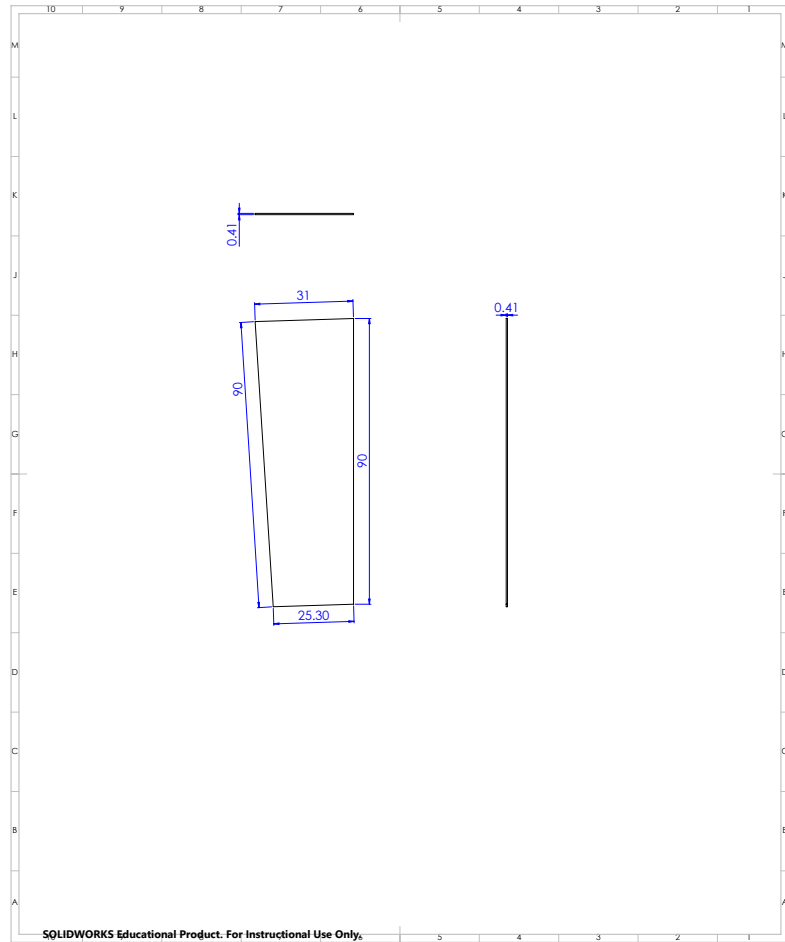


Figure 83: Side wall section of row A

Appendix C (Continued)

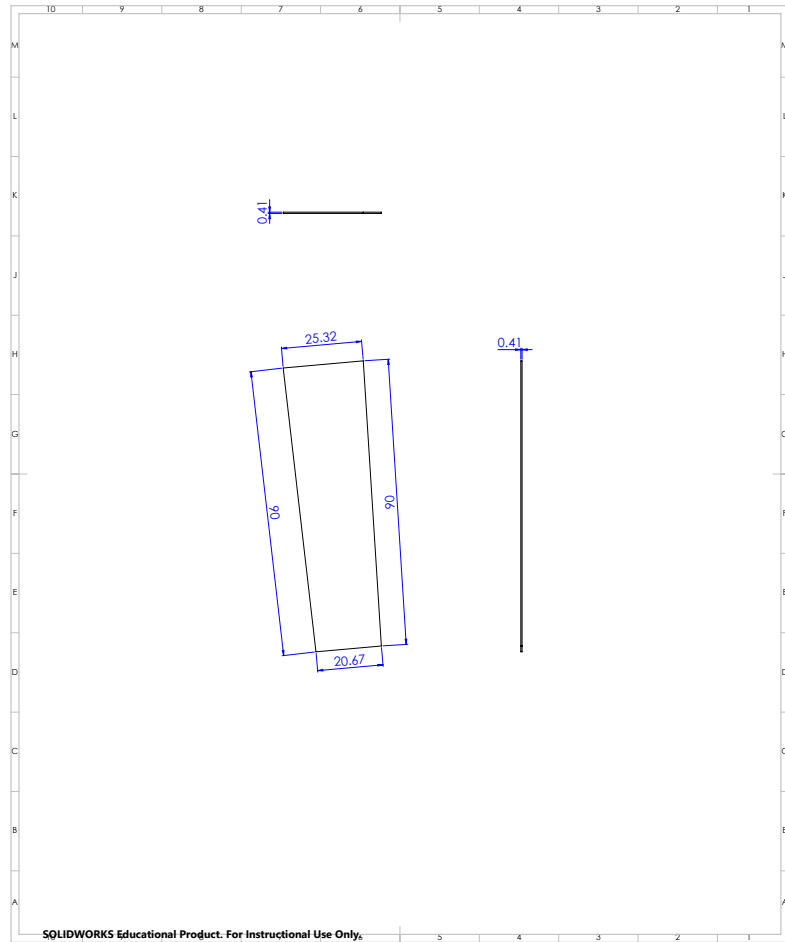


Figure 84: Side wall section of row B

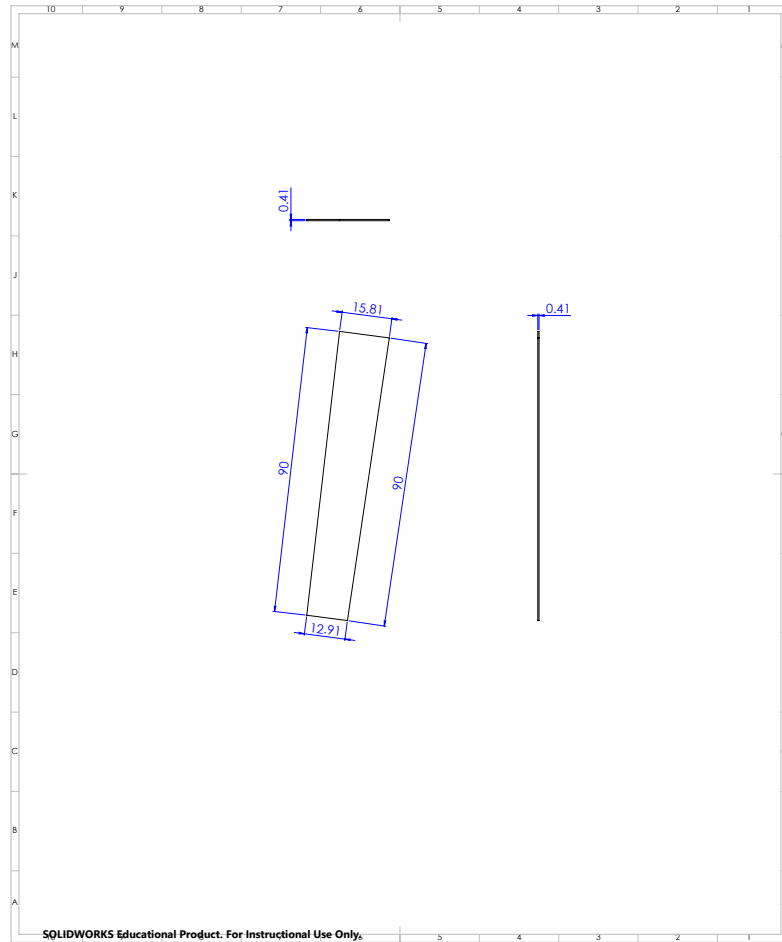
Appendix C (Continued)

Figure 85: Side wall section of row C

Appendix C (Continued)

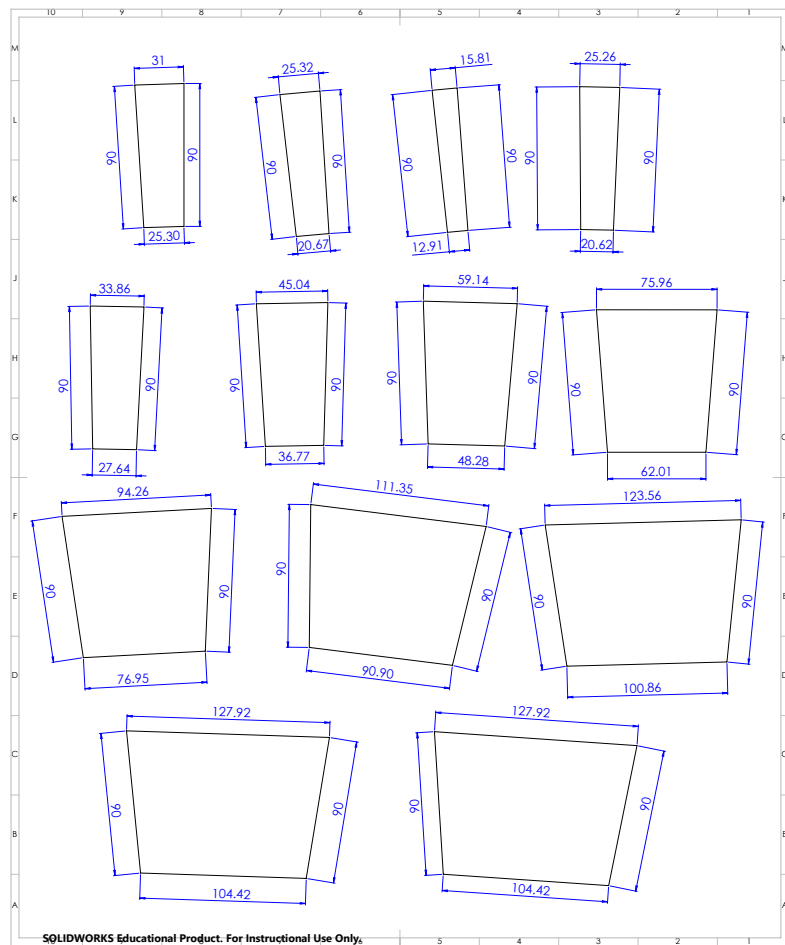


Figure 86: Side wall front view of each row (A-M)

Appendix D

PERMISSIONS TO REPRINT COPYRIGHT MATERIALS

Appendix D (Continued)

23/4/2019

RightsLink Printable License

ELSEVIER LICENSE TERMS AND CONDITIONS

Apr 23, 2019

This Agreement between Ms. Giulia Crocioni ("You") and Elsevier ("Elsevier") consists of your license details and the terms and conditions provided by Elsevier and Copyright Clearance Center.

License Number	4574280592169
License date	Apr 22, 2019
Licensed Content Publisher	Elsevier
Licensed Content Publication	Computers in Biology and Medicine
Licensed Content Title	Application of different imaging modalities for diagnosis of Diabetic Macular Edema: A review
Licensed Content Author	Muthu Rama Krishnan Mookiah,U. Rajendra Acharya,Hamido Fujita,Jen Hong Tan,Chua Kuang Chua,Sulatha V. Bhandary,Augustinus Laude,Louis Tong
Licensed Content Date	Nov 1, 2015
Licensed Content Volume	66
Licensed Content Issue	n/a
Licensed Content Pages	21
Start Page	295
End Page	315
Type of Use	reuse in a thesis/dissertation
Portion	figures/tables/illustrations
Number of figures/tables/illustrations	1
Format	electronic
Are you the author of this Elsevier article?	No
Will you be translating?	No
Original figure numbers	1
Title of your thesis/dissertation	Design, Fabrication and Testing of a Configurable Full-Field Stimulus Source for Electroretinography
Expected completion date	May 2019
Estimated size (number of pages)	190
Requestor Location	Ms. Giulia Crocioni 59 East Van Buren Street CHICAGO, IL 60605 United States Attn: Ms. Giulia Crocioni
Publisher Tax ID	98-0397604
Total	0.00 USD
Terms and Conditions	

INTRODUCTION

Appendix D (Continued)

23/4/2019

RightsLink Printable License

1. The publisher for this copyrighted material is Elsevier. By clicking "accept" in connection with completing this licensing transaction, you agree that the following terms and conditions apply to this transaction (along with the Billing and Payment terms and conditions established by Copyright Clearance Center, Inc. ("CCC"), at the time that you opened your Rightslink account and that are available at any time at <http://myaccount.copyright.com>).

GENERAL TERMS

2. Elsevier hereby grants you permission to reproduce the aforementioned material subject to the terms and conditions indicated.

3. Acknowledgement: If any part of the material to be used (for example, figures) has appeared in our publication with credit or acknowledgement to another source, permission must also be sought from that source. If such permission is not obtained then that material may not be included in your publication/copies. Suitable acknowledgement to the source must be made, either as a footnote or in a reference list at the end of your publication, as follows:

"Reprinted from Publication title, Vol /edition number, Author(s), Title of article / title of chapter, Pages No., Copyright (Year), with permission from Elsevier [OR APPLICABLE SOCIETY COPYRIGHT OWNER]." Also Lancet special credit - "Reprinted from The Lancet, Vol. number, Author(s), Title of article, Pages No., Copyright (Year), with permission from Elsevier."

4. Reproduction of this material is confined to the purpose and/or media for which permission is hereby given.

5. Altering/Modifying Material: Not Permitted. However figures and illustrations may be altered/adapted minimally to serve your work. Any other abbreviations, additions, deletions and/or any other alterations shall be made only with prior written authorization of Elsevier Ltd. (Please contact Elsevier at permissions@elsevier.com). No modifications can be made to any Lancet figures/tables and they must be reproduced in full.

6. If the permission fee for the requested use of our material is waived in this instance, please be advised that your future requests for Elsevier materials may attract a fee.

7. Reservation of Rights: Publisher reserves all rights not specifically granted in the combination of (i) the license details provided by you and accepted in the course of this licensing transaction, (ii) these terms and conditions and (iii) CCC's Billing and Payment terms and conditions.

8. License Contingent Upon Payment: While you may exercise the rights licensed immediately upon issuance of the license at the end of the licensing process for the transaction, provided that you have disclosed complete and accurate details of your proposed use, no license is finally effective unless and until full payment is received from you (either by publisher or by CCC) as provided in CCC's Billing and Payment terms and conditions. If full payment is not received on a timely basis, then any license preliminarily granted shall be deemed automatically revoked and shall be void as if never granted. Further, in the event that you breach any of these terms and conditions or any of CCC's Billing and Payment terms and conditions, the license is automatically revoked and shall be void as if never granted. Use of materials as described in a revoked license, as well as any use of the materials beyond the scope of an unrevoked license, may constitute copyright infringement and publisher reserves the right to take any and all action to protect its copyright in the materials.

9. Warranties: Publisher makes no representations or warranties with respect to the licensed material.

10. Indemnity: You hereby indemnify and agree to hold harmless publisher and CCC, and their respective officers, directors, employees and agents, from and against any and all claims arising out of your use of the licensed material other than as specifically authorized pursuant to this license.

11. No Transfer of License: This license is personal to you and may not be sublicensed, assigned, or transferred by you to any other person without publisher's written permission.

12. No Amendment Except in Writing: This license may not be amended except in a writing signed by both parties (or, in the case of publisher, by CCC on publisher's behalf).

13. Objection to Contrary Terms: Publisher hereby objects to any terms contained in any purchase order, acknowledgment, check endorsement or other writing prepared by you, which terms are inconsistent with these terms and conditions or CCC's Billing and Payment

Appendix D (Continued)

23/4/2019

RightsLink Printable License

terms and conditions. These terms and conditions, together with CCC's Billing and Payment terms and conditions (which are incorporated herein), comprise the entire agreement between you and publisher (and CCC) concerning this licensing transaction. In the event of any conflict between your obligations established by these terms and conditions and those established by CCC's Billing and Payment terms and conditions, these terms and conditions shall control.

14. **Revocation:** Elsevier or Copyright Clearance Center may deny the permissions described in this License at their sole discretion, for any reason or no reason, with a full refund payable to you. Notice of such denial will be made using the contact information provided by you. Failure to receive such notice will not alter or invalidate the denial. In no event will Elsevier or Copyright Clearance Center be responsible or liable for any costs, expenses or damage incurred by you as a result of a denial of your permission request, other than a refund of the amount(s) paid by you to Elsevier and/or Copyright Clearance Center for denied permissions.

LIMITED LICENSE

The following terms and conditions apply only to specific license types:

15. **Translation:** This permission is granted for non-exclusive world **English** rights only unless your license was granted for translation rights. If you licensed translation rights you may only translate this content into the languages you requested. A professional translator must perform all translations and reproduce the content word for word preserving the integrity of the article.

16. **Posting licensed content on any Website:** The following terms and conditions apply as follows: Licensing material from an Elsevier journal: All content posted to the web site must maintain the copyright information line on the bottom of each image; A hyper-text must be included to the Homepage of the journal from which you are licensing at <http://www.sciencedirect.com/science/journal/xxxx> or the Elsevier homepage for books at <http://www.elsevier.com>; Central Storage: This license does not include permission for a scanned version of the material to be stored in a central repository such as that provided by Heron/XanEdu.

Licensing material from an Elsevier book: A hyper-text link must be included to the Elsevier homepage at <http://www.elsevier.com>. All content posted to the web site must maintain the copyright information line on the bottom of each image.

Posting licensed content on Electronic reserve: In addition to the above the following clauses are applicable: The web site must be password-protected and made available only to bona fide students registered on a relevant course. This permission is granted for 1 year only. You may obtain a new license for future website posting.

17. **For journal authors:** the following clauses are applicable in addition to the above:

Preprints:

A preprint is an author's own write-up of research results and analysis, it has not been peer-reviewed, nor has it had any other value added to it by a publisher (such as formatting, copyright, technical enhancement etc.).

Authors can share their preprints anywhere at any time. Preprints should not be added to or enhanced in any way in order to appear more like, or to substitute for, the final versions of articles however authors can update their preprints on arXiv or RePEc with their Accepted Author Manuscript (see below).

If accepted for publication, we encourage authors to link from the preprint to their formal publication via its DOI. Millions of researchers have access to the formal publications on ScienceDirect, and so links will help users to find, access, cite and use the best available version. Please note that Cell Press, The Lancet and some society-owned have different preprint policies. Information on these policies is available on the journal homepage.

Accepted Author Manuscripts: An accepted author manuscript is the manuscript of an article that has been accepted for publication and which typically includes author-incorporated changes suggested during submission, peer review and editor-author communications.

Authors can share their accepted author manuscript:

- immediately

Appendix D (Continued)

23/4/2019

RightsLink Printable License

- via their non-commercial person homepage or blog
- by updating a preprint in arXiv or RePEc with the accepted manuscript
- via their research institute or institutional repository for internal institutional uses or as part of an invitation-only research collaboration work-group
- directly by providing copies to their students or to research collaborators for their personal use
- for private scholarly sharing as part of an invitation-only work group on commercial sites with which Elsevier has an agreement
- After the embargo period
 - via non-commercial hosting platforms such as their institutional repository
 - via commercial sites with which Elsevier has an agreement

In all cases accepted manuscripts should:

- link to the formal publication via its DOI
- bear a CC-BY-NC-ND license - this is easy to do
- if aggregated with other manuscripts, for example in a repository or other site, be shared in alignment with our hosting policy not be added to or enhanced in any way to appear more like, or to substitute for, the published journal article.

Published journal article (JPA): A published journal article (PJA) is the definitive final record of published research that appears or will appear in the journal and embodies all value-adding publishing activities including peer review co-ordination, copy-editing, formatting, (if relevant) pagination and online enrichment.

Policies for sharing publishing journal articles differ for subscription and gold open access articles:

Subscription Articles: If you are an author, please share a link to your article rather than the full-text. Millions of researchers have access to the formal publications on ScienceDirect, and so links will help your users to find, access, cite, and use the best available version. Theses and dissertations which contain embedded PJAs as part of the formal submission can be posted publicly by the awarding institution with DOI links back to the formal publications on ScienceDirect.

If you are affiliated with a library that subscribes to ScienceDirect you have additional private sharing rights for others' research accessed under that agreement. This includes use for classroom teaching and internal training at the institution (including use in course packs and courseware programs), and inclusion of the article for grant funding purposes.

Gold Open Access Articles: May be shared according to the author-selected end-user license and should contain a [CrossMark logo](#), the end user license, and a DOI link to the formal publication on ScienceDirect.

Please refer to Elsevier's [posting policy](#) for further information.

18. **For book authors** the following clauses are applicable in addition to the above:

Authors are permitted to place a brief summary of their work online only. You are not allowed to download and post the published electronic version of your chapter, nor may you scan the printed edition to create an electronic version. **Posting to a repository:** Authors are permitted to post a summary of their chapter only in their institution's repository.

19. **Thesis/Dissertation:** If your license is for use in a thesis/dissertation your thesis may be submitted to your institution in either print or electronic form. Should your thesis be published commercially, please reapply for permission. These requirements include permission for the Library and Archives of Canada to supply single copies, on demand, of the complete thesis and include permission for Proquest/UMI to supply single copies, on demand, of the complete thesis. Should your thesis be published commercially, please reapply for permission. Theses and dissertations which contain embedded PJAs as part of the formal submission can be posted publicly by the awarding institution with DOI links back to the formal publications on ScienceDirect.

Elsevier Open Access Terms and Conditions

You can publish open access with Elsevier in hundreds of open access journals or in nearly 2000 established subscription journals that support open access publishing. Permitted third

Appendix D (Continued)

23/4/2019

RightsLink Printable License

party re-use of these open access articles is defined by the author's choice of Creative Commons user license. See our [open access license policy](#) for more information.

Terms & Conditions applicable to all Open Access articles published with Elsevier:

Any reuse of the article must not represent the author as endorsing the adaptation of the article nor should the article be modified in such a way as to damage the author's honour or reputation. If any changes have been made, such changes must be clearly indicated.

The author(s) must be appropriately credited and we ask that you include the end user license and a DOI link to the formal publication on ScienceDirect.

If any part of the material to be used (for example, figures) has appeared in our publication with credit or acknowledgement to another source it is the responsibility of the user to ensure their reuse complies with the terms and conditions determined by the rights holder.

Additional Terms & Conditions applicable to each Creative Commons user license:

CC BY: The CC-BY license allows users to copy, to create extracts, abstracts and new works from the Article, to alter and revise the Article and to make commercial use of the Article (including reuse and/or resale of the Article by commercial entities), provided the user gives appropriate credit (with a link to the formal publication through the relevant DOI), provides a link to the license, indicates if changes were made and the licensor is not represented as endorsing the use made of the work. The full details of the license are available at <http://creativecommons.org/licenses/by/4.0>.

CC BY NC SA: The CC BY-NC-SA license allows users to copy, to create extracts, abstracts and new works from the Article, to alter and revise the Article, provided this is not done for commercial purposes, and that the user gives appropriate credit (with a link to the formal publication through the relevant DOI), provides a link to the license, indicates if changes were made and the licensor is not represented as endorsing the use made of the work. Further, any new works must be made available on the same conditions. The full details of the license are available at <http://creativecommons.org/licenses/by-nc-sa/4.0>.

CC BY NC ND: The CC BY-NC-ND license allows users to copy and distribute the Article, provided this is not done for commercial purposes and further does not permit distribution of the Article if it is changed or edited in any way, and provided the user gives appropriate credit (with a link to the formal publication through the relevant DOI), provides a link to the license, and that the licensor is not represented as endorsing the use made of the work. The full details of the license are available at <http://creativecommons.org/licenses/by-nc-nd/4.0>. Any commercial reuse of Open Access articles published with a CC BY NC SA or CC BY NC ND license requires permission from Elsevier and will be subject to a fee.

Commercial reuse includes:

- Associating advertising with the full text of the Article
- Charging fees for document delivery or access
- Article aggregation
- Systematic distribution via e-mail lists or share buttons

Posting or linking by commercial companies for use by customers of those companies.

20. Other Conditions:

v1.9

Questions? customercare@copyright.com or +1-855-239-3415 (toll free in the US) or +1-978-646-2777.

Appendix D (Continued)

04/22/2019

1200 W Harrison St, Chicago, IL 60607

I am writing to request permission to use “Scotopic Efficacy curve” figure from your publication in my thesis. This material will appear as originally published. Unless you request otherwise, I will use the conventional style of the Graduate College of the University of Illinois at Chicago as acknowledgment.

A copy of this letter is included for your records. Thank you for your kind consideration of this request.

Sincerely,

Giulia Crocioni
59 East Van Buren St, Chicago, IL 60605

The above request is approved.

Approved by: Rod Nave

Date: 04/22/2019

Appendix D (Continued)

23/4/2019

RightsLink Printable License

SPRINGER NATURE LICENSE TERMS AND CONDITIONS

Apr 23, 2019

This Agreement between Ms. Giulia Crocioni ("You") and Springer Nature ("Springer Nature") consists of your license details and the terms and conditions provided by Springer Nature and Copyright Clearance Center.

License Number	4574290954030
License date	Apr 22, 2019
Licensed Content Publisher	Springer Nature
Licensed Content Publication	Documenta Ophthalmologica
Licensed Content Title	ISCEV standard for clinical multifocal electroretinography (mfERG) (2011 edition)
Licensed Content Author	Donald C. Hood, Michael Bach, Mitchell Brigell et al
Licensed Content Date	Jan 1, 2011
Licensed Content Volume	124
Licensed Content Issue	1
Type of Use	Thesis/Dissertation
Requestor type	academic/university or research institute
Format	electronic
Portion	figures/tables/illustrations
Number of figures/tables/illustrations	1
Will you be translating?	no
Circulation/distribution	<501
Author of this Springer Nature content	no
Title	Design, Fabrication and Testing of a Configurable Full-Field Stimulus Source for Electroretinography
Institution name	n/a
Expected presentation date	May 2019
Order reference number	2
Portions	Figure 2: diagram of a mfERG response to show the designation of the major features of the waveform.
Requestor Location	Ms. Giulia Crocioni 59 East Van Buren Street CHICAGO, IL 60605 United States Attn: Ms. Giulia Crocioni
Total	0.00 USD

Terms and Conditions

Springer Nature Terms and Conditions for RightsLink Permissions

Springer Nature Customer Service Centre GmbH (the Licensor) hereby grants you a non-exclusive, world-wide licence to reproduce the material and for the purpose and requirements specified in the attached copy of your order form, and for no other use, subject to the conditions below:

1. The Licensor warrants that it has, to the best of its knowledge, the rights to license reuse of this material. However, you should ensure that the material you are requesting is original to the Licensor and does not carry the copyright of another entity (as credited in the published version).

If the credit line on any part of the material you have requested indicates that it was reprinted or adapted with permission from another source, then you should also seek permission from that source to reuse the material.

2. Where **print only** permission has been granted for a fee, separate permission must be obtained for any additional electronic re-use.

Appendix D (Continued)

23/4/2019

RightsLink Printable License

3. Permission granted **free of charge** for material in print is also usually granted for any electronic version of that work, provided that the material is incidental to your work as a whole and that the electronic version is essentially equivalent to, or substitutes for, the print version.
4. A licence for 'post on a website' is valid for 12 months from the licence date. This licence does not cover use of full text articles on websites.
5. Where '**reuse in a dissertation/thesis**' has been selected the following terms apply: Print rights of the final author's accepted manuscript (for clarity, NOT the published version) for up to 100 copies, electronic rights for use only on a personal website or institutional repository as defined by the Sherpa guideline (www.sherpa.ac.uk/romeo/).
6. Permission granted for books and journals is granted for the lifetime of the first edition and does not apply to second and subsequent editions (except where the first edition permission was granted free of charge or for signatories to the STM Permissions Guidelines <http://www.stm-assoc.org/copyright-legal-affairs/permissions/permissions-guidelines/>), and does not apply for editions in other languages unless additional translation rights have been granted separately in the licence.
7. Rights for additional components such as custom editions and derivatives require additional permission and may be subject to an additional fee. Please apply to Journalpermissions@springernature.com/bookpermissions@springernature.com for these rights.
8. The Licensor's permission must be acknowledged next to the licensed material in print. In electronic form, this acknowledgement must be visible at the same time as the figures/tables/illustrations or abstract, and must be hyperlinked to the journal/book's homepage. Our required acknowledgement format is in the Appendix below.
9. Use of the material for incidental promotional use, minor editing privileges (this does not include cropping, adapting, omitting material or any other changes that affect the meaning, intention or moral rights of the author) and copies for the disabled are permitted under this licence.
10. Minor adaptations of single figures (changes of format, colour and style) do not require the Licensor's approval. However, the adaptation should be credited as shown in Appendix below.

Appendix — Acknowledgements:

For Journal Content:

Reprinted by permission from [the Licensor]: [Journal Publisher (e.g. Nature/Springer/Palgrave)] [JOURNAL NAME] [REFERENCE CITATION (Article name, Author(s) Name), [COPYRIGHT] (year of publication)]

For Advance Online Publication papers:

Reprinted by permission from [the Licensor]: [Journal Publisher (e.g. Nature/Springer/Palgrave)] [JOURNAL NAME] [REFERENCE CITATION (Article name, Author(s) Name), [COPYRIGHT] (year of publication), advance online publication, day month year (doi: 10.1038/sj.[JOURNAL ACRONYM].)]

For Adaptations/Translations:

Adapted/Translated by permission from [the Licensor]: [Journal Publisher (e.g. Nature/Springer/Palgrave)] [JOURNAL NAME] [REFERENCE CITATION (Article name, Author(s) Name), [COPYRIGHT] (year of publication)]

Note: For any republication from the British Journal of Cancer, the following credit line style applies:

Reprinted/adapted/translated by permission from [the Licensor]: on behalf of Cancer Research UK: [Journal Publisher (e.g. Nature/Springer/Palgrave)] [JOURNAL NAME] [REFERENCE CITATION (Article name, Author(s) Name), [COPYRIGHT] (year of publication)]

For Advance Online Publication papers:

Reprinted by permission from The [the Licensor]: on behalf of Cancer Research UK: [Journal Publisher (e.g. Nature/Springer/Palgrave)] [JOURNAL NAME] [REFERENCE CITATION (Article name, Author(s) Name), [COPYRIGHT] (year of publication), advance online publication, day month year (doi: 10.1038/sj.[JOURNAL ACRONYM].)]

For Book content:

Reprinted/adapted by permission from [the Licensor]: [Book Publisher (e.g. Palgrave Macmillan, Springer etc)] [Book Title] by [Book author(s)] [COPYRIGHT] (year of publication)]

Other Conditions:

Version 1.1

Questions? customercare@copyright.com or +1-855-239-3415 (toll free in the US) or +1-978-646-2777.

Appendix D (Continued)

23/4/2019

RightsLink Printable License

SPRINGER NATURE LICENSE TERMS AND CONDITIONS

Apr 23, 2019

This Agreement between Ms. Giulia Crocioni ("You") and Springer Nature ("Springer Nature") consists of your license details and the terms and conditions provided by Springer Nature and Copyright Clearance Center.

License Number	4574291389840
License date	Apr 22, 2019
Licensed Content Publisher	Springer Nature
Licensed Content Publication	Documenta Ophthalmologica
Licensed Content Title	ISCEV standard for clinical pattern electroretinography (PERG): 2012 update
Licensed Content Author	Michael Bach, Mitchell G. Brigell, Marko Hawlina et al
Licensed Content Date	Jan 1, 2012
Licensed Content Volume	126
Licensed Content Issue	1
Type of Use	Thesis/Dissertation
Requestor type	academic/university or research institute
Format	electronic
Portion	figures/tables/illustrations
Number of figures/tables/illustrations	1
Will you be translating?	no
Circulation/distribution	<501
Author of this Springer Nature content	no
Title	Design, Fabrication and Testing of a Configurable Full-Field Stimulus Source for Electroretinography
Institution name	n/a
Expected presentation date	May 2019
Order reference number	1
Portions	Figure 1: a typical standard PERG.
Requestor Location	Ms. Giulia Crocioni 59 East Van Buren Street CHICAGO, IL 60605 United States Attn: Ms. Giulia Crocioni
Total	0.00 USD
Terms and Conditions	

Springer Nature Terms and Conditions for RightsLink Permissions
Springer Nature Customer Service Centre GmbH (the Licensor) hereby grants you a non-exclusive, world-wide licence to reproduce the material and for the purpose and requirements specified in the attached copy of your order form, and for no other use, subject to the conditions below:

Appendix D (Continued)

23/4/2019

RightsLink Printable License

1. The Licensor warrants that it has, to the best of its knowledge, the rights to license reuse of this material. However, you should ensure that the material you are requesting is original to the Licensor and does not carry the copyright of another entity (as credited in the published version).

If the credit line on any part of the material you have requested indicates that it was reprinted or adapted with permission from another source, then you should also seek permission from that source to reuse the material.

2. Where **print only** permission has been granted for a fee, separate permission must be obtained for any additional electronic re-use.
3. Permission granted **free of charge** for material in print is also usually granted for any electronic version of that work, provided that the material is incidental to your work as a whole and that the electronic version is essentially equivalent to, or substitutes for, the print version.
4. A licence for 'post on a website' is valid for 12 months from the licence date. This licence does not cover use of full text articles on websites.
5. Where '**reuse in a dissertation/thesis**' has been selected the following terms apply: Print rights of the final author's accepted manuscript (for clarity, NOT the published version) for up to 100 copies, electronic rights for use only on a personal website or institutional repository as defined by the Sherpa guideline (www.sherpa.ac.uk/romeo/).
6. Permission granted for books and journals is granted for the lifetime of the first edition and does not apply to second and subsequent editions (except where the first edition permission was granted free of charge or for signatories to the STM Permissions Guidelines <http://www.stm-assoc.org/copyright-legal-affairs/permissions/permissions-guidelines/>), and does not apply for editions in other languages unless additional translation rights have been granted separately in the licence.
7. Rights for additional components such as custom editions and derivatives require additional permission and may be subject to an additional fee. Please apply to Journalpermissions@springernature.com/bookpermissions@springernature.com for these rights.
8. The Licensor's permission must be acknowledged next to the licensed material in print. In electronic form, this acknowledgement must be visible at the same time as the figures/tables/illustrations or abstract, and must be hyperlinked to the journal/book's homepage. Our required acknowledgement format is in the Appendix below.
9. Use of the material for incidental promotional use, minor editing privileges (this does not include cropping, adapting, omitting material or any other changes that affect the meaning, intention or moral rights of the author) and copies for the disabled are permitted under this licence.
10. Minor adaptations of single figures (changes of format, colour and style) do not require the Licensor's approval. However, the adaptation should be credited as shown in Appendix below.

Appendix — Acknowledgements:

For Journal Content:

Reprinted by permission from [**the Licensor**]: [**Journal Publisher** (e.g. Nature/Springer/Palgrave)] [**JOURNAL NAME**] [**REFERENCE CITATION** (Article name, Author(s) Name), [**COPYRIGHT**] (year of publication)]

For Advance Online Publication papers:

Reprinted by permission from [**the Licensor**]: [**Journal Publisher** (e.g. Nature/Springer/Palgrave)] [**JOURNAL NAME**] [**REFERENCE CITATION** (Article name, Author(s) Name), [**COPYRIGHT**] (year of publication), advance online publication, day month year (doi: 10.1038/sj.[**JOURNAL ACRONYM**]).]

Appendix D (Continued)

23/4/2019

RightsLink Printable License

For Adaptations/Translations:

Adapted/Translated by permission from [the Licensor]: [Journal Publisher (e.g. Nature/Springer/Palgrave)] [JOURNAL NAME] [REFERENCE CITATION (Article name, Author(s) Name), [COPYRIGHT] (year of publication)

Note: For any republication from the British Journal of Cancer, the following credit line style applies:

Reprinted/adapted/translated by permission from [the Licensor]: on behalf of Cancer Research UK: : [Journal Publisher (e.g. Nature/Springer/Palgrave)] [JOURNAL NAME] [REFERENCE CITATION (Article name, Author(s) Name), [COPYRIGHT] (year of publication)

For Advance Online Publication papers:

Reprinted by permission from The [the Licensor]: on behalf of Cancer Research UK: [Journal Publisher (e.g. Nature/Springer/Palgrave)] [JOURNAL NAME] [REFERENCE CITATION (Article name, Author(s) Name), [COPYRIGHT] (year of publication), advance online publication, day month year (doi: 10.1038/sj. [JOURNAL ACRONYM])

For Book content:

Reprinted/adapted by permission from [the Licensor]: [Book Publisher (e.g. Palgrave Macmillan, Springer etc) [Book Title] by [Book author(s)] [COPYRIGHT] (year of publication)

Other Conditions:

Version 1.1

Questions? customercare@copyright.com or +1-855-239-3415 (toll free in the US) or +1-978-646-2777.

Appendix D (Continued)

April 23, 2019

200 First Street SW
Rochester, MN 55905
(507) 284-3335
Scientific Publications

Permissions: University of Illinois at Chicago
Richard & Loan Hill Department of Bioengineering
1200 W Harrison St.
Chicago, IL 60607

To Whom It May Concern:

On behalf of Mayo Foundation for Medical Education and Research, I grant Giulia Crocioni permission to reuse the attached image, for which Mayo Foundation for Medical Education and Research holds copyright, in the new work

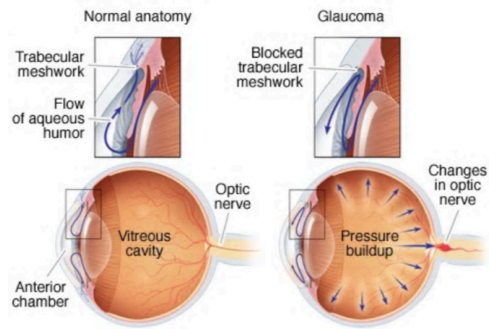
Crocioni G. Design, Fabrication and Testing of a Configurable Full-Field Stimulus Source for Electroretinography (thesis). [Chicago] IL: *University of Illinois at Chicago: Richard & Loan Hill Department of Bioengineering*; 2019.

As Copyright Agent for Mayo Foundation, I grant permission to include the aforementioned image, in print and electronic forms of the new work on the condition that credit be given as follows: "Used with permission of Mayo Foundation for Medical Education and Research, all rights reserved."

Sincerely,

Kenna Atherton, Copyright Agent
Mayo Foundation for Medical Education and Research

Appendix D (Continued)



© MAYO FOUNDATION FOR MEDICAL EDUCATION AND RESEARCH. ALL RIGHTS RESERVED.

Appendix D (Continued)

04/22/2019

1200 W Harrison St, Chicago, IL 60607

I am writing to request permission to use figures from “Pattern Electroretinography in Peripheral Retina: System Development and Validation in Human Subjects” (Thesis submitted as partial fulfillment of the requirements for the degree of Doctor of Philosophy in Bioengineering in the Graduate College of the UIC, 2018) in my thesis. This material will appear as originally published. Unless you request otherwise, I will use the conventional style of the Graduate College of the University of Illinois at Chicago as acknowledgment.

A copy of this letter is included for your records. Thank you for your kind consideration of this request.

Sincerely,

Giulia Crocioni
59 East Van Buren St, Chicago, IL 60605

The above request is approved.

Approved by: Shresta Patangay

Date: 04/22/2019

CITED LITERATURE

1. Nave, C. R.: Rods and cones, Last accessed 27-February-2019. <http://hyperphysics.phy-astr.gsu.edu/hbase/vision/rodcone.html>.
2. Mookiah, M. R. K., Acharya, U. R., Fujita, H., Tan, J. H., Chua, C. K., Bhandary, S. V., Laude, A., and Tong, L.: Application of different imaging modalities for diagnosis of Diabetic Macular Edema: A review. Computers in Biology and Medicine, 66:295–315, November 2015.
3. Kolb, H., Fernandez, E., Nelson, R., and Jones, B. W.: Webvision: The Organization of the Retina and Visual System, Last accessed 24-February-2019. <http://webvision.med.utah.edu/>.
4. Hood, D. C., Bach, M., Brigell, M., Keating, D., Kondo, M., Lyons, J. S., Marmor, M. F., McCulloch, D. L., and Palmowski-Wolfe, A. M.: ISCEV standard for clinical multifocal electroretinography (mfERG) (2011 edition). Documenta Ophthalmologica, 124(1):1–13, February 2012.
5. Bach, M., Brigell, M. G., Hawlina, M., Holder, G. E., Johnson, M. A., McCulloch, D. L., Meigen, T., and Viswanathan, S.: ISCEV standard for clinical pattern electroretinography (PERG): 2012 update. Documenta Ophthalmologica, 126(1):1–7, February 2013.
6. Frolov, S.: Oscilloscope cathode-ray tube, Last accessed 24-February-2019. https://commons.wikimedia.org/wiki/File:Oscilloscopic_tube.jpg.
7. Patangay, S.: Pattern electroretinography in peripheral retina: System development and validation in human subjects. Graduate College of the University of Illinois at Chicago, 2018.
8. Cree: Cree XLamp MC-E LED datasheet, 2008–2009.
9. Cree: Optimizing PCB Thermal Performance for Cree XLamp LEDs, 2010–2011. Rev. 1.
10. Texas Instruments: SNx4HC5958-Bit Shift Registers With 3-State Output Registers, Sept 2015. SN74HC595.
11. Morgan, J. E.: Retina ganglion cell degeneration in glaucoma: an opportunity missed? A review: RGC degeneration. Clinical & Experimental Ophthalmology, 40(4):364–368, May 2012.
12. Gurevich, L. and Slaughter, M.: Comparison of the Waveforms of the ON Bipolar Neuron and the b-Wave of the Electroretinogram. page 5.

13. McCulloch, D. L., Marmor, M. F., Brigell, M. G., Hamilton, R., Holder, G. E., Tzekov, R., and Bach, M.: ISCEV Standard for full-field clinical electroretinography (2015 update). Documenta Ophthalmologica, 130(1):1–12, February 2015.
14. Luminance, Last accessed 24-February-2019. <http://www.schorsch.com/en/kbase/glossary/luminance.html>.
15. Thompson, D. A., Fujinami, K., Perlman, I., Hamilton, R., and Robson, A. G.: ISCEV extended protocol for the dark-adapted red flash ERG. Documenta Ophthalmologica, 136(3):191–197, June 2018.
16. Frishman, L., Sustar, M., Kremers, J., McAnany, J. J., Sarossy, M., Tzekov, R., and Viswanathan, S.: ISCEV extended protocol for the photopic negative response (PhNR) of the full-field electroretinogram. Documenta Ophthalmologica, 136(3):207–211, June 2018.
17. Sustar, M., Holder, G. E., Kremers, J., Barnes, C. S., Lei, B., Khan, N. W., and Robson, A. G.: ISCEV extended protocol for the photopic On-Off ERG. Documenta Ophthalmologica, 136(3):199–206, June 2018.
18. Ramkumar, H. L., Epley, K. D., Tripathy, K., Karth, P. A., Kumar, U. R., and Shah, V. A.: Electroretinogram, Last accessed 4-March-2019. <https://eyewiki.aao.org/Electroretinogram>.
19. Miura, G., Wang, M. H., Ivers, K. M., and Frishman, L. J.: Retinal pathway origins of the pattern ERG of the mouse. Experimental Eye Research, 89(1):49–62, June 2009.
20. Bach, M. and Hoffmann, M. B.: Update on the Pattern Electroretinogram in Glaucoma. Optometry and Vision Science, 85(6):386–395, June 2008.
21. Holder, G. E.: Pattern Electroretinography (PERG) and an Integrated Approach to Visual Pathway Diagnosis. Progress in Retinal and Eye Research, 20(4):531–561, July 2001.
22. Viswanathan, S., Frishman, L. J., and Robson, J. G.: The Uniform Field and Pattern ERG in Macaques with Experimental Glaucoma: Removal of Spiking Activity. 41(9):14, 2000.
23. Bach, M., Sulimma, F., and Gerling, J.: Little correlation of the pattern electroretinogram (PERG) and visual field measures in early glaucoma. Documenta Ophthalmologica, 94(3):253–263, September 1997.
24. eds. J. R. Heckenlively and G. B. Arden Principles and Practice of Clinical Electrophysiology of Vision. The MIT Press, 2006.
25. LKC TECHNOLOGIES, I.: UTAS SunBurstTM. LKC TECHNOLOGIES, Inc., Last accessed 10-April-2019. https://www.lkc.com/wp-content/uploads/2017/02/LKC_SunBurst_Brochure_web.pdf.
26. Tomey: ELECTROPHYSIOLOGY EP-1000. Tomey Corporation, Last accessed 10-April-2019. https://tomey.de/images/product_flyer/EP-1000_br_w.pdf.

27. Metrovision: Vision Monitor - Visual electrophysiology systems. Metrovision, Last accessed 10-April-2019. https://metrovision.fr/pdf/HVM-MONPACKone_US.pdf.
28. LKC TECHNOLOGIES, I.: RETeval®. LKC TECHNOLOGIES, Inc., Last accessed 10-April-2019. https://www.lkc.com/wp-content/uploads/2018/06/LKC_RETeval_Brochure.pdf.
29. Diagnosys: Desktop Envoy™. Diagnosys, Last accessed 10-April-2019. <http://diagnosysllc.com/files/brochures/Diagnosys>
30. Diagnosys: ColorDome - Advanced Performance Ganzfeld Dome. Diagnosys, Last accessed 10-April-2019. <http://diagnosysllc.com/files/brochures/Diagnosys>
31. Diagnosys: LCD Monitor - Advanced High Brightness Monitor. Diagnosys, Last accessed 10-April-2019. <http://diagnosysllc.com/files/brochures/Diagnosys>
32. Hood, D., Xu, L., Thienprasiddhi, P., Greenstein, V., Odel, J., Grippo, T., Liebmann, J., and Ritch, R.: The pattern electroretinogram in glaucoma patients with confirmed visual field deficits. Invest Ophthalmol Vis Sci, 46:2411–2418, 2005.
33. Bach, M., Pfeieffer, N., and Birkner-Binder, D.: Pattern electroretinogram reflects diffuse retinal damage in early glaucoma. Clin Vision Sci, 32:1219—1223, 1992.
34. Tham, Y.-C., Li, X., Wong, T. Y., Quigley, H. A., Aung, T., and Cheng, C.-Y.: Global Prevalence of Glaucoma and Projections of Glaucoma Burden through 2040. Ophthalmology, 121(11):2081–2090, November 2014.
35. Foster, P. J.: The definition and classification of glaucoma in prevalence surveys. British Journal of Ophthalmology, 86(2):238–242, February 2002.
36. Glaucoma: What You Should Know. National Eye Institute - National Institute of Health, NIH Publication No: 10–651, September 2010.
37. Lucy, K. A. and Wollstein, G.: Structural and functional evaluations for the early detection of glaucoma. Expert Review of Ophthalmology, 11(5):367–376, August 2016.
38. Landers, J., Sharma, A., Goldberg, I., and Graham, S. L.: A comparison of visual field sensitivities between the medmont automated perimeter and the humphrey field analyzer. Clinical & Experimental Ophthalmology, 38:273–276, April 2010.
39. Quigley, H. A., Dunkelberger, G. R., and Green, W. R.: Retinal ganglion cell atrophy correlated with automated perimetry in human eyes with glaucoma. American Journal of Ophthalmology, 107(5):453–464, 2018/12/24 1989.
40. Banitt, M. R., Ventura, L. M., Feuer, W. J., Savatovsky, E., Luna, G., Shif, O., Bosse, B., and Porciatti, V.: Progressive Loss of Retinal Ganglion Cell Function Precedes Structural Loss by Several Years in Glaucoma Suspects. Investigative Ophthalmology & Visual Science, 54(3):2346, March 2013.
41. Visual fields. In Clinical Methods: The History, Physical, and Laboratory Examinations. 3rd edition., ed. H. J. Walker HK, Hall WD, chapter 116. Boston: Butterworths, 1990.

42. Traquair, H. M.: An Introduction to Clinical Perimetry, chapter 1, pages 4–5. London: Henry Kimpton, 1938.
43. Bach, M. and Holder, G. E.: Check size tuning of the pattern electroretinogram: a reappraisal. Documenta Ophthalmologica, 92(3):193–202, September 1996.
44. Poelman, D., Avci, N., and Smet, P. F.: Measured luminance and visual appearance of multi-color persistent phosphors. Optics Express, 17(1):358, January 2009.
45. 127 x 177.8 x 1mm high efficiency window, Last accessed 10-March-2019. <https://www.edmundoptics.com/p/127-x-1778-x-1mm-High-Efficiency-Window/17831/>.
46. #55, 8" x 10", 5 sheets, adhesive back flock paper, Last accessed 10-March-2019. <https://www.edmundoptics.com/p/55-8quot-x-10quot-5-sheets-adhesive-back-flock-paper/11265/>.
47. High reflectance film, Last accessed 21-March-2019. <https://www.whiteoptics.com/reflectance-film/>.
48. Optix 95 - ld, Last accessed 13-March-2019. https://www.delviesplastics.com/p/Optix95_LD.html.
49. Aswani, K.: Time-Lapse Imaging with Lamp & LED – Stability vs. Repeatability. Excelitas Technologies, October 2014. Rev: A.
50. Vishay Semiconductors: 1 Form A Solid-State Relay, June 2017. VO14642AT.
51. Maw, C. and Igoe, T.: Serial to parallel shifting-out with a 74hc595, Last accessed 24-March-2019. <https://www.arduino.cc/en/Tutorial/ShiftOut>.
52. National instruments VISA, Last accessed 24-March-2019. <https://www.ni.com/visa/>.
53. CAMERA EXPOSURE, Last accessed 7-April-2019. <https://www.cambridgeincolour.com/tutorials/camera-exposure.html>.
54. How to photograph an LED sign, Last accessed 10-April-2019. <https://sdgmag.com/tips/how-photograph-led-sign>.
55. Weitz, A.: The photographic eye, Last accessed 7-April-2019. <https://www.bhphotovideo.com/c/find/newsLetter/The-Photographic-Eye.jsp>.
56. Rowse, D.: ISO settings in digital photography, Last accessed 7-April-2019. <https://digital-photography-school.com/iso-settings/>.
57. rgb2gray, Last accessed 8-April-2019. <https://www.mathworks.com/help/matlab/ref/rgb2gray.html>.
58. Caldwell, B., Cooper, M., Guarino Reid, L., and Vanderheiden, G.: Web content accessibility guidelines (WCAG) 2.0, Last accessed 10-April-2019. <https://www.w3.org/TR/2008/REC-WCAG20-20081211/>.
59. Matkovic, K., Neumann, L., Neumann, A., Psik, T., and Purgathofer, W.: Global Contrast Factor - a New Approach to Image Contrast. pages 1–9, 2005.

CITED LITERATURE (Continued)

173

60. Metal Velvet Adhesive Foil Sheet 200 x 200 mm, Last accessed 10-April-2019. <https://www.edmundooptics.com/p/metal-velvet-adhesive-foil-sheet-200-x-200mm/41320/>.

VITA

NAME: Giulia Crocioni

EDUCATION: M.S., Bioengineering
University of Illinois at Chicago, Chicago, IL
August 2018 to present

M.S., Biomedical Engineering - Technologies for Electronics
Politecnico di Milano, Milano, Italy
September 2017 to present

B.S., Biomedical Engineering
Politecnico di Milano, Milano, Italy
September 2014 to July 2017

EXPERIENCE: University of Illinois at Chicago
Teaching Assistant in Neural Engineering
January 2019 to present

PUBLICATIONS: Bonfanti, S.B., Crocioni, G., Cunsolo, F., and Grusso, G.
"Implementation of an IoT node for biomedical devices"
2018 IEEE 4th International Forum on Research and
Technology for Society and Industry (RTSI)